UNIVERSITÀ DEGLI STUDI "G. d'Annunzio"

Chieti-Pescara

"G. d'Annunzio" School of Advanced Studies

Doctorate School in Biomolecular and Pharmaceutical Sciences

Cycle – XXXVIII

EXTRACTION, CHARACTERIZATION AND BIOLOGICAL EVALUATION OF SNAIL SLIME OBTAINED BY THE CHERASCO METHOD ON IN-VITRO CELL MODELS

Department of Pharmacy

Disciplinary Area BIOS-12/A

PhD student
Dr. Muhammad Rashad

Coordinator
Prof. Assunta Pandolfi

Tutor
Prof. Susi Zara

ACADEMIC YEARS 2022 – 2025

TABLE OF CONTENTS

ABSTRACT 1

1 INTRODUCTION 2

1.1 Extraction of SS 6

1.2 Composition of SS 8

1.3 Applications of SS 11

1.3.1 Wound Healing 12

1.3.2 Treating Skin Conditions 14

1.3.3 Antimicrobial Properties 15

1.3.4 Beauty and Cosmetic Uses 18

1.3.4.1 Anti-aging Properties 18

1.3.4.2 Moisturizing Effects 19

1.3.4.3 Skin Regeneration and Repair 20

1.3.4.4 Antioxidant Properties 20

1.3.4.5 Anti-inflammatory Activities 20

1.3.4.6 Acne Treatment 22

1.3.4.7 Skin Brightening 22

1.3.5 Emerging Applications 22

1.3.5.1 Cough Suppressant 23

1.3.5.2 Antiviral Activities 23

1.3.5.3 Antifungal Activities 24

1.3.5.4 Dental Applications 24

1.3.5.5 Osteoarthritis Treatment 24

1.3.5.6 Neuroprotective Effects 25

1.3.5.7 Gastrointestinal Health 25

1.3.5.8 Cancer Research 26

1.3.5.9 Tissue Engineering and Optimized Drug Delivery 26

1.3.5.10 Biochemical Marker and Diagnostic Applications 27

1.3.5.11 Ophthalmic Applications 27

2 MATERIALS AND METHODS 29

2.1 Extraction of SS 29

2.2 Sampling....30
2.3 Chemical Analysis....30
2.3.1 Nuclear Magnetic Resonance (NMR) Analysis....30
2.3.2 Gas Chromatography-Mass Spectrometry (GC-MS) Analysis....30
2.3.3 Solid-Phase Microextraction (SPME) Sampling....31
2.3.4 Fourier Transform Infrared-Attenuated Total Reflection Spectroscopy (FTIR-ATR) Analysis....32
2.3.5 Raman Spectroscopy Measurements....32
2.3.6 Thermal Analysis....32
2.3.7 Total Phenolic Content (TPC) Assessment....33
2.3.8 Determination of Antioxidant Effects....33
2.3.8.1 DPPH Radical Scavenging Ability....33
2.3.8.2 ABTS Radical Scavenging Ability....34
2.3.9 Reducing Power Assays....34
2.3.9.1 Cupric Ion Reducing Activity (CUPRAC)....34
2.3.9.2 Ferric Reducing Antioxidant Power (FRAP)....34
2.3.9.3 Phosphomolybdenum Assay....34
2.3.10 Metal Chelating Ability....35
2.3.11 Enzyme Inhibitory Assays....35
2.3.11.1 Cholinesterase (ChE) Inhibitory Assays....35
2.3.11.2 Tyrosinase Inhibitory Assay....35
2.3.11.3 α-Amylase Inhibitory Assay....35
2.3.11.4 α-Glucosidase Inhibitory Assay....35
2.4 Cell Culture....36
2.5 Cell Treatments....36
2.5.1 Cell Viability by MTT Assay....36
2.5.2 Wound Healing Assay....37
2.5.3 Flow Cytometry Analysis of ROS Release....37
2.5.4 Western Blot Analysis....38

2.6 HaCaT Experiments 39
2.6.1 Lactate Dehydrogenase (LDH) Cytotoxicity Assay 39
2.6.2 Measurement of Interleukin-6 (IL−6) Secretion by ELISA Assay 39
2.6.3 RNA Extraction, Reverse Transcription and Real-Time Polymerase Chain Reaction (RT-PCR) 39
2.7 NHDFs Experiments 41
2.7.1 Almar Blue Assay 41
2.7.2 Antioxidant Activity Assessment 41
2.7.3 Detection of Apoptosis and Necrosis by Flow Cytometry 42
2.7.4 Treatment and Sample Collection for Proteomic Analysis 42
2.7.4.1 Cell Lysis and Protein Quantification 42
2.7.4.2 Protein Digestion 43
2.7.4.3 LC-MS Analysis 43
2.7.4.4 Data Analysis 44
2.8 Statistical Evaluation 44
3 RESULTS 45
3.1 Chemical Analysis of SS 45
3.1.1 Nuclear Magnetic Resonance (NMR) Analysis of Metabolites 45
3.1.2 Solid-Phase Microextraction-Gas Chromatography/Mass Spectrometry (SPME-GC/MS) Analysis 46
3.1.3 Fourier Transform Infrared Spectroscopy (FT-IR) Measurements 51
3.1.4 Raman Spectroscopy Analysis 53
3.1.5 Thermogravimetric Assessment 55
3.1.6 Antioxidant Capacity Evaluation 56
3.1.7 Enzyme Inhibition Assessment 57
3.2 Biological Evaluation of SS on Different Cell Models 58
3.2.1 Human Keratinocytes (HaCaT) 58
3.2.1.1 Assessment of Viability after SS and GA Treatment 58
3.2.1.2 Evaluation of GA's and SS's Effects on Cytotoxicity 59

3.2.1.3 Measurement of ROS Level after SS and GA Treatment 60
3.2.1.4 Effect of SS and GA Treatment on PI3K/Akt/NF-κB Protein levels 61
3.2.1.5 Assessment of SS Modulated Inflammatory Response 63
3.2.1.6 Analysis of Matrix Metalloproteinases (MMPs) Gene Expression 65
3.2.1.7 Wound Healing Assessment after SS and GA Treatment 66
3.2.2 Human Endothelial Cells (ECs) (EA.hy926) 67
3.2.2.1 Evaluation of Cell Viability 67
3.2.2.2 Wound Healing Assessment after SS and GA Treatments 68
3.2.3 Normal Human Dermal Fibroblasts (NHDFs) 69
3.2.3.1 Evaluation of Cell Viability 69
3.2.3.2 Proteomics Results 70
3.2.3.3 Evaluation of programmed cell death occurrence 73
3.2.3.4 Pro and Antiapoptotic Protein Expression Analysis 74
3.2.3.5 Antioxidant Capacity Assessment 75
3.2.3.6 Wound Healing Analysis 76
4 DISCUSSION 78
4.1 Chemical Characterization of Snail Slime 78
4.2 Biological Evaluation of Snail Slime 83
4.3 Proteomics Analysis 89
5 CONCLUSIONS 94
6 FUTURE PROSPECTIVES 96
7 FUNDING 97
8 ACKNOWLEDGMENTS 97
9 REFERENCES 98
10 PUBLICATIONS 106
11 CONFERENCES AND SEMINARS 107

ABSTRACT

This study provides a comprehensive chemical, biological, and proteomic characterization of snail slime (SS), highlighting its potential as a multifunctional biomaterial for dermatological and therapeutic applications. Advanced analytical techniques (NMR, GC–MS, IR, Raman, and thermal analyses) revealed a complex composition rich in glycoproteins, organic acids, phenolics, and trace elements, with processing conditions significantly influencing its chemical profile and functional properties. Stabilized SS exhibited enhanced antioxidant capacity and enzyme inhibitory potential, while non-stabilized samples showed superior metal-chelating activity, underscoring formulation-dependent bioactivity. Biological evaluation demonstrated that SS is highly biocompatible and promotes skin regeneration through coordinated modulation of inflammation, oxidative stress, and extracellular matrix remodeling. In keratinocytes, SS induced a controlled and transient activation of the PI3K/Akt/NF-κB pathway, avoiding the prolonged inflammatory and cytotoxic effects observed with glycolic acid (GA) alone. SS reduced COX-2 and IL-6 expression, regulated ROS levels in a concentration-dependent manner, and significantly enhanced cell migration and wound closure. Additionally, SS promoted endothelial cell viability and migration, supporting its pro-angiogenic potential. Proteomic analysis in dermal fibroblasts further revealed that SS regulates key biological processes, including apoptosis, oxidative stress response, cell migration, and wound healing, with central involvement of hub proteins such as AKT, PI3K, SRC, and KRAS. The observed hormetic redox modulation and balanced apoptotic signaling indicate a controlled cellular turnover conducive to tissue regeneration. Collectively, these findings establish SS as a bioactive natural matrix capable of orchestrating multiple regenerative pathways, supporting its application as a safer and effective alternative to synthetic agents in wound healing, anti-aging, and skin repair strategies.

Keywords: Snail slime; Cherasco muller method; Cruelty free; Spectroscopic analysis; Wound healing; Redox modulation; Proteomics; LC-MS analysis

1 INTRODUCTION

Gastropods, a diverse class of mollusks comprising snails and slugs, have long captivated scientific curiosity owing to their unique adaptations and intriguing biological activities [1]. They inhabit an extensive range of ecosystems, spanning terrestrial landscapes, freshwater bodies, and marine environments, where they have developed mucus-based strategies to ensure survival and ecological success [2]. The most representative species include *Cornu aspersum* (formerly *Helix aspersa*), *Helix pomatia*, *Archachatina marginata, Achatina fulica, Hexaplex trunculus, Conus magus, Bolinus brandaris*, and *Eremina desertorum*, while among slugs, *Arion subfuscus* is one of the most well-documented representatives [3]. These species, although unified by their ability to secrete slime, exhibit significant differences in the biochemical composition and biological functions of their secretions, reflecting evolutionary adaptations to their respective habitats. A comparative overview of different snail species and their slime composition is provided in Table 1.

Helix aspersa, widely distributed across Europe, North Africa, and many temperate regions, due to natural dispersion and human-mediated introduction, has been the most intensively studied terrestrial snail [4]. Belonging to the family Helicidae, this species produces mucus particularly rich in glycoproteins, glycolic acid (GA), hyaluronic acid (HA), and antimicrobial peptides [5, 6]. These compounds are increasingly valued in biomedical and cosmetic fields for their regenerative, antioxidant, and antimicrobial effects. *Helix pomatia*, commonly known as the Roman snail, differs in its slime profile, which contains higher levels of mucopolysaccharides and antioxidant molecules, making it particularly relevant in antioxidant therapies and cosmetic formulations [7, 8]. *Archachatina marginata* and *Achatina fulica*, two giant African land snails, are characterized by their ability to produce larger volumes of slime with abundant glycosaminoglycans (GAGs) and antimicrobial peptides, an adaptation that supports survival in humid and microbe-rich environments [9]. In contrast, desert-dwelling species such as *Eremina desertorum* secrete more viscous and resistant mucus to withstand desiccating conditions, reducing water loss during extended drought periods [10].

Marine gastropods show even greater biochemical diversity in their secretions. *Hexaplex trunculus* and *Bolinus brandaris* are historically known for their role in producing Tyrian purple dye, but recent studies have revealed that their mucus is rich in sulfated GAGs with potential anticoagulant and anti-inflammatory properties [11]. *Conus magus*

represents another unique case, producing both mucus and highly specialized venom (conotoxins), which have been extensively studied for their neuroactive properties, leading to the development of novel analgesics such as ziconotide [12]. Slugs like *Arion subfuscus,* lacking a protective shell, rely heavily on their slime as a multifunctional defense, producing copious adhesive mucus with exceptional viscoelastic and antimicrobial characteristics, making it distinct from snail mucus both in quantity and chemical complexity [13].

The adaptive functions of snail slime (SS) are central to gastropod survival. When threatened, both snails and slugs release copious amounts of mucus that act as a physical barrier, reducing predation risks by creating a slippery or adhesive surface [13]. In several species, this mucus also contains chemical deterrents that further enhance survival, exemplifying the integration of mechanical and biochemical defense strategies. Beyond defense, slime fulfills crucial ecological and biological roles, including hydration, locomotion, and reproductive interactions, while also serving as a protective shield against microbial colonization. Recent research highlights that bioactive molecules in slime are capable of stimulating cellular proliferation, accelerating wound closure, and exhibiting antimicrobial activity, making them promising candidates for therapeutic applications in wound healing, tissue regeneration, and infection control.

The biological process underlying slime secretion is a complex one. Snails produce different types of mucus through specialized glands; each is adapted for distinct functions. The pedal glands, located in the foot, are primarily responsible for locomotory mucus, which facilitates smooth movement across surfaces and reduces mechanical stress. This secretion is composed of more than 99% water, along with GAGs and minerals that provide adhesion and lubrication. Proteomic analyses of *Cornu aspersum* pedal mucus have revealed only three predominant protein bands (82, 97, and 175 kDa), suggesting that this mucus has limited bioactive roles compared to other glandular secretions [14]. In contrast, mantle glands, located near the shell, produce a secretion chemically richer, containing GAGs, mucopolysaccharides, proteins, enzymes, and minerals crucial for shell repair, protection against environmental stress, and antimicrobial defense [15]. This mantle-derived mucus is also the principal source of bioactive components currently exploited in medicine and cosmetics. The slime formation process involves the secretion of mucin precursors that swell and hydrate upon exposure to water, forming a cross-linked polymeric network that confers the characteristic viscoelastic and protective properties of gastropod mucus [14, 16].

Taken together, gastropod species exhibit remarkable diversity in the composition and function of their mucus, shaped by their ecological niches and evolutionary pressures. Terrestrial species have optimized their slime for hydration, adhesion, and defense, whereas marine gastropods show a broader spectrum of bioactivities with unique pharmacological applications. Slugs, on the other hand, rely heavily on adhesive and defensive mucus as a substitute for shell protection. These interspecies differences emphasize the importance of comparative biochemical analyses to better understand gastropod adaptations and to harness their mucus as a valuable source of novel biomaterials and therapeutic agents.

Among the various gastropods, *Helix aspersa*, now correctly classified as *Cornu aspersum*, occupies a particularly important position owing to its broad distribution, ecological adaptability, and extensive biomedical applications. Native to the Mediterranean basin but now naturalized across Europe, North America, South Africa, and Australia, this species thrives in highly variable environments ranging from humid coastal regions to semi-arid landscapes. Its adaptability has been facilitated by versatile physiology, including the ability to aestivate during unfavorable conditions, and by its capacity to produce mucus that is both protective and multifunctional. Unlike other terrestrial snails that show more restricted ecological ranges, *Helix aspersa* has emerged as a model organism for studying mucus biology due to the abundance, accessibility, and unique biochemical richness of its secretions.

The biomedical potential of *Helix aspersa* mucus has been increasingly highlighted in recent decades. Its slime is particularly rich in glycoproteins, GA, HA, allantoin, antimicrobial peptides, and bioactive enzymes that collectively contribute to skin regeneration, hydration, and antimicrobial defense. These properties have led to its widespread incorporation into dermatological and cosmetic formulations, particularly for wound healing, scar reduction, anti-aging, and anti-inflammatory applications. Furthermore, studies have demonstrated that its mucus stimulates fibroblast proliferation and extracellular matrix remodeling, processes critical to tissue repair and regeneration. Compared to related species such as *Helix pomatia*, *Helix aspersa* secretes a higher proportion of low-molecular-weight bioactive compounds that are more readily absorbed by human tissues, further supporting its prominence in biomedical research. Its mucus has also shown inhibitory activity against common bacterial pathogens, highlighting potential as a natural source of novel antimicrobial agents in an era of rising antibiotic resistance.

Table 1: Comparative table illustration of snail species slime differences.

Species	Extraction Method	Physical Properties	Chemical Composition	Biological Activities	References
Archachatina marginata	Chemical extraction (acetic acid, ammonium bicarbonate), physical scraping	Variable colors; higher volume and degree of sliminess; viscosity higher than *Achatina achatina* and *Lissachatina fulica*	Rich in antimicrobial proteins; variable protein content based on extraction; metabolites contributing to antimicrobial activity	Strong antibacterial effects against Gram-positive and Gram-negative bacteria; notable inhibition zones (19.5-24.0 mm); potential in addressing antibiotic resistance	[11, 17]
Achatina achatina	Chemical extraction (acetic acid, ammonium bicarbonate), physical scraping	Moderate volume and viscosity; slime color lighter compared to *A. marginata*	Contains bioactive peptides; protein profile is less potent antibacterial compared to *A. marginata*	Moderate antimicrobial effects against bacterial species; relevant in wound infection control	[17]
Lissachatina fulica	Physical scraping; comparisons of mantle vs. foot mucus; cold extraction methods	Mucus varies with anatomical origin; mantle mucus is more viscous and protein-rich	Contains achacin and other antibacterial proteins; antioxidant metabolites; high mucin content	Antibacterial, antioxidant, and anti-inflammatory activities; promotes nitric oxide inhibition; effective against bacterial pathogens in wound infections	[18, 19]
Helix aspersa	Cruelty-free Muller	Color variable;	Rich in allantoin,	Strong wound healing	[11, 20, 21]

	method; chemical analyses via ICP-OES, GC-MS	slime presents moderate viscosity and volume	mucin, minerals; presence of peptides and metabolites supporting regeneration	promotion via fibroblast viability enhancement; anti-inflammatory effects; antimicrobial against wound pathogens	
Pomacea canaliculata	Physical collection of mucus from freshwater snails	Viscous mucus with distinctive antioxidant capacity	Contains antioxidant proteins and metabolites; lower antibacterial protein concentration compared to land snails	Better reducing power activity compared to *Lissachatina fulica*; anti-inflammatory properties	[19]

1.1 Extraction of SS

There are several methods for extracting snail mucin, ranging from traditional to more modern techniques. Non-lethal methods include stimulated production, where snails are induced to produce mucin through acid stimulation [22]. Unfortunately, some lethal methods are still in use, such as crushing whole snails or using solvent extraction, mechanical stimulation, or centrifugation [23] which raises significant ethical concerns (Figure 1).

After extraction, the raw mucin undergoes several processing steps. These typically include filtration to remove debris and impurities, centrifugation to separate different components of the mucin, lyophilization (freeze-drying) to produce a stable powder form, and sterilization to ensure product safety for cosmetic or pharmaceutical use. Advanced techniques such as ultrafiltration and chromatography may be employed to isolate specific bioactive compounds from the mucin [24].

Adopting sustainable and ethical practices is crucial for the future of the SS industry, as it ensures long-term viability, minimizes environmental harm, and addresses animal welfare [25]. Key sustainability goals involve optimizing farms to reduce resource use,

developing humane and non-lethal extraction methods, and finding valuable uses for farming by-products to eliminate waste [21]. On the ethical front, the primary concerns are animal welfare, which is addressed by prioritizing extraction methods that avoid harm to snails, and environmental impact, which is mitigated through strict biosecurity measures to prevent farmed snails from becoming invasive species [22].

There is a growing demand for transparency in the cosmetics industry regarding the sourcing and production methods of snail mucin. Some companies, such as Lumacheria Italiana srl. have developed an innovative "cruelty-free" Muller Cherasco method for their snail mucin products [26, 27]. Additionally, the production of snail mucin for cosmetic or pharmaceutical use must comply with relevant regulations and safety standards. This includes ensuring that extraction and processing methods do not introduce harmful contaminants [28]. Lumacheria Italiana srl. Cherasco, Italy, is extracting SS using the Muller Cherasco method, a cruelty-free process that uses a machine, namely Muller One, to stimulate snails to release slime while complying with the safety standards and regulations. This method involves washing healthy snails, then subjecting them to a cycle of antimicrobial ozonated water and a citric acid solution that encourages slime secretion without harming the animals.

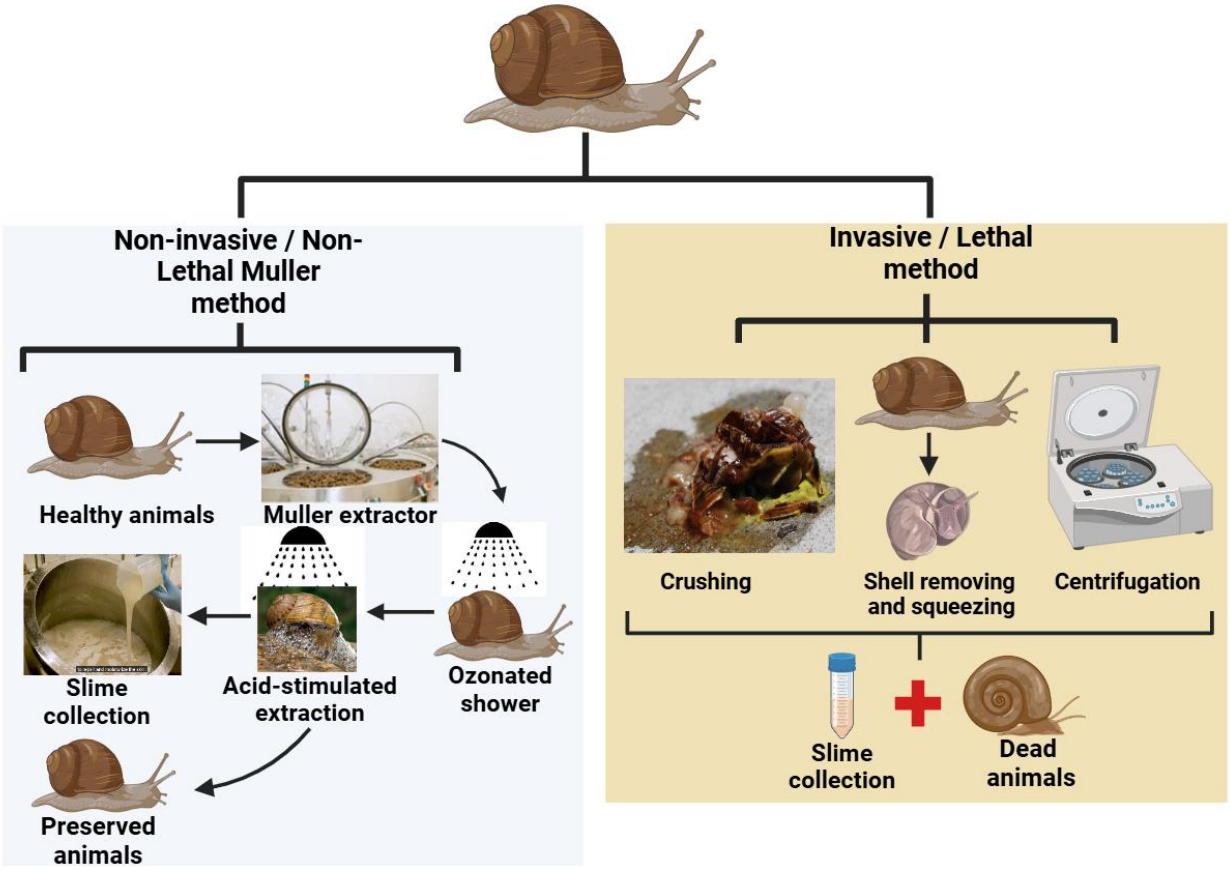


Figure 1: Comparative illustration of non-lethal SS Muller extraction and production method (left panel) and lethal (right panel) SS extraction and production method.

1.2 Composition of SS

SS, a complex bioactive substance, is primarily composed of water (90-99.7%) and a diverse array of compounds. The dry weight typically includes 5-9% proteins, 3-5% GAGs, and 1.3-1.6% mucopolysaccharides. Key components include HA (<1 mg/g), GA (up to 4%), and allantoin (0.3-0.5%). The slime also contains collagen, elastin, and various glycoproteic enzymes [14], each contributing to its purported skincare benefits. GA acts as a gentle exfoliant, promoting cell turnover and improving skin texture [29]. HA is a powerful humectant capable of holding up to 1000 times water of its weight, drawing moisture to the skin and helping maintain hydration [30]. This substance helps to hydrate the skin deeply, plumping it up and reducing the appearance of fine lines. The presence of HA contributes to the moisturizing properties often associated with SS-based products. Allantoin is known for its soothing and healing properties, while the proteins and peptides in the mucin may support collagen production and skin elasticity. Collagen and elastin, both proteins crucial for skin structure and elasticity, are also present in SS.

These proteins are essential for maintaining skin firmness and reducing the appearance of fine lines and wrinkles. Their presence in snail mucin has led to its inclusion in many anti-aging products. This natural substance offers a potent blend of moisturizing, exfoliating, and healing properties as its components work synergistically to promote skin regeneration, boost collagen production, and provide powerful antioxidant effects [28].

Chemical analysis has revealed that trace amounts of mineral salts (Ca, Mg, Zn, Cu, Fe) and vitamins (A, C, E) are also present in SS [31]. Antimicrobial peptides and copper peptides contribute to their bioactive properties. The exact composition varies depending on the snail species, environmental conditions, and extraction methods used. The major components of SS, along with their concentrations and detection techniques, are listed in Table 2.

Growing scientific interest in the chemical composition of SS reflects its expanding applications in pharmaceutical, cosmetic, and biomedical domains. Numerous analytical investigations have identified a wide array of bioactive molecules in the slime of *Helix aspersa*. Notably, antimicrobial and antifungal peptides such as achacin and the helix amide mytimacin-AF have been isolated and characterized in *Achatina fulica* [32, 33]. SS is also a natural source of antioxidant compounds, including polyphenols and flavonoids, further highlighting its biological significance [28].

Recent advancements in analytical methodologies have considerably deepened the understanding of SS's chemical complexity. Vassilev *et al*. [34] employed mass spectrometry (MS) and nuclear magnetic resonance (NMR) spectroscopy to characterize over 20 metabolites in *Helix aspersa* slime, shedding light on its multifunctional bioactivity. Similarly, gas chromatography–mass spectrometry (GC–MS) analyses identified nine major volatile compounds in the mucus of *Monacha obstructa*, *Theba pisana*, and *Eobania vermiculata*, with hexamethylcyclotrisiloxane (molecular weight 222.06) and methoxy phenyl oxime (151.06) reported as dominant constituents [35]. Elemental analyses using inductively coupled plasma atomic emission spectroscopy (ICP-AES) and flame atomic absorption spectroscopy (FAAS) further revealed that *A. fulica* slime contains appreciable concentrations of trace minerals such as Ca, Mg, Fe, Zn, Cu, and Co [31, 36].

Table 2: Composition of SS, including the source species and analytical techniques used to measure the specific compound.

Component	Concentration	Species	Analytical Technique	References
Water	90-99.7%	Various species	Gravimetric analysis	[31, 37]
Proteins	5-9% of dry weight	*Helix aspersa*	Bradford assay, SDS-PAGE, and LC-MS/MS	[18, 31, 38]
Glycosaminoglycans	3-5% of dry weight	*Helix aspersa*	^{1}H and ^{13}C NMR	[31, 38]
Hyaluronic acid	<1 mg/g	*Helix aspersa*	ELISA	[39]
Glycolic acid	Up to 4%	*Helix aspersa*	HPLC	[38, 40]
Allantoin	0.3-0.5%	*Helix aspersa*	HPLC	[40, 41]
Collagen	85 mg/L	*Cornu aspersum*	Fastin-Elastin Assay	[42-44]
Elastin	0.099 g/100 g	*Cornu aspersum*	Fastin-Elastin Assay	[42, 44]
Glycoprotein	Present	*Achatina fulica*	DEAE-Toyopearl 650 M ion exchange chromatography	[45]
Copper peptides	Present	*Helix aspersa*	ICP-MS	[42, 46]
Antimicrobial peptides	Present	Various species	Radial diffusion assay	[47]
Mineral salts (Ca, Mg, Zn, Cu, Fe)	Trace amounts	Various species	ICP-OES	[46, 48]
Vitamins A, C, E	Trace amounts	Various species	HPLC	[27, 38]
Mucopolysaccharide	1.3-1.6% of	*Helix aspersa*	Carbazole assay	[15]

s	dry weight			
Proteoglycans	Present	Various species	Western blot	[15]
Amino acids profile	Varied	*Helix aspersa*	HPLC-MS/MS	[49]
Fatty acids profile	Varied	*Cryptomphalus aspersa*	GC-MS	[23]
Molecular weight distribution	10-1000 kDa	*Helix aspersa*	SEC-MALS	[25]
Secondary structure of proteins	α-helix, β-sheet, random coil	*Helix aspersa*	CD spectroscopy	[36]
Functional groups	-OH, -COOH, -NH2	Various species	FTIR spectroscopy	[50]
Mucin glycosylation	Complex N- and O-linked glycans	*Achatina fulica*	Lectin microarray	[51]

1.3 Applications of SS

SS has been extensively used for treating inflammation, burns, and other skin disorders since ancient times. Its traditional therapeutic applications have triggered researchers to make contributions to advance and explore the beneficial effects of this unique secretion. As the popularity of snail mucin in health and beauty products continues to grow, so does the need for more comprehensive research. The scientific community is still working to fully understand its mechanisms of action and long-term effects on skin health.

Based on the use of SS in cosmetic products, future studies aim to explore its use in health and medical applications with a more specific and targeted approach. The wide applications of SS in cosmetics and its continuous use in health-related applications have led researchers to focus on SS's emerging applications and future prospects while achieving sustainability (Figure 2).

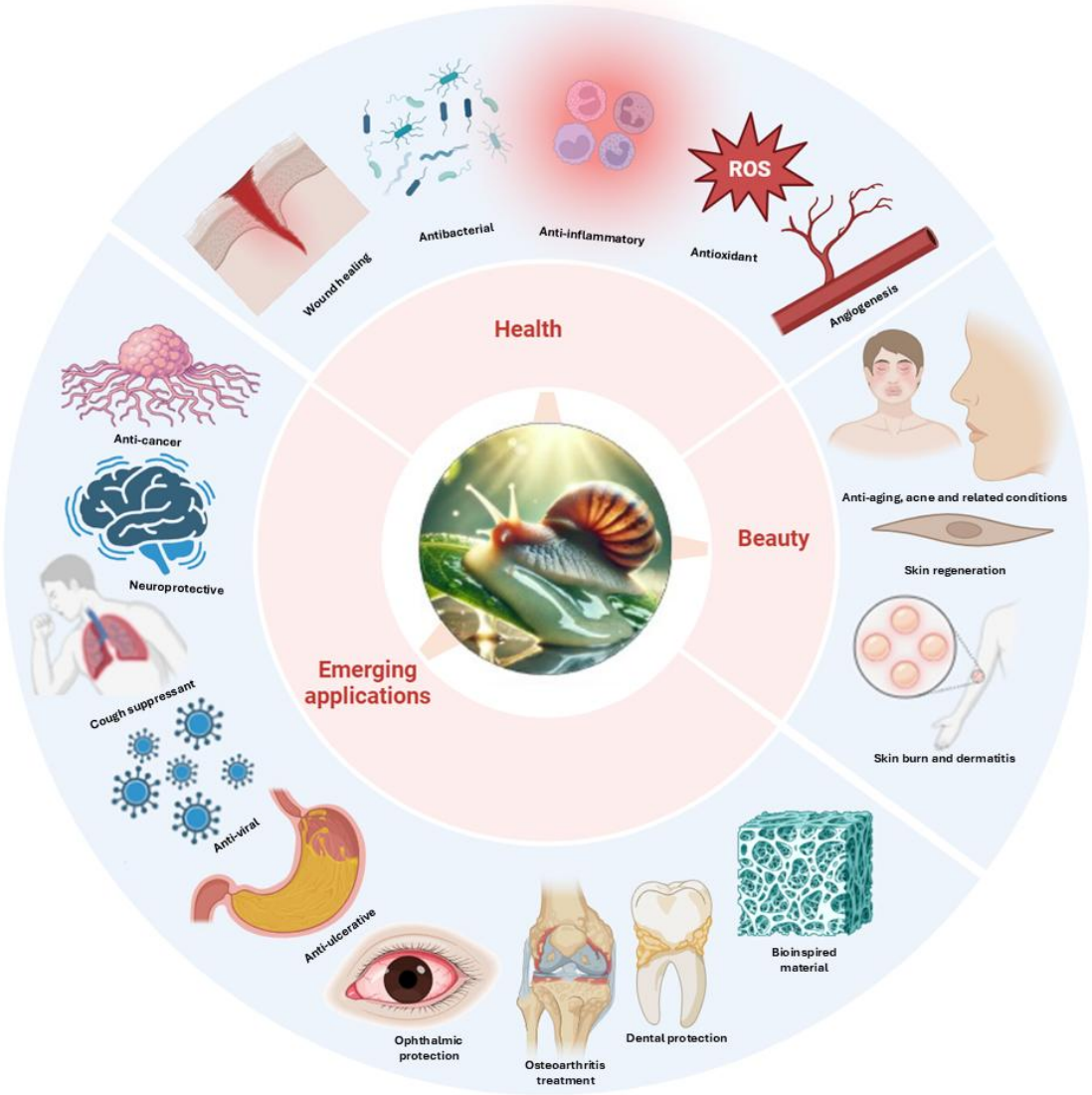


Figure 2: An overview of the SS applications in different fields.

1.3.1 Wound Healing

SS has demonstrated significant potential in wound healing and closure, primarily due to its unique composition of bioactive compounds. The mucus contains several key components that contribute to its wound-healing properties. Allantoin, present at 0.3-0.5% in *Helix aspersa* slime, promotes cell proliferation and accelerates wound healing. Tsoutsos *et al.* found that *Helix aspersa* extract significantly improved healing in partial-thickness burns compared to standard treatments of moist exposure burn ointment, an oil-based herbal paste, purported to be efficacious in managing burn wounds and more commonly used in Asia and the Middle East [28]. GAGs, comprising 3-5% of the slime's dry weight, play a crucial role in maintaining skin hydration and supporting the

extracellular matrix, both essential for optimal wound healing; HA, a specific GAG found in SS, contributes to this process.

The presence of antimicrobial peptides, as reported by Pitt *et al.* helps prevent wound infection, further supporting the healing process [47]. Additionally, collagen and elastin in the slime provide a scaffold for new tissue growth and contribute to the strength and elasticity of healed skin. Deng T. *et al.* demonstrated that a hydrogel containing 10% snail mucin accelerated wound closure in a rat model by 23% compared to standard treatment [52]. This effect is likely due to the synergistic action of the slime's components.

The viscous nature of SS also aids in forming a protective barrier over the wound, maintaining a moist environment conducive to faster healing and reduced scar formation. Furthermore, research by Ellijimi *et al.* showed that SS extract increased the production of growth factors such as Transforming Growth Factor-beta 1 (TGF-β1), Fibroblast Growth Factor-2 (FGF-2) and Interleukin-6 (IL-6), crucial for wound healing in human fibroblasts [24]. Wound healing and closure properties of SS are attributed to its unique combination of allantoin, GAGs, antimicrobial peptides, and structural proteins, which collectively promote cell proliferation, tissue regeneration, and wound protection. The components present in SS and their role in wound healing are listed in Table 3.

Table 3: Wound healing properties of various components present in SS.

Component	Property	Reference
Allantoin	Promotes cell proliferation and wound healing	[28]
Glycolic Acid	Enhance skin cell turnover	[23]
Glycosaminoglycans	Maintains skin hydration	[38]
Hyaluronic Acid	Contributes to extracellular matrix	[25]
Collagen	Provides scaffold for new tissue	[53]
Elastin	Contributes to skin elasticity	[53]
Antimicrobial Peptides	Prevents wound infection	[47]
Proteoglycans	Modulates inflammatory response	[15]

1.3.2 Treating Skin Conditions

SS has shown promising potential in treating various skin conditions, particularly in burns, diabetic wounds, and dermatitis treatment. Its unique composition of bioactive compounds contributes to its therapeutic effects beyond cosmetic applications.

In burn treatment, SS has demonstrated significant efficacy. A study by Tsoutsos *et al.* examined the use of *Helix aspersa* Müller extract in treating partial-thickness burns [28]. The researchers found that the snail mucus extract significantly accelerated healing compared to standard treatments. The allantoin content present in the slime is believed to be a key factor in promoting cell proliferation and wound healing in burn cases. For general skin conditions, SS has shown remarkable properties; this effect is attributed to the synergistic action of various components in the slime, including GAGs and HA, which maintain skin hydration and support the extracellular matrix.

SS has also shown potential in treating diabetic wounds, a condition often resistant to standard treatments. The antimicrobial properties of the slime, as demonstrated by Pitt *et al.* help to prevent infection in these vulnerable wounds [47]. Additionally, the presence of collagen and elastin in the slime provides a scaffold for new tissue growth, which is particularly beneficial in chronic wounds associated with diabetes.

In cases of radiation dermatitis, a side effect of radiation therapy in cancer treatment, SS has shown promising effects. The anti-inflammatory and hydrating properties of snail mucin suggest potential benefits in soothing and healing irradiated skin. Sarkar *et al.* confirmed the snail mucus's effects on the regulation of inflammation to control atopic dermatitis, an allergic skin disease that affects many. The results demonstrated the capacity of *Helix aspersa* mucus filtrate to counteract the production of proinflammatory cytokines produced in canine epidermal keratinocytes, suggesting natural and safe treatment strategies for dermatitis and related skin diseases [54]. For eczema and psoriasis, the moisturizing and anti-inflammatory properties of SS offer potential benefits. The high concentration of GAGs and HA in the slime can help maintain skin hydration, while its reported ability to modulate inflammatory responses may help in managing these chronic skin conditions. Snail mucin from *Cryptomphalus aspersa* enhances the growth and migration of keratinocytes and fibroblasts, which are key cell populations for skin repair. This effect increases with higher doses and over time. Additionally, the mucin

boosts the production of important adhesion proteins like β1-integrin, β-catenin, E-cadherin, and vinculin, indicating its potential role in promoting scar healing [45].

It's important to note that while these applications show promise, many are still in the research phase. The use of SS in treating skin conditions requires further clinical studies to establish standardized treatments and ensure safety and efficacy across different patient populations. As research progresses, SS may emerge as a valuable natural resource in dermatological treatments, offering alternatives or complementary approaches to conventional therapies for various skin conditions.

1.3.3 Antimicrobial Properties

Studies conducted over the past two decades have shown that various snail species produce mucus with antibacterial properties. For instance, *Achatina fulica* (giant African land snail) mucus has exhibited inhibitory effects against *Staphylococcus aureus, Escherichia coli,* and *Pseudomonas aeruginosa*. The mucus from *Helix aspersa* has also shown promise, particularly against *Staphylococcus epidermidis* and *Propionibacterium acne*, making it potentially useful in treating skin infections and acne. The antibacterial activity of snail mucus is attributed to several components, including antimicrobial peptides such as myticin, defensin, and cecropin-like peptides, lysozyme such as muramidase and glycoconjugates. These compounds work through various mechanisms, such as disrupting bacterial cell membranes, inhibiting bacterial growth, and interfering with bacterial communication systems.

Research has demonstrated that the effectiveness of snail mucus varies depending on the snail species, bacterial strain, and concentration of the mucus extract. Notably, some studies have shown that snail mucus can be effective against antibiotic-resistant bacteria, including *methicillin-resistant Staphylococcus aureus.* Some peptides like mytimacin-AF isolated from *Achatina fulica*, and seventeen other peptides (MW: 3 – 30 kDa) including proline-rich and cysteine-rich peptides isolated from *Cornu aspersum* by Dolashki *et al.* [55] using MALDI-TOF/TOF (Matrix-Assisted Laser Desorption/Ionization equipped with dual Time-of-Flight detectors) showed promising antibacterial effects against various species of Gram-negative and Gram-positive bacteria. This finding is particularly significant given the growing concern over antibiotic resistance worldwide. A detailed list of SS activities obtained from different snail species on a specific strain of bacteria and mold is listed in Table 4.

While these results are promising, it's important to note that much of the research is still in its early stages. Many studies have been conducted *in vitro*, and more extensive *in vivo* research and clinical trials are needed to fully understand the potential of snail mucus as an antibacterial agent in practical applications. Additionally, standardization of extraction methods and quality control measures will be crucial for the development of snail mucus-based antibacterial products in the future.

Table 4: Anti-bacterial/mold activities of SS obtained from different species on particular strains with an experimental minimum inhibitory concentration (MIC).

Snail Species	Bacteria/Mold	Strain	MIC	Reference
Achatina fulica	*Staphylococcus aureus*	ATCC 9080	9.3 mm	[56, 57]
	Staphylococcus spp		15.4±2.04 mm	[53, 58]
	Streptococcus epidermidis	ATCC 19606	10.29 mm	[23, 56]
	Streptococcus spp		17.5±2.72 mm	[15, 58]
	Pseudomonas spp		17.1±1.30 mm	[3, 59]
	Escherichia coli	PBR 322	21 mm	[46, 55, 60]
	Vibrio cholerae		16 mm	[3, 61]
Archachatina marginata	*Escherichia coli*		0.098 µg/ml	[62, 63]
	Salmonella spp		0.049 µg/ml	[3, 24]
	Staphylococcus aureus		50 µg/ml	[3, 64, 65]
	Pseudomonas spp		50 µg/ml	[3, 47]
	Escherichia coli		0.050 µg/ml	[62, 66]
	Salmonella spp		0.098 µg/ml	[3, 67]
	Staphylococcus aureus		100 µg/ml	[3, 68]
	Pseudomonas spp		100 µg/ml	[3, 61]
	Staphylococcus spp		17.4±1.20 mm	[58, 69]
	Pseudomonas spp		19.2±1.10 mm	[3, 70]
	Streptococcus spp		18.6±2.14 mm	[3, 71]
	Staphylococcus spp		15.6±1.44 mm	[58, 71]
	Pseudomonas spp		19.8±0.88 mm	[58]
	Streptococcus spp		19.3±1.90 mm	[3]
Helix aspersa	*Staphylococcus aureus*	ATCC 25923	>50 µg/µl	

	Streptococcus pyogenes	NCIMB 13285	5.5 mm	[61]
	Escherichia coli	ATCC 25922	25 µg/µl	[47]
	Klebsiella pneumoniae	NCTC 11228	0 mm	[61]
	Pseudomonas aeruginosa	NCTC 8626	11.12±2.57 mm	[47]
		NCTC 10548	11.63±1.52 mm	[3]
		ATCC BAA-47	25 µg/µl	[3]
	Candida albicans	ATCC 10231	>50 µg/µl	[61]
	Enterococcus faecalis	WDCM 00087	23.42 ± 0.68 mm	[72]
	Staphylococcus epidermidis	WDCM 00036	24.79 ± 0.21 mm	
	Staphylococcus aureus	WDCM 00034	25.04 ± 0.50	
	Methicillin-resistant Staphylococcus aureus	BAA1708	19.58 ± 0.37 mm	
	Streptococcus pyogenes	ATCC 19615	23.85 ± 0.18 mm	
	Bacillus subtilis	WDCM 00003	22.05 ± 0.28 mm	
	Bacillus cereus	WDCM 00001	19.88 ± 0.20 mm	
	Clostridium perfringens	WDCM 00,007	21.35 ± 0.33 mm	
	Pseudomonas aeruginosa	WDCM 00025	20.31 ± 0.53 mm	
	Enterobacter cloacae	WDCM 00,083	18.60 ± 0.96 mm	
	Escherichia coli	WDCM 00,013	19.85 ± 0.20 mm	
	Klebsiella pneumoniae	WDCM 00,097	18.57 ± 0.37 mm	
	Proteus mirabilis	WDCM 00,023	19.36 ± 0.29 mm	
	Pseudomonas aeruginosa	PA-9	15 µg/µl	[73]
	Escherichia coli	EC-3	20 µg/µl	
	Staphylococcus aureus	SA-17	15 µg/µl	
	Aspergillus niger	AN-05	32 µg/µl	
	R. stolonifera	RS	25 µg/µl	
	Trichoderma harzianum	TH	25 µg/µl	
	Candida albicans	CA-11	20 µg/µl	
Eremina	*Pseudomonas*	PA-9	7 µg/µl	

desertorum	*aeruginosa*			
	Escherichia coli	EC-3	5 µg/µl	
	Staphylococcus aureus	SA-17	5 µg/µl	
	Aspergillus niger	AN-05	7 µg/µl	
	R. stolonifera	RS	10 µg/µl	
	Trichoderma harzianum	TH	10 µg/µl	
	Candida albicans	CA-11	12 µg/µl	

1.3.4 Beauty and Cosmetic Uses

SS has gained significant attention in the beauty and cosmetics industry due to its potential anti-aging, moisturizing, and skin-regenerating properties. The unique composition of snail mucin, rich in bioactive compounds, has led to its incorporation in various skincare products. Some of the major uses of SS in cosmetics or beauty are explained below.

1.3.4.1 Anti-aging Properties

One of the primary cosmetic uses of SS is in anti-aging products. The mucin contains glycoproteins, proteoglycans, and GAGs which are known to promote collagen and elastin production. Glycoproteins and peptides present in SS promote proliferation of fibroblasts and production of collagen and elastin which decrease with time in elderly people thus inhibiting the aging signs [45]. The antioxidants present in SS also contribute to detoxing the oxidation process thus promoting skin's fineness and texture. A study by Fabi *et al.* demonstrated that a topical gel containing purified snail secretion improved the appearance of fine lines and wrinkles after 12 weeks of use [74]. The presence of allantoin and GA in snail mucin contributes to its skin-renewing properties, potentially reducing the visible signs of aging [28]. Vitamins A, E, and C present in SS have caring properties.

In the case of photoaging, compelling evidence exists for the protective effects of snail mucin against UV-induced photoaging. *Achatina fulica* mucus has been demonstrated to ameliorate UVB-induced fibroblast photoaging through modulation of the TGF-β/Smad signaling pathway, a crucial pathway involved in collagen production [75]. Specifically,

the mucus upregulates TGF-β and Smad3 expressions while downregulating Smad7, thereby promoting pro-collagenogenic responses in UVB-irradiated skin cells.

Oral administration studies provide additional support, showing that edible snail extract powder significantly prevents UVB-induced skin damage through multiple mechanisms [76]. These included restored expression of hyaluronic acid synthases (necessary for skin hydration), suppression of matrix metalloproteinase-1 (MMP-1), and upregulation of antioxidant enzyme superoxide dismutase (SOD). The protective effects translated to reduced wrinkle formation and improved skin barrier function in UVB-exposed animal models.

1.3.4.2 Moisturizing Effects

Snail mucin is highly valued for its moisturizing properties. The high concentration of HA in SS, as reported by Gubitosa *et al.*, helps to maintain skin hydration by attracting and retaining moisture [25]. HA has the property to hold water 1000 times its molecular weight, thus this natural moisturizer can help improve skin texture and reduce the appearance of dry, flaky skin. GAGs present in the SS support skin moisture retention and improve skin hydration [76]. These components work to maintain the stratum corneum integrity while increasing trans-epidermal hydration, thereby reducing water loss and supporting the appearance of plump, youthful skin. Studies examining snail mucus preparations have documented increased skin hydration, reduced trans-epidermal water loss, and improved skin thickness in both topical and oral application models. The regenerative properties of the mucus, including stimulation of natural regenerative processes and cellular proliferation, further support barrier recovery and long-term skin rejuvenation [77].

The effect of SS on skin elasticity was evaluated using the Cutometer dualMPA580 on 27 volunteer women for 15 days, and post-treatment skin pliability/firmness, skin ability to recover its original structure, net elasticity, and skin ability to return to its original position after deformation were evaluated, showing positive results. This suggests that SS can improve skin elasticity, making it suitable for dermatological applications. *In vitro* experiments on keratinocytes revealed that SS promotes cellular well-being, which is essential for maintaining healthy and hydrated skin [78].

1.3.4.3 Skin Regeneration and Repair

The regenerative properties of snail mucin make it a popular ingredient in products aimed at improving skin texture and reducing scarring. Brieva *et al.* found that snail secretion filtrate stimulated the proliferation of fibroblasts and the production of extracellular matrix components, suggesting potential benefits for skin regeneration [23]. SS stimulates the proliferation and migration of fibroblasts and keratinocytes, essential for tissue repair and regeneration. It also enhances the expression of genes like TGF-β1 and VEGF, which are critical for wound healing. SS has exhibited a significant role in stimulating the skin's innate regenerative mechanisms, potentially via its impact on the immune response and make the wound healing process smoother by preventing the formation of thick scar tissue known as keloids, improving the cosmetic appearance of the skin [73]. Beyond direct collagen and elastin production, SS demonstrates positive modulation of angiogenesis and increased *Angiopoietin-1* gene expression has been observed following SS treatment, indicating enhanced vascular support for skin tissue. Improved blood supply to the dermis facilitates nutrient delivery and waste removal, supporting overall skin health and reducing the appearance of aging-related skin changes, ultimately giving better and good looking skin [76].

1.3.4.4 Antioxidant Properties

Snail mucin contains antioxidants that can help protect the skin from free radical damage. These include vitamins A, C and E, as well as antioxidants (*e.g.,* polyphenols) and enzymes (SOD and glutathione S-transferase - GST) [39]. A study by Mubarak *et al.* confirms the antioxidant properties of snail mucus extract by 2,2-Diphenyl-1-picrylhydrazyl (DPPH) assay, and the content of catalase, GST, SOD, and reduced glutathione was also assessed, suggesting SS's potential in protecting skin cells from oxidative stress [79]. SS has been used to synthesize chitosan and gold-based nanoparticles, which exhibit significant antioxidant activity. This was demonstrated through DPPH and ABTS (2,2'-azino-bis(3-ethylbenzothiazoline-6-sulfonic acid)) assays, indicating their potential use in cosmetics as multifunctional ingredients [80].

1.3.4.5 Anti-inflammatory Activities

SS has been shown to possess anti-inflammatory properties. Research indicates it can help reduce inflammation and promote healing [27]. Specifically, the mucus derived from

snails like *Helix aspersa* and *Achatina fulica* contains GAGs, proteoglycans, mucopolysaccharides, carotenoids and phenolic contents having anti-inflammatory and antioxidant properties that may alleviate conditions such as colon inflammation and enhance overall wound healing [81]. Ricci *et al.* evidenced that SS reduces the inflammatory events by downregulating the cyclooxygenase-2 (COX-2) gene expression in human gingival fibroblasts exposed to an inflammatory stimulus represented by hydrogen peroxide [11] (Figure 3). SS-based gold nanoparticles significantly reduced LPS-induced interleukins (IL) levels, such as IL1-β and IL-6, in murine macrophages, and completely abrogated the synthesis of inducible Nitric Oxide Synthase [11, 25]. The mucin fraction of *Eremina desertorum* showed antioxidant and anti-inflammatory effects in experimentally induced intestinal inflammation and testicular damage in mice [82]. SS significantly modulated the expression of inflammatory mediators in canine progenitor epidermal keratinocytes, showing a protective effect on cell viability when stimulated with LPS [83]. SS from *Helix aspersa* and *Eremina desertorum* exhibited anti-inflammatory activities *in vitro*, including membrane stabilization of human red blood cells, albumin denaturation, and proteinase inhibitory activity [73].

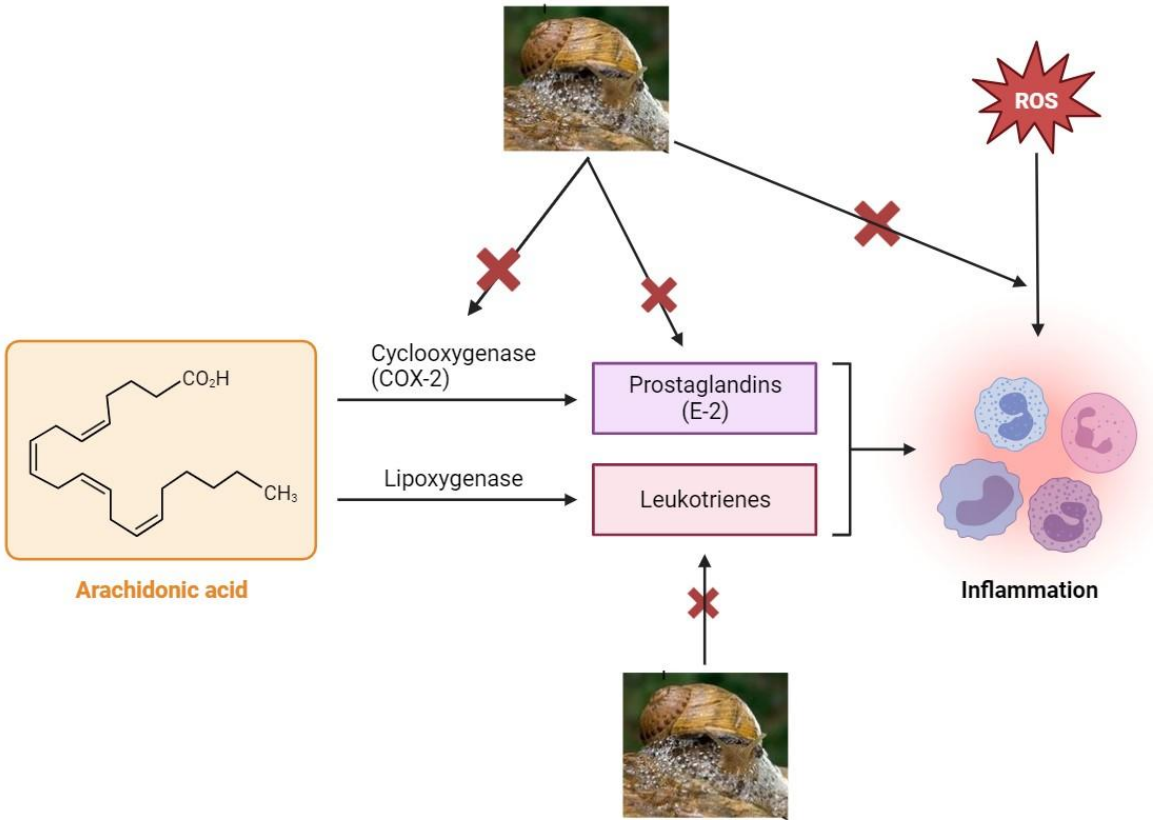


Figure 3: A proposed SS mechanism of action to counteract inflammation.

1.3.4.6 Acne Treatment

SS has also been investigated for its potential in treating acne and acne scars. The GA content helps in gently exfoliating the skin, which unclogs pores filled with oil and dead skin cells and promotes skin cell turnover, which potentially reduces the appearance of acne scars [11]. The role of GA is further enhanced by the antimicrobial properties of SS, as reported by Pitt *et al.*, may help in managing acne-causing bacteria [47]. Three promising peptides from mucus of *Achatina fulica* that could have antimicrobial, anti-biofilm, cytotoxic, and cell-penetrating properties were selected, modified with lectins to enhance their desired activities and then tested against *Propionibacterium acnes* isolates. The modified peptides showed strong antimicrobial activity against several strains, suggesting their potential for acne treatment and other medical uses [84]. In fact, a pilot study demonstrated that a facial cream containing the probiotic strain *Weissella viridescens* UCO-SMC3, derived from *Helix aspersa* mucus, effectively reduced acne lesions in volunteers. This suggests that SS-based products can be effective in clinical settings for acne treatment [85].

1.3.4.7 Skin Brightening

Some cosmetic products claim that snail mucin can help in evening out skin tone and reduce hyperpigmentation. This effect is often attributed to the presence of GA, which is known for its gentle exfoliating properties and brightens skin by acting as a chemical exfoliant, dissolving dead skin cells to reveal a brighter, smoother complexion underneath [28]. It promotes cell turnover and renewal, which fades dark spots and improves skin tone and texture. Additionally, it stimulates collagen production, helping to firm the skin and reduce the appearance of fine lines [28]. This effect is further supported by the skin regenerative properties of SS.

1.3.5 Emerging Applications

SS, beyond its applications in wound healing, burn treatment, and cosmetics, has shown potential in various other health-related fields. These applications, even if some are still in the early research stages, demonstrate the versatility of this unique biological substance [86, 87].

1.3.5.1 Cough Suppressant

SS moisturizes and lubricates the mucous membranes of the respiratory tract and promotes the regeneration of the epithelium. Some studies suggest that preparations derived from snails can decrease morbid activities in pulmonary inflammation, potentially alleviating cough related to these conditions. Due to its emollient and antibacterial properties, SS is considered as an attractive remedy for whooping cough and chronic bronchitis such as tuberculosis [88]. While snail mucus possesses multiple properties theoretically relevant to cough suppression, including anti-inflammatory activity, epithelial protection, and compositional similarity to airway mucus, only a few scientific studies currently support its use as a cough suppressant. The gap between traditional use and scientific validation represents an important opportunity for future investigation. Rigorous clinical and preclinical research is essential to determine whether the well-documented anti-inflammatory and tissue-protective properties of snail secretions translate into measurable antitussive efficacy and to establish appropriate dosing and formulation for respiratory applications.

1.3.5.2 Antiviral Activities

Recent research has explored the antiviral properties of snail mucus. Hemocyanins isolated from the mucus of *Rapana venosa* showed antiviral activity against *herpes simplex virus type 1* (HSV-1) and *human immunodeficiency virus type 1* (HIV-1) [89]. Furthermore, Cilia and Fratini (2018) confirmed that slime obtained from *Phyllocaulis boraceiensis* is effective against the single-stranded Measles virus, and this property is probably due to the presence of polyunsaturated fatty acids, specifically hydroxy-tritriacontapentaenoic acid and hydroxy-pentatriacontapentaenoic acid [42]. Toledo-Piza *et al.* tested the antiviral activity of the mucus of the land slug *P. boraceiensis* was demonstrated *in vitro* using Vero cells infected with measles virus. The crude sample and four fractions were tested in cultures infected with measles virus and the antiviral activity was assessed by the cytopathic effect in infected cell cultures as well as by immunofluorescence and qPCR. Two fractions of the mucus from *P. boraceiensis* were analyzed by HPLC-DAD-ESI-MS/MS and infrared spectroscopy. A mixture of polyunsaturated fatty acids was found in the two fractions. A reduction in the growth of the measles virus was observed, measured by qPCR, with a protection index of 80% in Vero cells infected with measles and treated with fraction 39. Fraction 39 exhibited the

best antiviral action *in vitro* and high contents of hydroxy-tritriacontapentaenoic acid and hydroxy-pentatriacontapentaenoic acid were found in this fraction. This finding opens up possibilities for SS components in antiviral therapy development.

1.3.5.3 Antifungal Activities

Several studies have also reported the antifungal effects of snail mucus therapy. One possible mechanism through which snail mucus exerts its antifungal activity is through the presence of lectins and peptides [54]. These bioactive molecules disrupt fungal cell membranes, inhibit fungal growth, and interfere with crucial metabolic processes, suppressing fungal proliferation. Additionally, snail mucin's high glycoprotein content may contribute to its antifungal effects by enhancing the host's immune response against invading fungal pathogens. Studies have demonstrated the efficacy of snail mucin extracts against fungal pathogens, including *Candida albicans, Aspergillus fumigatus, Penicillium chrysogenum,* and *Mucor racemosus* [54].

1.3.5.4 Dental Applications

The potential use of snail mucin in dental care is an emerging area of interest. A study by Kanthi *et al.* investigated the effects of snail mucin on dental remineralization. They found that snail mucin enhanced the remineralization of enamel, suggesting its potential use in preventing dental caries [90-92]. SS has been shown to decrease the number of osteoclasts in rats with periodontitis when administered both orally and topically. This suggests its potential in reducing bone resorption associated with periodontal disease [93]. Kantawong *et al.* also confirm the changes in gene expressions related to mineralization when snail mucus was applied to human dental pulp cells (hDPCs) *in vitro,* and a decreasing NF-κB expression level revealed its negative role in odontoblastic differentiation of DPCs. However, the expression of some inflammatory genes should be a concern, because the proinflammatory cytokines (IL-1β and IL-6) and the inflammatory mediator COX-2 play dual roles in bone differentiation and mineralization. The effect of snail mucus on the inflammation of DPCs needs further investigation [90].

1.3.5.5 Osteoarthritis Treatment

The GAGs present in snail mucin, particularly chondroitin sulfate, have been studied for their potential in treating osteoarthritis. While most research has focused on marine snails, the principles could potentially apply to terrestrial snail mucin as well. A review by Zhu

et al. highlighted the potential of marine snail-derived compounds in managing osteoarthritis [94]. *Achatina fulica* snail mucin gel has been evaluated for enhancing osteoblast viability in periodontitis models, demonstrating statistically significant increases in osteoblast populations compared to control groups [95]. The mucin's glycosaminoglycan content provides building blocks and signaling cues that support bone cell differentiation and bone matrix production. In veterinary medicine, snail mucin has been investigated for managing osteoarthritis progression. Intramuscular injection of snail mucin produced plasma MMP-3 reductions comparable to glucosamine supplementation, suggesting utility in slowing cartilage degradation in degenerative joint diseases [94]. These findings suggest potential applications in human orthopaedic conditions, though clinical translation remains preliminary.

1.3.5.6 Neuroprotective Effects

Some components of SS have shown neuroprotective properties. A study by Guo *et al.* found that a peptide derived from *Achatina fulica* mucus exhibited neuroprotective effects in a cellular model of Parkinson's disease [27]. This suggests potential applications in developing treatments for neurodegenerative disorders by acting as an antioxidant against various reactive oxygen species and elevating the level of first-line enzymatic antioxidants *i.e.,* SOD, catalase, reductase, and glutathione peroxidase, essential for neuroprotective effects [96-100]. Walker *et al*. investigated the microRNA from *L. stagnalis*, a freshwater snail used extensively in neurological research [54]. They found that the snail species has benefits in improving long-term memory and can potentially manage neurodegenerative diseases like Alzheimer's and dementia. While promising results have been found in cell and animal studies, most research into the neuroprotective properties of snail mucus is still in its early stages. Further rigorous clinical trials in humans are required to fully establish its efficacy and safety for treating neurodegenerative diseases.

1.3.5.7 Gastrointestinal Health

The mucoadhesive properties of snail mucin have been explored for potential applications in gastrointestinal health. Adikwu and Nnamani (2005) investigated the use of snail mucin as a bioadhesive polymer for drug delivery in the gastrointestinal tract, potentially improving the efficacy of orally administered medications [27, 53]. SS forms an adhesive and protective layer on the internal lining of the gastrointestinal tract and thus prevents

the ulcerative effects of acid-base digestive enzymes. SS also contains copper, which is proven to have anti-ulcerative properties [44].

1.3.5.8 Cancer Research

While still in the very early stages, some studies have investigated the potential anticancer properties of snail mucus components. Matusiewicz *et al.* reported that lectins isolated from the mucus of *Helix aspersa* showed antiproliferative effects on *in vitro* human colon cancer cells (Caco-2) [101]. Chien *et al.* reported that snail mucus enhances chemosensitivity of triple-negative breast cancer via activation of the Fas pathway [102]. Likewise, Bo-Rong and Wei-Chien (2023) reported that snail mucus increased the anti-cancer activity of anti-PD-L1 antibody in melanoma [103]. Rashad *et al.* stated that *Helix aspersa* slime inhibits the growth of IGR-39 and SK-MEL-28 melanoma cells by increasing expression of the cytokine Tumor Necrosis Factor (TNF-α), and inhibits the transcription process by blocking NF-κB-activated B cells, which, in proper regulation, has been linked to cancer progression [27]. Research conducted on the impact of *Helix aspersa* mucus on melanoma cell lines has revealed compelling results. Studies have shown that snail mucus may significantly reduce the growth of cancerous cells and prevent melanoma cell metastasis. Some studies indicate that the reduction in cell viability can be attributed to an apoptotic mechanism linked to the cleavage of Poly (ADP-ribose) polymerase (PARP). El Ouar *et al*. showed that *Helix aspersa* mucus may inhibit the growth of two human melanoma cell lines and induce necrosis in tumor cells, specifically the breast cancer cell line Hs578T [104]. This inhibition is attributed to an increase in the expression of the cytokine TNFα and the suppression of NF-κB, a transcriptional process closely associated with cancer progression [54]. However, much more research is needed to understand the implications and potential applications in cancer treatment.

1.3.5.9 Tissue Engineering and Optimized Drug Delivery

The complex composition of snail mucin has attracted interest in the field of tissue engineering. Gubitosa *et al.* suggested that snail mucus could potentially be used as a bioactive scaffold in tissue engineering applications [25]. Furthermore, the gel-like nature and interlinking properties make SS an attractive biomaterial candidate for targeted and/or sustained drug delivery with an impactful, beneficial effect on gastric mucosa, offering superb gastrointestinal protection. The glycoprotein and GAG components

provide both structural and biological cues supporting cell adhesion, migration, and differentiation. These properties position snail-derived biomaterials as candidates for engineering three-dimensional tissue constructs for regenerative medicine applications. Emerging research explores snail mucin's potential in engineered skin tissue platforms, dental regeneration, and bone tissue scaffolds. The ability to provide cell-instructive signals while supporting vascularization and tissue organization makes snail mucus-derived biomaterials attractive alternatives to synthetic polymers for biomedical applications where biological compatibility and regenerative capacity are prioritized.

1.3.5.10 Biochemical Marker and Diagnostic Applications

As research characterizes the full complement of bioactive molecules in snail mucus, emerging applications in diagnostics and biomarker detection are being explored. Lectins and other recognition proteins present in snail secretions demonstrate specificity for particular carbohydrate structures and cellular markers [105]. This property could support the development of diagnostic assays for detecting abnormal cells or disease-associated biomarkers.

The ability of snail-derived compounds to modulate immune responses and support tissue repair may also position certain mucus components as candidates for therapeutic monitoring, where changes in biomarker profiles could assess tissue response to snail-derived treatments or predict clinical outcomes.

1.3.5.11 Ophthalmic Applications

The lubricating and healing properties of snail mucin have led to investigations into its potential use in ophthalmic treatments. While research is limited, there is interest in exploring snail mucin as a component in eye drops for dry eye syndrome or in promoting corneal wound healing [43].

In conclusion, while many of these applications are still in the early research stages, they highlight the diverse potential of SS in various health-related fields. From antimicrobial and antiviral applications to potential uses in dental care, osteoarthritis treatment, and even neurological and cancer research, snail mucin continues to intrigue researchers with its unique properties. As research progresses, it's crucial to maintain ethical considerations in snail farming and mucin extraction practices while exploring these potential health benefits.

AIM OF THE PhD PROJECT

The main aim of my PhD project has been to extract, characterize, and biologically evaluate SS obtained through the Cherasco Muller method, a cruelty-free extraction process preserving the integrity and natural bioactivity of the mucus along with the animal life. This thesis is designed to provide a comprehensive understanding of the chemical composition, functional properties, and cellular effects of *Helix aspersa* slime through a multidisciplinary analytical and biological approach.

Specifically, the objectives of the research are to:

1. Chemically characterize the SS obtained by the Cherasco method, ensuring the preservation of its natural composition. Advanced analytical techniques, including FTIR, NMR, HS-SPME/GC–MS, thermal analysis, and Raman spectroscopy, were employed to identify and quantify the principal bioactive molecules. Compare natural non-stabilized and stabilized SS to assess the effect of preservation and stabilization on the chemical integrity and biological functionality of the slime by different biochemical assays.

2. Investigate the biological properties of SS on *in-vitro* cellular models represented by cell lines of keratinocytes, namely HaCaT; endothelial cells, namely EA.hy926.and primary Normal Human Dermal Fibroblasts (NHDFs). The analysis focused on assessing SS biocompatibility, cytoprotective potential, anti-inflammatory response, and pro-regenerative activity, as well as its ability to promote angiogenesis and wound repair mechanisms. The biological effects of SS were also compared to GA, one of its key bioactive components.

3. Elucidate the molecular mechanisms underlying SS bioactivity through Liquid Chromatography equipped with Mass Spectrometer (LC-MS) based proteomic profiling of SS-treated NHDFs and to discover the proteins involved in the highly influenced biological functions by the SS treatment with the help of Gene Ontology (GO), string analysis, and cytohubba. Those selected biological functions were further validated using different non-proteomics methodologies.

2 MATERIALS AND METHODS

2.1 Extraction of SS

Helix aspersa's slime was extracted using the cruelty-free Cherasco Muller method at Lumacheria Italiana srl (Cherasco, Italy), as already described [11, 27, 106, 107]. Live healthy snails, aged 12–15 months, were pre-washed in running water at room temperature in order to remove the dust and debris as well as awaken the animal. Washed snails were then transferred to the Muller extractor, where they first received an antimicrobial treatment with ozonated water shower, followed by 10% sodium citrate stimulated slime extraction for 30 min each (Figures 4 and 5). The extracted slime (natural and non-stabilized SS) was collected and filtered through a 0.2 µm filter and mixed with sodium benzoate (0.1%) and potassium sorbate (0.1%) preservatives to be suitable for the market and other industrial processing (commercial and stabilized SS). The final products were stored in the dark at +4 °C to be used within six months.



Figure 4: A flowchart describing the extraction and production of SS using non-lethal Muller method.



Figure 5: Depiction of Muller extraction, a cruelty-free process (figures obtained from Lumacheria Italiana srl.)

2.2 Sampling

Samples of SS (with or without the addition of 0.1% potassium sorbate and sodium benzoate as natural preservatives and 10% sodium citrate as a stimulating solution) were kindly provided by Lumacheria Italiana srl. Cherasco, Italy. For the chemical analysis, samples were freeze-dried with a Buchi Lyovapor L-200 at -55 °C and 0.200 mbar conditions, obtaining a solid residue weight of 21.5 mg and 24.8 mg from 1 mL of slime without (non-stabilized) and with preservatives (stabilized), respectively. For biological and proteomics analysis, stabilized samples without freeze-drying were used.

2.3 Chemical Analysis

2.3.1 Nuclear Magnetic Resonance (NMR) Analysis

Following the drying of a 2 mL sample of SS, the resulting solid residue was dissolved in 700 µL of a 200 mM phosphate buffer prepared with deuterium oxide (D_2O). The solution included 0.3 mM of 3-(Trimethylsilyl)Propionic Acid Sodium Salt (TSP) as an internal standard for metabolite quantification. This prepared solution was transferred into a 5 mm NMR tube, and analysis was performed using a Jeol JNM-ECZ 600R spectrometer (JEOL Ltd., Tokyo, Japan) operating at a proton frequency of 600.17 MHz and equipped with a JEOL 5 mm FG/RO DIGITAL AUTOTUNE probe. The metabolite identification process involved acquiring a series of NMR experiments, including one-dimensional ^{1}H spectra, as well as two-dimensional ^{1}H-^{1}H TOCSY, ^{1}H-^{13}C heteronuclear single quantum correlation (HSQC), and ^{1}H-^{13}C heteronuclear multiple bond correlation (HMBC) spectra. All experiments were conducted under consistent conditions as established in prior methodology [108]. Spectral processing, analysis, and integration of metabolite signals were carried out using JEOL Delta software (version 5.3.1). Each sample was prepared and analyzed in five independent replicates, and quantitative metabolite data were presented as mean value ± SD µg/mL of SS.

2.3.2 Gas Chromatography-Mass Spectrometry (GC-MS) Analysis

Volatile metabolites were examined using a Perkin Elmer Clarus 500 GC coupled to a MS and equipped with a flame ionization detector (FID). Separation was performed on an Agilent VF-1ms capillary column (60 m × 0.32 mm ID, 1.0 µm DF; nonpolar 100%

dimethylpolysiloxane stationary phase). The oven temperature was programmed from 40 to 220 °C at a rate of 6 °C/min, followed by a 15-min hold. Helium served as the carrier gas at a constant flow of 1 mL/min. Electron ionization was conducted at 70 eV, and mass spectra were recorded over the 40–500 m/z range. Compound identification was achieved by matching the obtained spectra with the NIST 11 library and by comparing linear retention indices (LRIs), calculated using n-alkanes (C8–C25), with literature values from the NIST Chemistry WebBook. Relative abundances were determined from FID peak areas, averaged from triplicate runs, without the use of internal standards or correction factors.

2.3.3 Solid-Phase Microextraction (SPME) Sampling

SPME was used to assess the volatile composition of all slime samples. A Supelco SPME device (Bellefonte, PA) fitted with a 1 cm fiber coated with 50/30 µm Divinylbenzene/Carboxen/Polydimethylsiloxane (DVB/CAR/PDMS) was employed. After the system reached equilibrium, the fiber was exposed to the sample headspace at 40 °C for 25 min. The captured analytes were then thermally desorbed in a splitless GC injector set at 250 °C. Gas chromatographic and mass spectrometric conditions were identical to those described in Section 2.3.2, and all the measurements were performed in duplicate.GC-MS Analysis of Derivatized Samples

For compositional analysis of both stabilized and non-stabilized freeze-dried SS, approximately 0.5 mg of each sample was combined with 50 µL of Bis(trimethylsilyl)trifluoroacetamide (BSTFA) and 150 µL of pyridine. The mixture was heated at 70 °C for 30 min to achieve derivatization. Subsequently, 1 µL of the silylated sample was manually injected into the GC in splitless mode at an injector temperature of 270 °C. The oven program started at 70 °C, increased at 6 °C/min to 170 °C (held for 1 min), and then ramped at 8 °C/min to 250 °C (held for 30 min). Mass spectra were acquired using electron ionization, and compound identification was carried out by comparison with the NIST library, considering both spectral similarity and contribution to the total ion chromatogram (TIC). Quantification was performed via electronic integration of GC-FID peak areas, without applying internal standards or response factor corrections. All experiments were conducted in duplicate.

2.3.4 Fourier Transform Infrared-Attenuated Total Reflection Spectroscopy (FTIR-ATR) Analysis

Fourier-transform infrared spectroscopy was performed using a Shimadzu IRAffinity-1S FTIR spectrophotometer (Shimadzu Italia Srl., Milan, Italy), which features a sealed, desiccated interferometer and a Deuterated Triglycine Sulphate doped with L-Alanine (DLATGS) detector. A single-reflection diamond ATR crystal (QATR 10, Shimadzu Italia Srl., Milan, Italy) was used for sample analysis. Spectral data for the lyophilized samples were collected across the 4000–400 cm^{-1} range by averaging 45 interferograms at a resolution of 4 cm^{-1}, with Happ–Genzel apodization applied. Before each measurement, the ATR crystal was meticulously cleaned, and a new background spectrum was recorded. Every sample analysis was conducted in triplicate. The resulting spectra were processed and analyzed using LabSolution IR software (version 2.27, Shimadzu Italia Srl., Milan, Italy).

2.3.5 Raman Spectroscopy Measurements

Raman spectra were collected using a high-performance confocal Raman microscope (XploRA PLUS, HORIBA, Japan) equipped with a deep-cooled CCD (charge-coupled device) detector. Data acquisition, optimization, and preliminary processing were performed using LabSpec software (version 6.6.1.14, HORIBA, Japan), while further analysis and refinement were carried out in Origin 8.5. To avoid interference from the strong fluorescence of fresh samples, measurements were conducted on lyophilized specimens. Spectra were recorded over the 400–3400 cm^{-1} range using an 1800-line/mm grating. A 532 nm laser was employed, with an exposure time of 30 secs and 5 accumulations per spectrum to reduce the risk of sample overheating.

2.3.6 Thermal Analysis

Thermogravimetric analysis (TGA) was carried out using a Discovery SDT (Simultaneous Differential Thermogravimetric) 650 system (TA Instruments, Waters). Each sample was first stabilized through an initial isothermal conditioning step, after which the temperature was increased at 10 °C/min until reaching 900 °C. Experiments were performed under both nitrogen and air atmospheres to assess the thermal characteristics of the materials in different controlled environments. A constant gas flow of 100 mL/min was maintained throughout the runs to ensure consistent and reproducible

measurements. All thermograms were processed and evaluated using the TRIOS software package.

Differential Scanning Calorimetry (DSC) was performed on the commercial stabilized SS samples with a Discovery DSC 25 (TA Instruments, Waters), using TRIOS for instrument control and data interpretation. Freeze-dried (lyophilized) slime samples were heated from the storage temperature (4 °C) at 10 °C/min to successive temperature plateaus of 20, 25, 30, 35, 40, 50, 70, 80, 90, and 100 °C. At each temperature, the sample was held isothermally for 1 min to allow full thermal equilibration. Cooling was carried out at the same ramp rate, returning the sample to the starting temperature. This complete sequence represented one thermal cycle. For extended stability assessments, 20 cycles were applied, with temperatures limited to 70 °C to minimize thermal degradation. Stabilized liquid slime samples were analyzed using the same heating rate, with temperature steps at 20, 25, 30, and 35 °C, each followed by a 1-min hold. For cyclic stability testing, the upper temperature limits were increased to 40 and 50 °C. All measurements were performed in triplicate to ensure data consistency and reproducibility.

2.3.7 Total Phenolic Content (TPC) Assessment

Phenolic content was determined using a modified version of the Folin–Ciocalteu assay [104]. Briefly, 0.25 mL of the sample was combined with 1 mL of Folin–Ciocalteu reagent diluted at a 1:9 (v/v) ratio. After allowing the reaction to proceed for 3 min, 0.75 mL of a 1% Na_2CO_3 solution was added. The mixture was then left to stand at room temperature for 2 h. Absorbance readings were taken at 760 nm, and phenolic concentrations were calculated using Eq. 1 and expressed as milligrams of gallic acid equivalents (GAE)/g.

$$TPC = \frac{c \times V}{m} \qquad \text{(Eq. 1)}$$

Where, c = gallic acid concentration (mg/mL), V = sample volume (mL), m = sample mass (g).

2.3.8 Determination of Antioxidant Effects

2.3.8.1 DPPH Radical Scavenging Ability

An aliquot of the sample was mixed with 4 mL of a 0.004% DPPH (1, 1-diphenyl 2 picrylhydrazyl) solution prepared in methanol. The reaction mixture was kept in the dark

at room temperature for 30 min, after which its absorbance was measured at 517 nm. The DPPH scavenging capacity was determined using Eq. 2 and the results were expressed as milligrams of Trolox equivalents (TE) per gram of sample (TE)/g [109-111].

$$\text{Inhibition activity (\%)} = \frac{Ac \times As}{Ac} \times 100 \qquad \text{(Eq. 2)}$$

Where, Ac = absorbance of control, As = absorbance of sample.

2.3.8.2 ABTS Radical Scavenging Ability

The $ABTS^{+}$ (2,2′-azino-bis(3-ethylbenzothiazoline)-6-sulfonic acid) radical solution was generated by reacting 7 mM ABTS with 2.45 mM potassium persulfate and allowing the mixture to stand in the dark for 12–16 h. This stock solution was subsequently diluted with methanol until an absorbance of 0.700 ± 0.02 at 734 nm was achieved. For the assay, the sample was combined with 2 mL of the prepared $ABTS^{+}$ reagent and incubated for 30 min at 25 °C. Absorbance was then measured at 734 nm, and antioxidant activity was expressed as TE/g based on Eq. 2 [112].

2.3.9 Reducing Power Assays

2.3.9.1 Cupric Ion Reducing Activity (CUPRAC)

Samples were mixed with the CUPRAC working reagent, consisting of 10 mM cupric chloride, 7.5 mM neocuproine, and 1 M ammonium acetate buffer (pH 7.0). Following a 30-min incubation period, absorbance was recorded at 450 nm. Antioxidant activity was determined using Eq. 2 and reported as TE/g [113].

2.3.9.2 Ferric Reducing Antioxidant Power (FRAP)

FRAP working solution, composed of 10 mM TPTZ (2,4,6-tris(2-pyridyl)-*s*-triazine) in 40 mM HCl, 20 mM $FeCl_3$, and 0.3 M acetate buffer (pH 3.6) mixed in a 1:1:10 (v/v/v) ratio, was combined with the sample and left to react. After a 30-min incubation, the absorbance was measured at 593 nm. Ferric-reducing antioxidant capacity was calculated using Eq. 2 and reported as TE/g [114].

2.3.9.3 Phosphomolybdenum Assay

Following the addition of the reagent mixture consisting of 28 mM sodium phosphate, 0.6 M sulfuric acid, and 4 mM ammonium molybdate, the samples were incubated for 90 min at 95 °C. After incubation, absorbance was recorded at 695 nm. Antioxidant capacity was determined using Eq. 2 and expressed as mmol TE/g [115].

2.3.10 Metal Chelating Ability

Metal-chelating activity was evaluated by combining the sample with 2 mM $FeCl_2$, after which the reaction was initiated by adding 5 mM ferrozine. The mixture was then allowed to stand for 10 min. Absorbance was measured at 562 nm, and the chelation capacity was calculated using Eq. 2 and expressed as milligrams of EDTA (ethylenediaminetetraacetic acid) equivalents (EDTAE/g) [116].

2.3.11 Enzyme Inhibitory Assays

2.3.11.1 Cholinesterase (ChE) Inhibitory Assays

Samples were incubated with 5,5-dithio-bis(2-nitrobenzoic) acid (DTNB) and either acetylcholinesterase (AChE) or butyrylcholinesterase (BChE) in Tris–HCl buffer (pH 8.0) at 25 °C for 15 min. Reactions were started with the addition of acetylthiocholine iodide (ATCI) and butyrylthiocholine iodide (BTCI), respectively. Absorbance was taken at 405 nm after 10 min, and inhibition activities were expressed as mg Galantamine Equivalents(GALAE)/g, determined by Eq. 2 [117].

2.3.11.2 Tyrosinase Inhibitory Assay

The samples were mixed with tyrosinase and phosphate buffer (pH 6.8) and incubated at 25 °C for 15 min. The reaction was then initiated by adding L-DOPA, and after a further 10-min incubation, absorbance was measured at 492 nm. Tyrosinase inhibitory activity was calculated using Eq. 2 and reported as mg Kojic acid Equivalents (KAE)/g [118].

2.3.11.3 α-Amylase Inhibitory Assay

Samples were pre-incubated with α-amylase in phosphate buffer containing 6 M NaCl (pH 6.9) at 37 °C for 10 min. The enzymatic reaction was initiated by adding 0.05% starch solution and allowed to proceed for an additional 10 min at 37 °C. The reaction was terminated by 1 M HCl, followed by the addition of iodine–potassium iodide (KI) reagent. Absorbance was measured at 630 nm, and α-amylase inhibitory activity was calculated using Eq. 2, expressed as mmol Acarbose Equivalents (ACE)/g [119].

2.3.11.4 α-Glucosidase Inhibitory Assay

Samples were incubated with α-glucosidase in phosphate buffer (pH 6.8) along with glutathione and 4-nitrophenyl-α-D-glucopyranoside (PNPG) at 37 °C for 15 min. The reaction was terminated by adding 0.2 M Na_2CO_3, and absorbance was measured at 405

nm. α-Glucosidase inhibitory activity was calculated using Eq. 2 and expressed as mmol ACE/g [120].

2.4 Cell Culture

A human keratinocyte cell line (HaCaT), purchased from AddexBio (San Diego, CA, USA, catalog number T0020001), a somatic hybrid endothelial cell line, namely (EA.hy926), obtained from the human umbilical vein, purchased from the American Type Culture Collection (ATCC), and primary normal human dermal fibroblasts (NHDFs), purchased from Merck Life Science (Milan, Italy, catalog number c-12302), were cultured in high-glucose Dulbecco's Modified Eagle Medium (DMEM), supplemented with 10 % Fetal Bovine Serum (FBS) and 1% penicillin/streptomycin at 37 °C with 5% CO_2.

2.5 Cell Treatments

Cells were treated with specific dilutions of SS and GA in DMEM. The SS was applied at dilutions of 1:40 (0.508 mg/mL), 1:60 (0.31 mg/mL), and 1:80 (0.247 mg/mL). GA was applied at concentrations of 4.1 mM (0.31 mg/mL), 2.73 mM (0.21 mg/mL), and 2.05 mM (0.15 mg/mL), where relevant. The control condition consisted of cells cultured in DMEM containing only the stabilizers present in the SS formulation: 0.1% potassium sorbate and sodium benzoate, and 10% sodium citrate. This control was essential to normalize and isolate the biological effects of SS and GA from those of the preservatives and stabilizers. These specific treatment concentrations were selected based on prior experimental data [11].

2.5.1 Cell Viability by MTT Assay

Both HaCaT and EA.hy926, were seeded at a density of 7000 cells per well, while NHDFs at 6700 cells per well in a tissue culture-treated 96-well plate overnight. Following treatments, cell viability was assessed via the MTT (3-(4,5-dimethylthiazol-2-yl)-2,5-diphenyltetrazolium bromide) assay in HaCaT cells after 24 and 48 h with SS and GA, in EA.hy926 cells after 24, 48, and 72 h with SS and GA (concentration 4.1 mM only), and in NHDFs after 24 and 48 h with SS.

The culture medium was replaced after treatment with 100 µL per well of a 0.5 mg/mL MTT solution in DMEM. The plates were incubated for 4 h in the case of HaCaT and

EA.hy926, and for 5 h in the case of NHDFs, at 37°C in the dark. The resulting formazan crystals were then solubilized by adding 100 µL of dimethyl sulfoxide (DMSO) per well, followed by a 20-min incubation at 37°C. The absorbance of the resulting colored solution, indicative of viable cell presence, was measured at 540 nm using a GO microplate spectrophotometer (Thermo Fisher Scientific, Waltham, MA, USA). The percentage of metabolically active cells for each sample was calculated relative to the control group, which was set to 100% viability.

2.5.2 Wound Healing Assay

HaCaT cells were seeded at 240000 cells/well and NHDFs at 300000 cells/well in tissue-culture-treated 6-well plates, while EA.hy926 cells were seeded at 80,000 cells/well in a 12-well plate to perform wound healing. A uniform wound was created in the confluent cell monolayer in each well using a sterile 200 µL micropipette tip. The dislodged cells and debris were then rinsed away with DMEM. The remaining adherent HaCaT and EA.hy926 cells were treated with SS and GA (concentration 4.1 mM only) and NHDFs with SS only and a control for each cell type, prepared in FBS-free DMEM to specifically assess cell migration independently of proliferation. Photos were taken using an inverted light microscope (Leica DMi1, Wetzlar, Germany) equipped with a camera, using Leica LAS EZ software (LAS EZ 3.4 DVD 272), at different time intervals (0 h and 18 h of treatment for EA.hy926 cells and 0 h, 24 h, and 48 h for HaCaT and 0 h, and 24 h for NHDFs). The scratch distance and area were measured using Fiji imageJ 1.54f software. The percentage of cut reduction after treatment was then normalized to the cut at T0.

2.5.3 Flow Cytometry Analysis of ROS Release

HaCaT and NHDFs were seeded in a tissue-culture-treated 6-well plates at a density of 180,000 cells/well, and HaCaT cells were treated with SS and GA for 6 and 18 h, while NHDFs were treated with SS only for 6 or 24 h. After treatment, cells were incubated with 5 µM 5-(and-6)-chloromethyl-2′,7′-dichlorodihydrofluorescein diacetate, and acetyl ester (CM-H_2DCFDA, Cat. C6827, Molecular Probes, Invitrogen, Life Sciences Division, Milan, Italy) for 1 h at 37 °C, following the procedure described previously [121]. CM-H_2DCFDA is a cell-permeable probe that, upon oxidation by intracellular reactive oxygen species (ROS), emits green fluorescence. Fluorescence was recorded using a CytoFLEX flow cytometer (Beckman Coulter, Miami, FL, USA) equipped with an FL1 detector in logarithmic mode. The median fluorescence intensity (MFI) was quantified with

CytExpert software (v 2.3) to evaluate ROS generation. Dead cells were excluded by staining with propidium iodide (PI; 5 µg/mL, Cat. P4864, Sigma-Aldrich, St. Louis, MO, USA). For each sample, a minimum of 10,000 events were acquired for analysis.

2.5.4 Western Blot Analysis

Protein expression was analyzed via western blot in HaCaT and NHDF cells. HaCaT cells were seeded at a density of 240,000 cells/well in a 6-well plate and treated with SS and GA (4.1 mM) and protein expression was measured after 14, 24, and 48 h of treatment. NHDFs were seeded at 200,000 cells/well in a 6-well plate and treated with SS and protein expression was measured after 24 and 48 h of treatment. Following treatment, cells were detached, centrifuged, and the resulting cell pellet was lysed in RIPA buffer containing protease inhibitors (1 mM sodium orthovanadate, 50 µg/mL leupeptin, 10 µg/mL aprotinin, and 100 µg/mL PMSF (Phenylmethyl sulfonyl fluoride)). After further centrifugation, the supernatant was collected and total protein concentration was quantified using a Bicinchoninic acid (BCA) assay according to the manufacturer's protocol.

For immunoblotting, for HaCaT 25 µg of protein per sample was separated by electrophoresis on 8% or 12% while for NHDFs 30 µg on 10 % SDS-polyacrylamide gels and transferred onto nitrocellulose membranes. Membranes were blocked with 5% non-fat milk or 3% bovine serum albumin and then incubated overnight at 4°C with the following primary antibodies: anti-PI3K (cat.# 4292S, rabbit, 1:1000), anti-p-Akt (cat.# 9271S, rabbit, 1:1000), anti-Akt (cat.# 9272S, rabbit, 1:1000) (purchased from Cell Signaling Technology, Danvers, MA, USA), anti-NF-κB (cat.# sc-8008, rabbit, 1:800), anti-Bcl-2 (cat.# sc-7382, mouse, 1:100), anti-Bax (cat.# sc-7480, mouse, 1:100) anti-COX-2 (cat.# sc-19999, mouse, 1:1000) (purchased from Santa Cruz Biotechnology, Inc. Oregon, USA), anti-Tubulin (cat.# T6074, mouse, 1:1000) (purchased from Merck Life Science, Milan, Italy) for HaCaT, and anti-Actin (cat.# MA1-80729, mouse, 1:10000) (purchased from Thermofisher Scientific, Waltham, Massachusetts, USA) for NHDFs. The next day, membranes were washed and incubated with appropriate IgG horseradish peroxidase (HRP)-conjugated secondary antibodies (Calbiochem, Darmstadt, Germany). Immunoreactive protein bands were visualized using LiteAblot Extend Chemiluminescent Substrate (EuroClone S.p.a., Milan, Italy) and imaged with a ChemiDoc™ XRS system for HaCaT and Invitrogen iBright 1500 Imaging Systems (Thermofisher Scientific,

Waltham, Massachusetts, USA) for NHDFs. Densitometric analysis was performed using QuantityOne 1D analysis software (v4.6.6) (BIORAD, Richmond, CA, USA) for HaCaT and iBright Analysis Software v5.0.1 (Thermo Fisher Scientific, USA) for NHDFs, and the optical density of each protein band was normalized to that of the internal loading control, tubulin.

2.6 HaCaT Experiments

2.6.1 Lactate Dehydrogenase (LDH) Cytotoxicity Assay

HaCaT cells were seeded at 8000 cell/well in a tissue culture treated 96-well plate and cytotoxicity was assessed by measuring LDH release into the culture supernatant, an indicator of cell membrane damage. This was performed using the CytoTox 96 non-radioactive assay kit. Cells were treated with SS and GA (4.1 mM) for 14 and 24 h. The assay was conducted following the manufacturer's protocol. Following the treatment period, the optical density (OD) of the assay solution was measured at 490 nm, with background absorbance measured at 690 nm. The raw LDH release values were normalized to the corresponding MTT assay OD values for each sample, as described in a previous report [122].

2.6.2 Measurement of Interleukin-6 (IL−6) Secretion by ELISA Assay

HaCaT cells were seeded at 8000 cells/well in a tissue culture treated 96-well plate and the secretion of the pro-inflammatory cytokine IL-6 was quantified from HaCaT cell supernatants using a commercial ELISA kit (Enzo Life Sciences, Farmingdale, NY, USA). Following 48 h of treatment with SS and GA (4.1 mM), the supernatant was collected and analyzed according to the manufacturer’s instructions. The absorbance of each sample was measured at 450 nm using a multimode microplate reader (Varioskan™ LUX Multimode Microplate Reader, Thermo Scientific, Waltham, MA, USA). The IL-6 concentration (pg/mL) for each sample was determined by interpolating the absorbance value on a standard curve generated with known concentrations, and the final IL-6 concentration values were normalized to the corresponding MTT OD values.

2.6.3 RNA Extraction, Reverse Transcription and Real-Time Polymerase Chain Reaction (RT-PCR)

HaCaT cells were seeded at 240,000 cells/well in a tissue culture treated 6-well plate and treated with SS and GA (4.1 mM) for 6 and 24 h. Cell pellets were obtained by

centrifugation and lysed using a buffer containing 1% 2-mercaptoethanol, followed by the addition of an equal volume of 70% ethanol (v/v) prepared in RNase-free water. Samples were transferred to spin cartridges, provided by the PureLink® RNA Mini Kit (Life Technologies, Carlsbad, CA, USA); to avoid DNA contamination, before RNA extraction, samples were incubated for 15 min with 80 µL of DNase mixture (On-column PureLink® Dnase Treatment, Life Technologies, Carlsbad, CA, USA). RNA was then eluted in 30 µL of RNase free-water, and concentrations were measured (ng/µL) using the Qubit® RNA BR Assay kit using a Qubit® 4.0 Fluorometer reader (ThermoFisher Scientific Waltham, MA, USA).

For cDNA obtainment, 360 ng of RNA from each sample was reverse-transcribed using a high-capacity cDNA reverse transcription kit (Life Technologies, Carlsbad, CA, USA). The reaction was performed in a thermal cycler under the following conditions: 25°C for 10 min, 37°C for 120 min, and 85°C for 5 min. Gene expression was assessed by quantitative PCR using PowerUp™ SYBR™ Green 2X Master Mix (Thermo Fisher Scientific, Waltham, MA, USA). Each 20 µL reaction contained 10 ng of cDNA, 1 µM of each forward and reverse primer (sequences provided in Table 5), and SYBR Green 2X Master Mix in RNase-free water. Mixture was then transferred to MicroAmp Optical 96-well plate (Life Technologies, Carlsbad, CA, USA) and amplification was carried out in a QuantStudio 3.0 (Thermo Fisher Scientific, Waltham, MA, USA) instrument with the following cycling parameters: initial steps at 50°C for 2 min and 95°C for 2 min, followed by 40 cycles of 95°C for 15 sec and 60°C for 60 sec. A melt curve analysis was performed to confirm the specificity of amplification.

Gene expression data were analyzed using QuantStudio™ Design and Analysis Software (v1.5.1) (Thermo Fisher Scientific, Waltham, MA, USA). The expression of each target gene was normalized to the endogenous reference gene glyceraldehyde 3-phosphate dehydrogenase (*GAPDH*). Relative mRNA levels were calculated using the comparative $2^{-\Delta\Delta Ct}$ method to determine fold changes in gene expression relative to control samples.

Table 5: Sequence of primers used for qPCR gene expression.

Gene	Sequence (5′ to 3′)	Source
GAPDH-Fr	GGGTGTGAACCATGAGAAGTA	Primer blast
GAPDH-Rv	ACTGTGGTCATGAGTCCTTC	Primer blast
COX2-Fr	CCCTTCTGCCTGACACCTTT	Primer blast
COX2-Rv	TTCTGTACTGCGGGTGGAAC	Primer blast
MMP−2-Fr	GCTACGATGGAGGCGCTAAT	Primer blast
MMP−2-Rv	GGGCAGCCATAGAAGGTGTT	Primer blast
MMP−9-Fr	CGACGTCTTCCAGTACCGAG	Primer blast
MMP−9-Rv	GTTGGTCCCAGTGGGGATTT	Primer blast

2.7 NHDFs Experiments

2.7.1 Almar Blue Assay

To measure the viability, the Alamar blue assay was done in triplicate for each experimental group at each time point. NHDFs were seeded at 8000 cells/well in a tissue culture treated 96-well plate and treated with SS for 24, 48, and 72 h. Alamar blue assay is based on the capability of viable cells to reduce Alamar blue reagent into a red product. At established time points, the medium was replaced by a fresh one containing Alamar blue reagent (Thermo Scientific, Rockford, IL, USA) in 10% of the volume, probed with cells for 4 h at 37°C, and read at 570 and 600 nm. Value obtained in the absence of cells was considered as a negative control. The % reduction of Alamar blue reagent was calculated according to the manufacturer's instructions.

2.7.2 Antioxidant Activity Assessment

The total antioxidant capacity (TAC) of SS was determined by evaluating its power to reduce Cu^{2+} to Cu^{+} using the antioxidant assay kit (MAK334, Sigma-Aldrich, St. Louis, MO, USA) according to the manufacturer's instructions. NHDFs were seeded in a 6-well plate at a cell density of 200,000 cells/well. After 24 h of SS treatment (1:40, 1:60, 1:80), cell supernatants were collected for each condition to measure TAC. Briefly, 20 µL of cell supernatants were plated in a flat bottom 96-well plate, and 100 µL of Reaction Mix was added and maintained for 10 min at room temperature. Absorbance was read at 570 nm wavelength by using a spectrophotometer (Multiskan GO, Thermo Scientific,

Waltham, MA, USA), obtained values were interpolated with a standard Trolox curve to obtain the concentration of antioxidant molecules (μM).

2.7.3 Detection of Apoptosis and Necrosis by Flow Cytometry

NHDFs were seeded at 200,000 cells/well in a tissue culture treated 6-well plate and treated with SS for 24 and 48 h and after the prescribed time, cells were collected together with the supernatants. Cells were then stained with Annexin-V and Propidium Iodide (PI) (eBioscience, Thermo Fisher Scientific, Waltham, MA, USA) to discriminate against both apoptotic and necrotic cells, according to the manufacturer's instructions. Samples were probed in binding buffer and Annexin V FITC (197 μL +3 μL, respectively) in the dark for 15 min at room temperature. After that, the volumes were doubled with binding buffer, and the cells were centrifuged and resuspended in binding buffer with PI. A CytoFlex flow cytometer (Beckman Coulter, Brea, CA, USA) was used to quantify fluorescence. A 530/30 bandpass filter was used to analyze FITC fluorescence (FL-1), and a 650 nm long pass filter for PI fluorescence (FL-3). Data were acquired (2 × 104 events/sample) and analyzed by means of the CytExpert 5.0 Software (Beckman Coulter, Brea, CA, USA). Viable cells percentage (Annexin V-; PI-) were revealed in the lower left quadrant (unstained) of density plots, cells in apoptosis in the lower right quadrant (Annexin V+/PI-), cells in late apoptosis in the upper right quadrant (Annexin V+/PI+), and cells in necrosis in the upper left quadrant (Annexin V-/PI+).

2.7.4 Treatment and Sample Collection for Proteomic Analysis

NHDFs cells were grown in culture-treated T75cm^2 flask to reach 80-90% confluence, washed twice with Dulbecco's phosphate-buffered saline (DPBS), and then treated with 1:40, 1:60, and 1:80 dilutions of SS for 24 and 48 h, and control for 0, 24, and 48 h (in triplicate) in FBS-free DMEM. After the aforementioned time points, the medium was removed, and cells were collected by trypsinization, washed with DPBS, and pellets were stored in -80 °C for future use.

2.7.4.1 Cell Lysis and Protein Quantification

All the SS treatments were performed in triplicate, and the collected samples were divided into three equal groups by randomly selecting one sample from each treatment condition (3 x 9 samples) in order to avoid the handling errors between the replicates. Samples were handled group-wise, each cell pellet was lysed with 100 μL of S-TRAP 1X

lysis buffer (5% SDS + 50 mM Triethylammonium Bicarbonate (TEAB) in distilled water), vortexed, and subjected to probe sonication (HD 2200, Bandelin Sonopuls, Berlin, Germany) for 40 sec (4 cycles x10%) at 50% power (MS 72). Samples were centrifuged at 13000 xg for 8 min, and the supernatant was collected. The protein amount in each sample was measured by the BCA (Sigma-Aldrich) assay. For the standard curve, 0, 0.5, 1, 2, 5, 8 and 10 µg BSA were used. Measured quantities of BSA and 1 µl of 5X diluted samples (in duplicate) were transferred to a flat bottom 96-well plate and volume was made up to 200 µl with freshly prepared BCA solution by mixing 50 parts of Reagent-A with 1 part of Reagent-B (4% copper (II) sulphate pentahydrate) (50:1). Plate was incubated at 37 ℃ for 30 min, cooled down the plate at room temperature post incubation and measured the absorbance at 570 nm using Synergy HT microplate reader (BioTek, Winooski, Vermont, USA).

2.7.4.2 Protein Digestion

Protein (100 µg/sample) was digested using the S-TRAP protocol. Protein was reduced by incubating for 15 min at 55 °C with 10 mM dithiothreitol (DTT) final concentration, followed by disulfide alkylation by incubating for 10 min at room temperature with 20 mM iodoacetic acid (IAA) final concentration. Samples were acidified with 12% phosphoric acid to completely denature the protein and trap them efficiently. Each sample was diluted 6X with binding buffer (100 mM TEAB in 90% methanol) and filtered through S-TRAP mini spin column (4000 xg for 30 sec) to trap protein. Samples were washed thrice (4000 xg for 30 sec) with binding buffer to clean the protein and then incubated overnight at 37 °C with trypsin/lys-C mix (Pierce Trypsin/Lys-C Protease Mix, MS Grade, USA, Lot# YJ380698) in 50 mM TEAB at a 1:25 enzyme to protein ratio (w/w). Peptides were eluted with 80 µL of 50 mM TEAB, 0.2% formic acid (FA), and 50% acetonitrile (ACN) at 4000 xg for 1 min stepwise and dried in a speedvac (RVT 400, Thermo Scientific, USA).

2.7.4.3 LC-MS Analysis

Samples were redissolved in 0.1% FA to make a final concentration of 0.5 µg/µL of digested peptides. Peptides were injected at a concentration of 1 µg per sample in EvoSep ONE liquid chromatography (Evosep Biosystems, Odense, Denmark) equipped with an Orbitrap Fusion Lumos Tribrid (ThermoFisher Scientific, Waltham, Massachusetts, USA) mass spectrometer. The analytical column, EvoSep Endurance column (EV1106) (Evosep

Biosystems, Odense, Denmark): 150 mm (L) × 0.15 mm (D), ReproSil-Pur C18, 1.9 µm beads, with a column temperature of 30 °C, was used for peptide fractionation. A 44-min gradient program, 30 samples per day (SPD) was employed using two solvents (Solvent-A: 0.1% FA in water, Solvent-B: 0.1% FA in ACN). Samples were measured using data-independent acquisition (DIA), and for each sample, a DIA scan was performed using a 50%-staggered 12 Da isolation windows scheme.

2.7.4.4 Data Analysis

The raw files obtained from TraceFinder Quick Acquisition Software (v 5.1) for each sample's analysis were run in DIA-NN Academic (v. 2.2) against a human FASTA file downloaded from www.uniprot.org. Before the run, DIA-NN was set to mark reannotate, contaminants, FASTA digest for library free search, and deep learning-based spectra, RTs and IMs prediction. Missed cleavages set to 2 with a maximum of 3 variable modifications along with N-terminal M-excision, C-carbamidomethylation, Ox(M) and Ac(N-terminal). Peptide length set to 5-30, precursor charge range 1-4, precursor m/z range 300-1800 and fragment ion m/z range 200-1800 with active match between runs (MBR). The DIA-NN output file was then used to sort the protein groups (PG) with at least 2-peptide hits with the help of Knime analytics platform.

2.8 Statistical Evaluation

The results of repeated readings were combined and displayed as mean ± SD. The student t-test (α=0.05) was used to compare the results of chemical analysis. Differences at $p < 0.05$ were considered significant. The analysis of biological results was performed using the statistical software GraphPad Prism v.8.0 software (San Diego, CA, USA) using one-way and two-way ANOVA (Analysis of variance) followed by Dunnett's and Turkey's post hoc test while proteomics datasets were analyzed by RStudio software v.2025.09.0.

3 RESULTS

3.1 Chemical Analysis of SS

3.1.1 Nuclear Magnetic Resonance (NMR) Analysis of Metabolites

NMR-based metabolomic analysis provides a comprehensive snapshot of multiple metabolite classes within slime samples through a single experimental run, allowing both qualitative and quantitative comparisons related to slime production and processing. In the ^{1}H NMR spectra (Figure 6), seven organic acids, acetate, succinate, citrate, fumarate, formate, sorbate, and benzoate, were detected along with alanine, betaine, and glucose. Their identification and quantification were achieved using characteristic ^{1}H spectral features (chemical shifts, peak multiplicities, and J-coupling patterns), supported by two-dimensional NMR correlation data. Table 6 summarizes all detected metabolites, the specific ^{1}H NMR resonances employed for their quantification, and the corresponding concentration values.

Table 6: Metabolites identified in the ^{1}H spectra of SS, together with signal used for quantification (chemical shift, multiplicity, *J* coupling constant) and quantitative results expressed as µg/mL of slime (mean value ± SD).

Metabolite	^{1}H ppm, multiplicity *J* [123]	Stabilized slime	Non-stabilized slime
Acetate	1.92, s	18.00 ± 1.38	16.63 ± 1.59
Succinate	2.41, s	44.46 ± 1.07*	14.85 ± 0.43
Citrate	2.55, d [15.3]	51893.59 ± 4515.05*	64198.46 ± 2212.68
Fumarate	6.53, s	28.50 ± 1.89	51.72 ± 1.22
Formate	8.46, s	11.84 ± 1.26	5.41 ± 0.56
Sorbate	5.83, d [15.3]	547.76 ± 8.80*	282.44 ± 18.24
Benzoate	7.88, d [7.1]	1052.05 ± 15.38*	478.79 ± 16.98
Alanine	1.48, d [7.2]	7.09 ± 0.27	9.25 ± 0.40
Betaine	3.27, s	68.07 ± 5.67*	25.95 ± 0.26
Glucose	4.66, d [8.1]	16.09 ± 0.15	6.55 ± 0.35

*statistically significant difference respect to no stabilized slime, ($p < 0.05$).

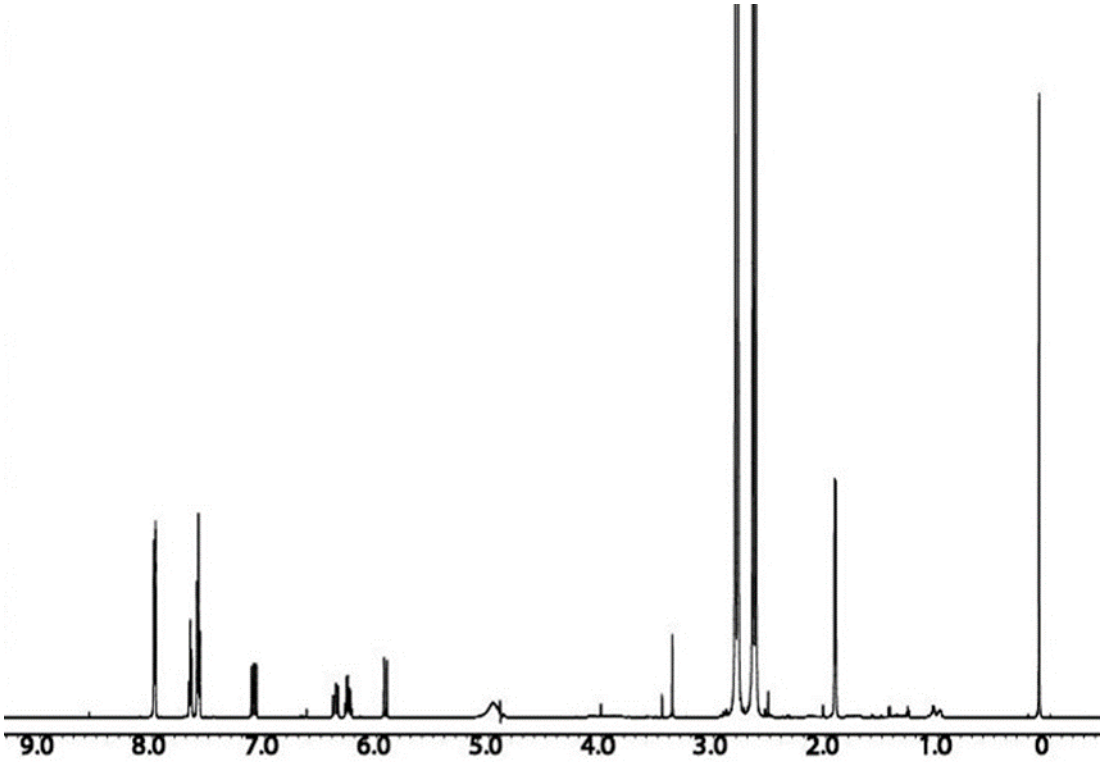


Figure 6: 600.17 MHz ^{1}H NMR spectrum of stabilized SS in 200 mM phosphate buffer/D_2O containing 0.3 mM TSP.

3.1.2 Solid-Phase Microextraction-Gas Chromatography/Mass Spectrometry (SPME-GC/MS) Analysis

The SPME–GC/MS analysis enabled the detection and semi-quantitative assessment of 13 volatile and semi-volatile compounds spanning multiple chemical classes, as summarized in Table 7. Organic acids, particularly sorbic and benzoic acids were the predominant constituents in both stabilized and non-stabilized freeze-dried slime samples, with the latter also showing trace levels of fatty acids. In the stabilized formulation, benzoic acid accounted for the highest mean relative abundance (69.4%), followed by 2,4-dimethylbenzaldehyde (17.7%). Vanillin was present in both preparations, representing 4.8% in the stabilized sample and 8.4% in the non-stabilized sample. Conversely, the non-stabilized slime exhibited a distinct volatile profile, with benzene emerging as the dominant component (43.8%). Notably, 1,3-dioxolane (16.1%) and methoxy phenyl oxime (23.2%) were detected exclusively in the non-stabilized sample. Representative chromatograms are shown in Figures 7–10.

Table 7: Metabolites identified (percentage mean values ± SD) in all samples of SS as determined by SPME-GC/MS technique.

Metabolite	LRI^{exp}	LRI^{lit}	Stabilized freeze-dried slime	Non-stabilized freeze-dried slime	Stabilized slime	Non-stabilized slime
1,3-dioxolane	588	590	-	-	-	16.1± 1.05
2-methyl-furan	600	605	-	-	-	6.6± 0.05
Benzene	660	663	-	-	-	43.8± 2.01
N-ethylformamide	701	706	-	-	-	1.9± 0.07
sorbic acid	1050	1056	27.8± 0.12	24.7± 0.20	-	-
2,4-dimethylbenzaldehyde	1185	1181	-	-	17.7± 1.02	-
benzoic acid	1193	1191	72.2± 1.35	71.9± 1.28	69.4± 1.21	-
methoxy phenyl oxime	1305	1301	-	-	-	23.2± 1.04
Vanillin	1414	1410	-	-	4.8± 0.04	8.4± 0.08
3,5-di-*t*-butylphenol	1560	1555	-	-	8.1± 0.05	-
tridecanoic acid	1662	1658	-	0.5± 0.02	-	-
oleic acid	2148	2151	-	1.0± 0.03	-	-
stearic acid	2182	2187	-	1.8± 0.04	-	-

-: not detected.

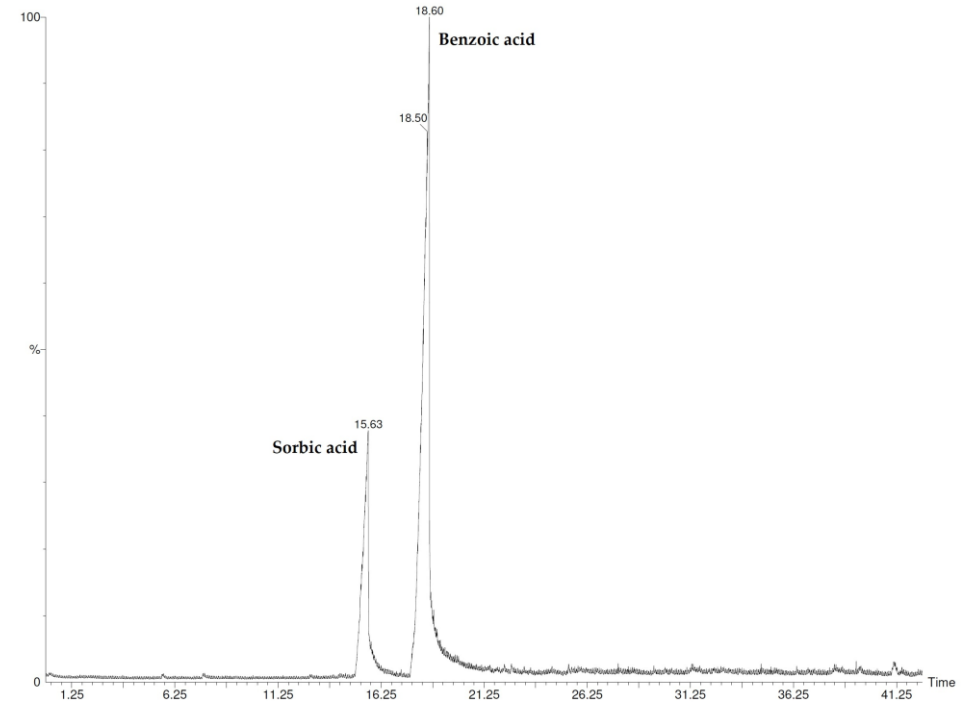


Figure 7: GC-MS chromatogram of stabilized freeze-dried snail slime.

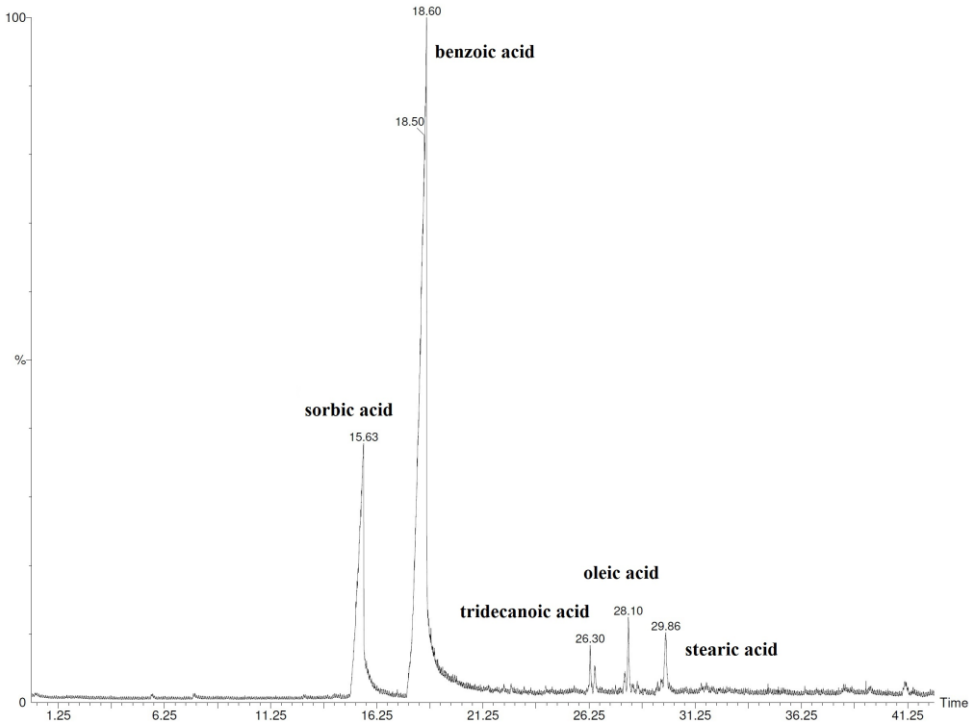


Figure 8: GC-MS chromatogram of non-stabilized freeze-dried snail slime.

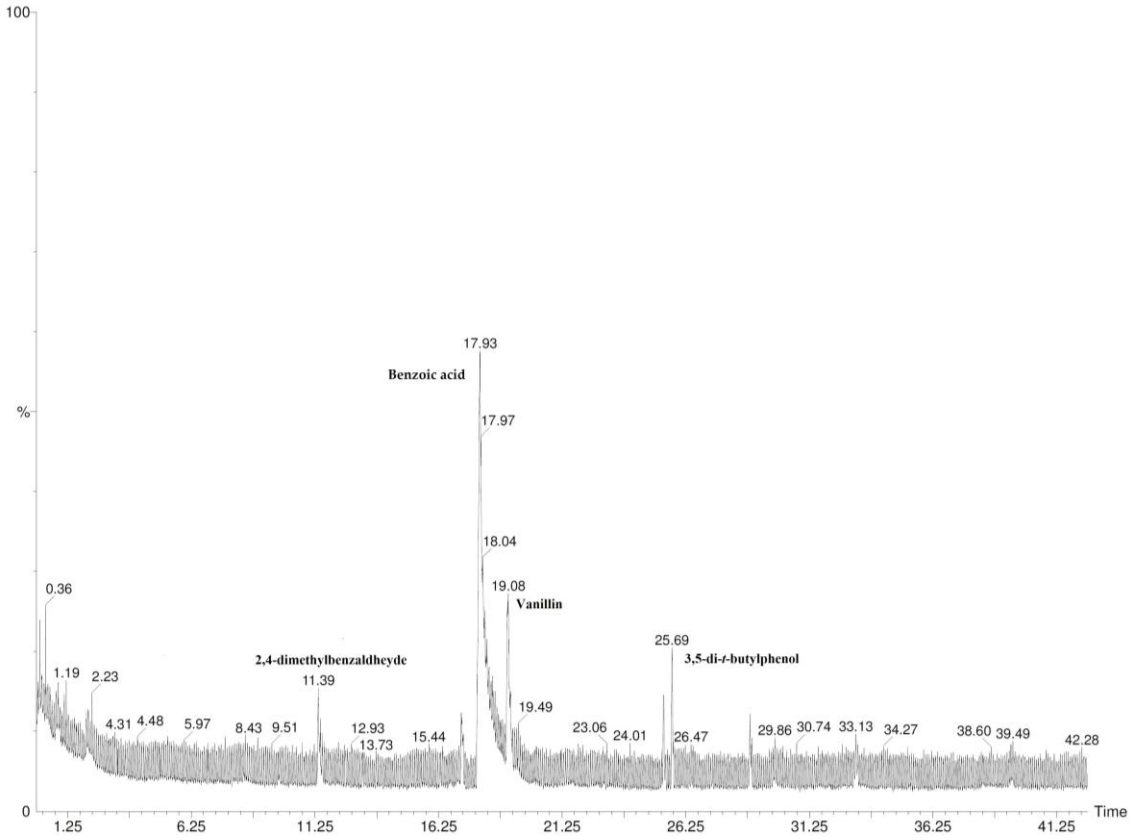


Figure 9: GC-MS chromatogram of stabilized snail slime.

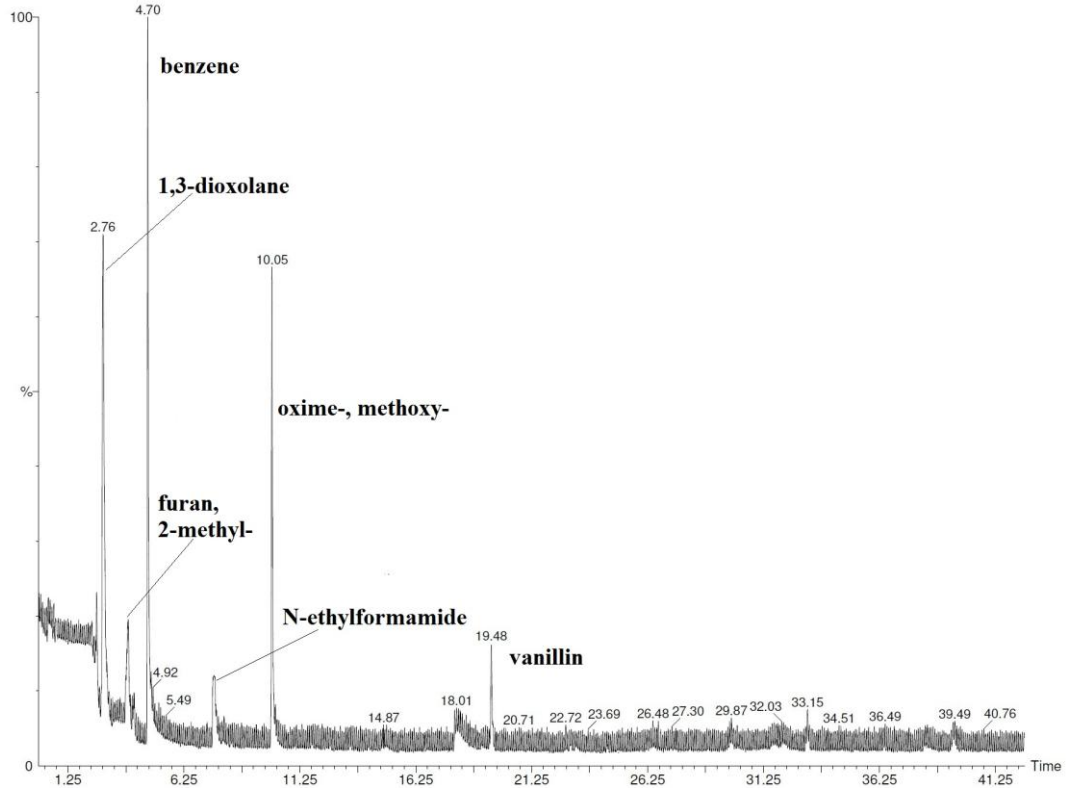


Figure 10: GC-MS chromatogram of non-stabilized snail slime.

Analysis of the derivatized stabilized and non-stabilized freeze-dried slime samples revealed the presence of several furan-related compounds. Among these, 2,5-furandione, 3-methyl-, and 2-furoic acid were the predominant constituents, as detailed in Table 8 and illustrated in Figures 11–12.

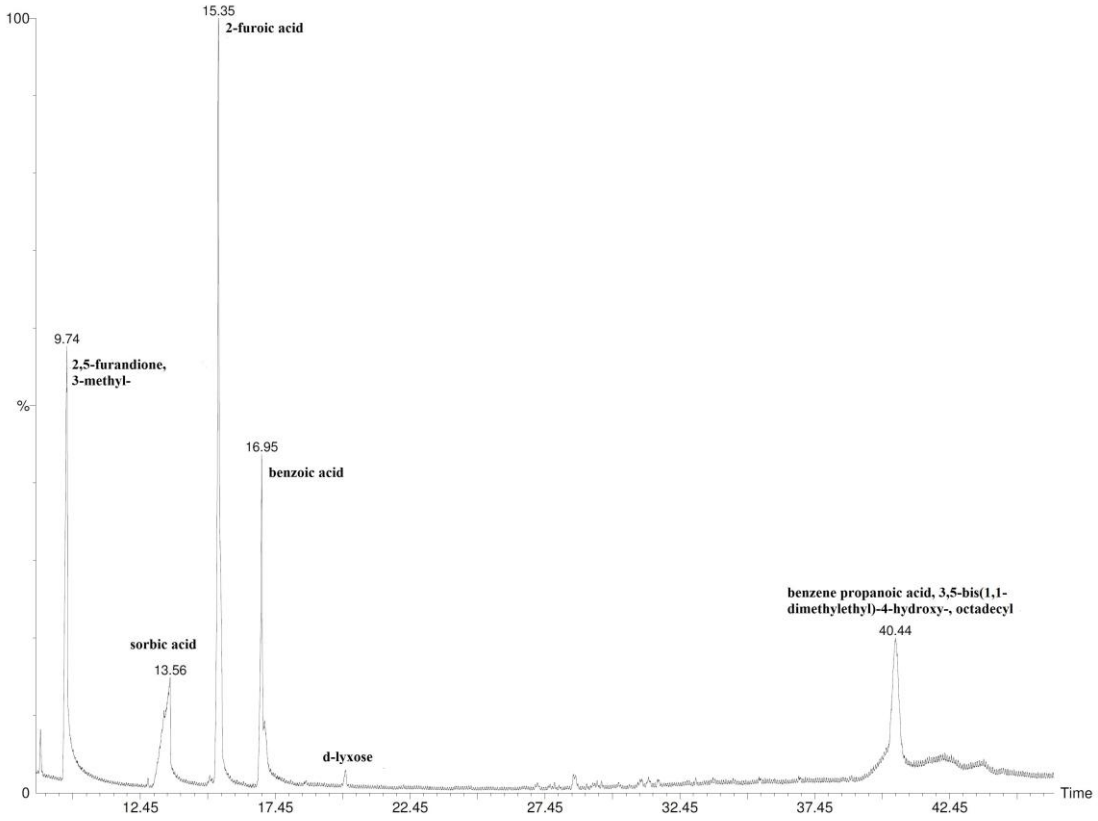


Figure 11: GC-MS chromatogram of stabilized snail slime freeze-dried after derivatization.

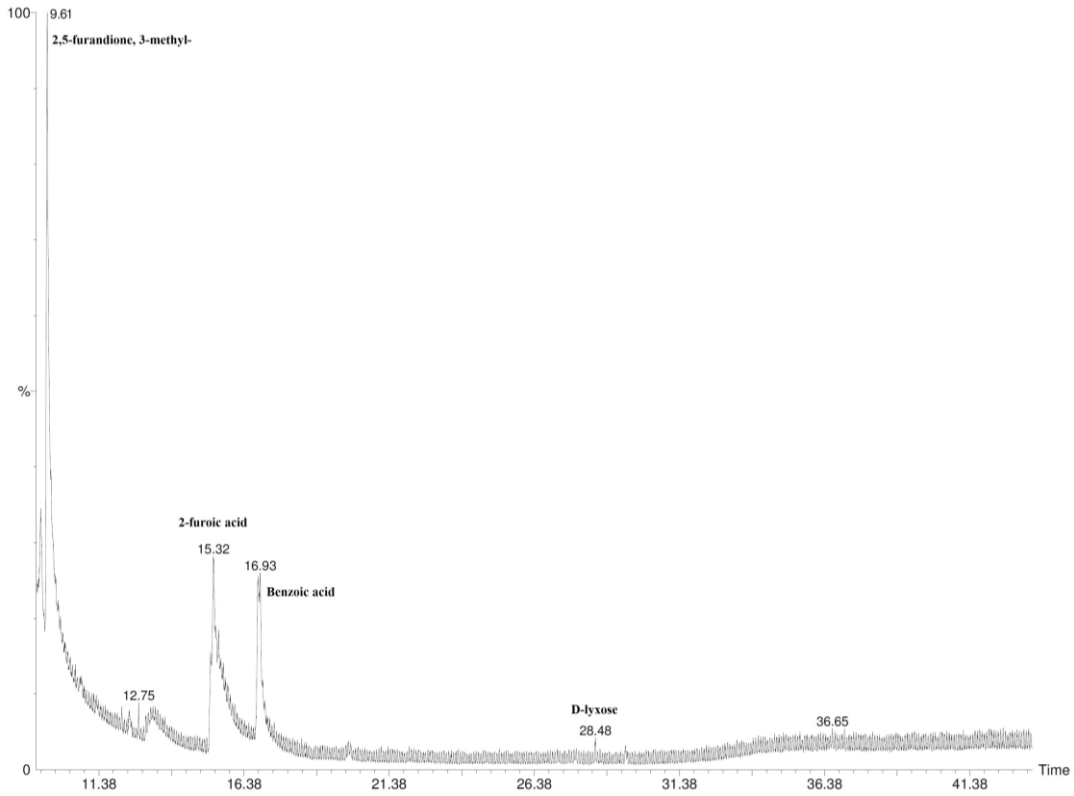


Figure 12: GC-MS chromatogram of non-stabilized snail slime freeze-dried after derivatization.

Table 8: Metabolites identified (percentage mean values ± SD) in the stabilized and non-stabilized freeze-dried SS after derivatization as determined by GC-MS.

Metabolite	Stabilized slime freeze-dried	Non-stabilized slime freeze-dried
3-methyl-2,5-furandione	18.8± 0.14	67.0± 2.52
sorbic acid	12.3± 0.08	tr
2-furoic acid	27.1± 0.21	19.9± 0.32
benzoic acid	7.2	12.3
D-lyxose	0.4	0.8
methyl 3-(3,5-di-tert-butyl-4-hydroxyphenyl) propionate	34.3	-

tr: percent mean value <0.1%.

3.1.3 Fourier Transform Infrared Spectroscopy (FT-IR) Measurements

IR spectroscopy allows the detection of distinct vibrational modes of molecular bonds, offering important evidence for the presence and distribution of specific functional groups

within the SS. The main absorption features observed are summarized in Table 9 and depicted in Figure 13.

Table 9: Infrared absorption bands and their corresponding vibrational modes identified in the sample.

Wavenumber (cm^{-1})	Vibration Type	Molecules
516	Skeletal bending	Polysaccharides, complex carbohydrates
594	Out-of-plane C–H bending	Polysaccharides, glycosidic linkages
651, 682	C–S stretching	Sulfur-containing compounds, cysteine residues (proteins)
798, 887	C–C and C–O bending	Mucopolysaccharides
933	C–H rocking	Carbohydrate backbones
1126	C–O stretching	Glycosylated proteins, glycoproteins
1198	Amide III (secondary structure)	Proteins (predominantly α-helices)
1323	Symmetric CH_2 bending, N–H deformation	Amino acids, polysaccharides
1400	Vibrations of sugars and amino acid chains	Sugars, amino acids
1581	Amide II (N–H bending, C–N stretching)	Proteins
1700	C=O stretching	Citric acid (from the industrial process)
2538	Weak hydrogen-bonded SH groups or unknown interactions	Possible thiol-containing compounds
2947	Aliphatic C–H stretching	Lipids, proteins
3078	Aromatic C–H stretching	Phenyl groups (protein aromatic residues)
3417	O–H stretching	Hydroxyl groups (water, polysaccharides, glycoproteins)



Figure 13: FT-IR spectrum of stabilized SS in the lyophilized form.

3.1.4 Raman Spectroscopy Analysis

The biochemical composition of the SS was characterized by its Raman spectrum, which displayed several distinct vibrational peaks. These spectral features provide specific insights into the molecular constituents such as polysaccharides, amide, tryptophan, phenylalanine, carbohydrates, proteins, citric acid and other carboxylic groups present in the sample, as detailed in Figure 14 and Table 10.

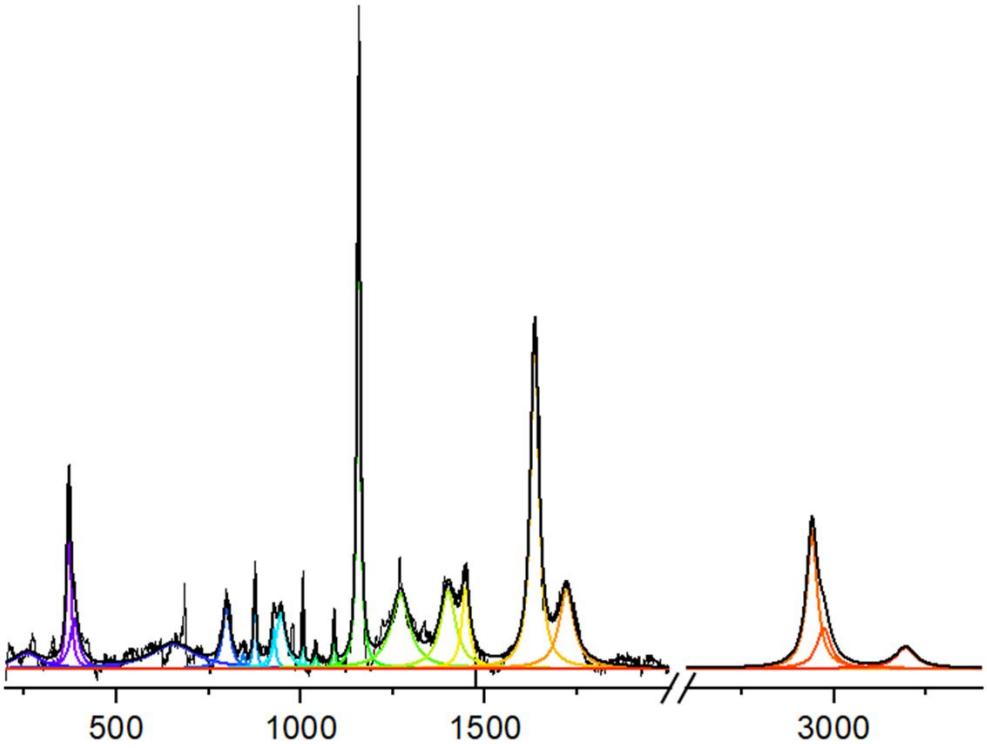


Figure 14: Raman spectrum of stabilized and lyophilized SS. The black line represents the raw spectrum, the colored lines correspond to the individual deconvoluted components.

Table 10: Raman peak assignments for stabilized and lyophilized SS. The table reports the Raman shift (cm^{-1}), the relative assignment and the corresponding species.

Raman Shift	Assignment	Species
369 cm^{-1}	lattice vibrations	Polysaccharides
684 cm^{-1}	OCN bending	Amide IV-VII
795 cm^{-1}	Indole ring vibration	Tryptophan
877 cm^{-1}	Indole ring vibration	Tryptophan
1005 cm^{-1}	Benzene ring breathing	Phenylalanine
1092 cm^{-1}	C–O stretching	Carbohydrates
1157 cm^{-1}	Indole ring	Tryptophan
1268 cm^{-1}	Amide III	Proteins
1390 cm^{-1}	N-C-N Imidazole	Histidine
1449 cm^{-1}	C-H deformation	Alkyl chains
1630 cm^{-1}	Amide I	Random coil (Hexamer in crystalline

		phase)
1717 cm^{-1}	C=O Stretch.	Citric acid and other carboxylic groups
2943 cm^{-1}	C-H_{sym} aliphatic stretching	Fatty acid chains
2990 cm^{-1}	C-H_{asym} aliphatic stretching	Fatty acid chains
3078 cm^{-1}	C-H aromatic stretching	Aromatic amino acids
3195 cm^{-1}	N-H stretching	Amides (proteins)

3.1.5 Thermogravimetric Assessment

TGA of the freeze-dried SS provides valuable information on its thermal decomposition patterns under oxidative (air) and inert (nitrogen) atmospheres. The mass-loss curves obtained in the two conditions display clear differences, highlighting the distinct contributions of oxidation versus pyrolytic processes (Figure 15).

For the commercial liquid formulations, TGA performed up to 50 °C revealed no meaningful changes in sample integrity across repeated heating cycles (Figure 16a), indicating that these preparations remain structurally stable within this temperature interval. In contrast, the lyophilized material demonstrated a wider range of thermal resilience (Figure 17b).

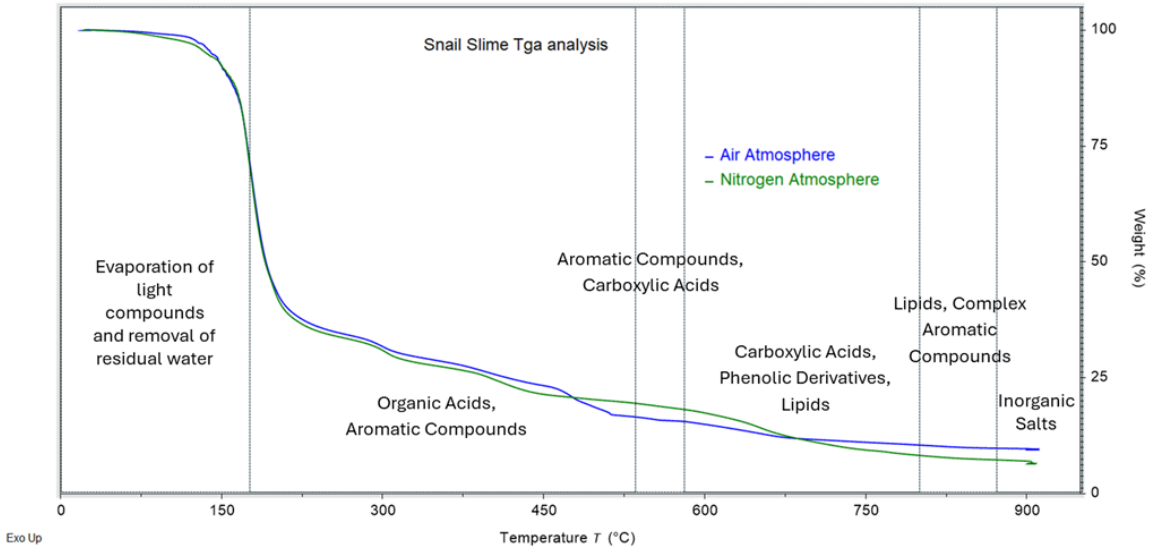


Figure 15: TGA of freeze-dried SS in air and nitrogen atmospheres. The graph shows the temperature ranges at which different compound families undergo decomposition.

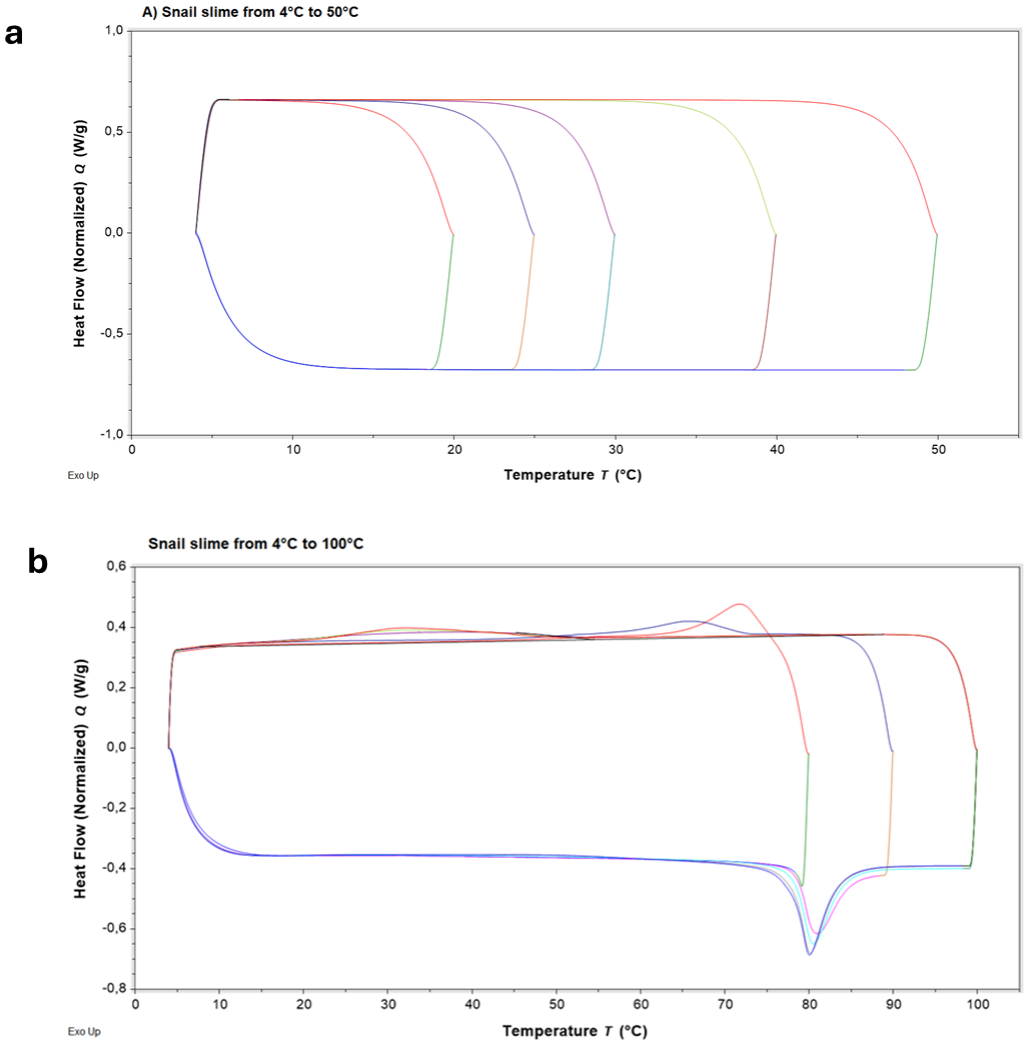


Figure 16: DSC of stabilized a) liquid and b) lyophilized SS.

3.1.6 Antioxidant Capacity Evaluation

The stabilized formulation exhibited a higher phenolic concentration (2.56 mg GAE/g) compared with the non-stabilized sample (1.48 mg GAE/g), a difference likely attributable to the protective action of the stabilizing agents over time (Figure 17).

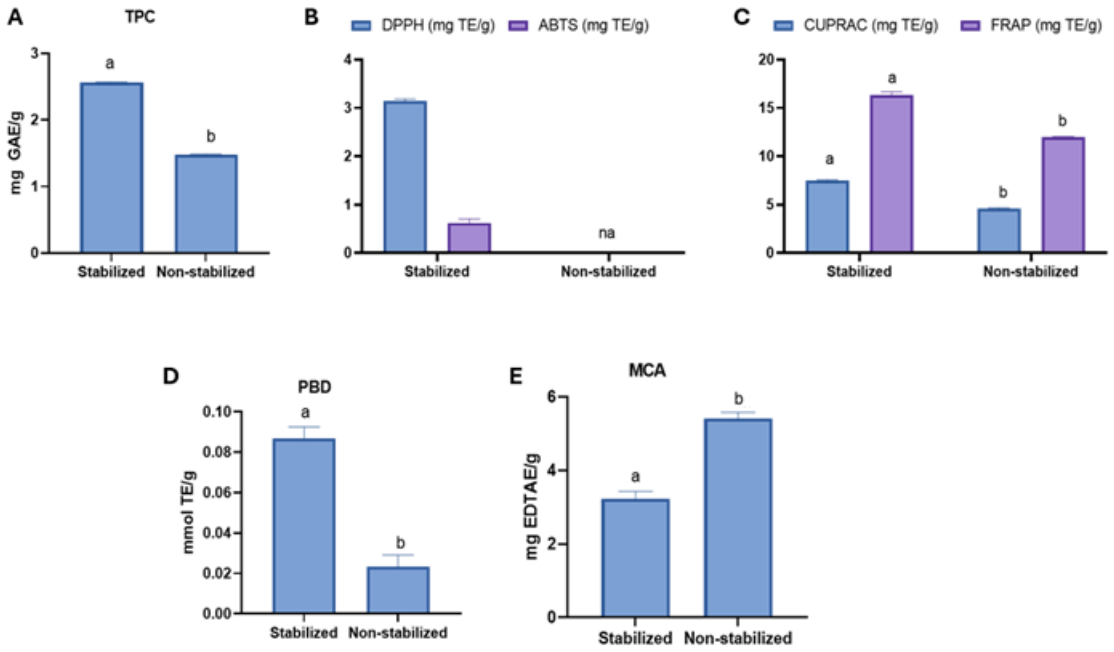


Figure 17: Total phenolic content (TPC) (**A**), and antioxidant properties of stabilized and non-stabilized SS measured by DPPH and ABTS radical scavenging assays (**B**), CUPRAC and FRAP ion reducing activities (**C**), phosphomolybdenum (PBD) assay (**D**), and metal chelating ability (MCA) (**E**). Values are reported as mean ± SD of three parallel measurements. GAE: Gallic Acid Equivalent TE: Trolox Equivalent; EDTAE: EDTA Equivalent; na: not active. Letter "a" indicates the statistical significance (p<0.05) of stabilized SS *vs* control and letter "b" indicates the statistical significance (p<0.05) of non-stabilized SS *vs* control.

3.1.7 Enzyme Inhibition Assessment

The enzyme inhibitory activities of the stabilized and non-stabilized slime samples were evaluated against a panel of enzymes, including glucosidases, cholinesterases, amylase, and tyrosinase, with the corresponding outcomes presented in Figure 18. Both samples demonstrated comparable inhibitory effects on BChE, whereas the non-stabilized slime exhibited no detectable activity against AChE. The stabilized sample showed slightly greater tyrosinase inhibition (21.54 mg KAE/g) relative to the non-stabilized sample (20.85 mg KAE/g). Inhibition of amylase was observed for both samples, while glucosidase inhibition was exclusive to the non-stabilized slime.

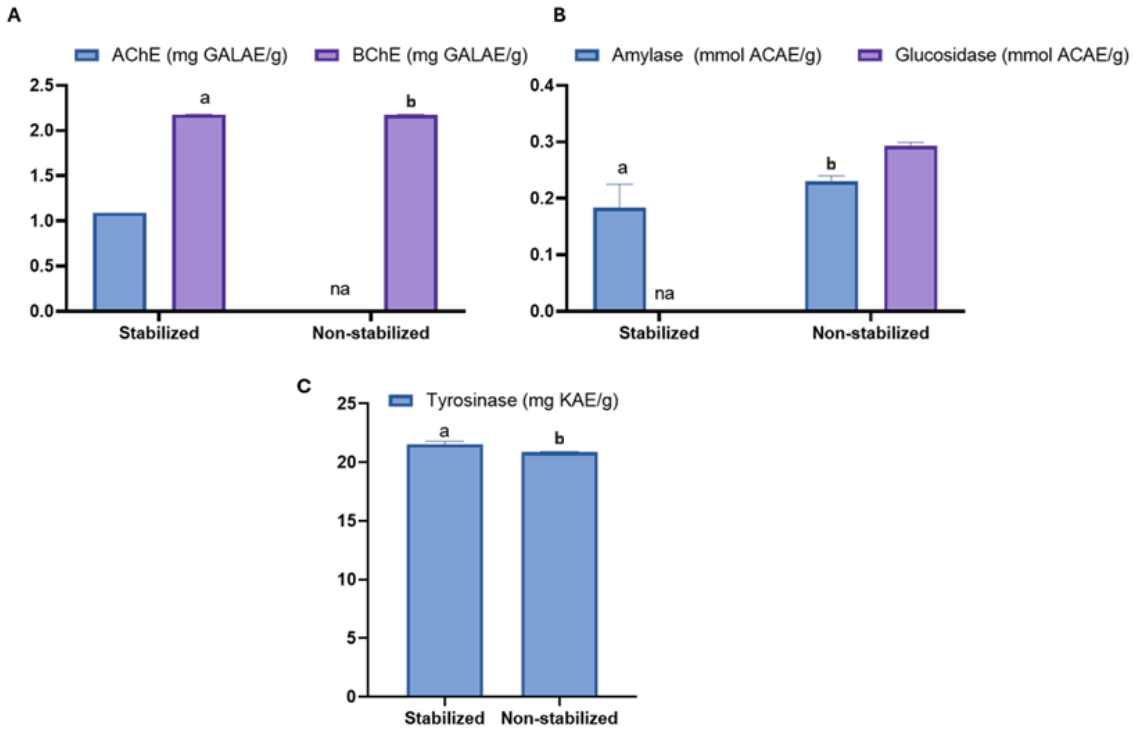


Figure 18: Enzyme inhibition properties of stabilized and non-stabilized SS measured against the acetylcholinesterase (AChE) and butyrylcholinesterase (BChE) inhibition (**A**), α-amylase and α-glucosidase inhibition (**B**) and tyrosinase inhibition (**C**). Values are reported as mean ± SD of three parallel measurements. Letter "a" indicates the statistical significance (p<0.05) of stabilized SS *vs* control and letter "b" indicates the statistical significance (p<0.05) of non-stabilized SS *vs* control. GALAE: Galantamine equivalent; ACAE: Acarbose equivalent; KAE: Kojic acid equivalent; na: not active.

3.2 Biological Evaluation of SS on Different Cell Models

3.2.1 Human Keratinocytes (HaCaT)

3.2.1.1 Assessment of Viability after SS and GA Treatment

HaCaT viability was evaluated using the MTT assay following 24 and 48 h of exposure to various dilutions of SS (1:40, 1:60, and 1:80) and GA (4.1, 2.73, and 2.05 mM, corresponding to the concentrations present in the SS dilutions), with results compared to those of untreated control. Across both time points, cells treated with SS exhibited no significant alterations in viability relative to the control group. Conversely, GA treatment produced no notable change at 24 h; however, after 48 h, GA at 4.1 and 2.73 mM induced

a significant reduction in cell viability compared with the control, as shown in Figure 19B.

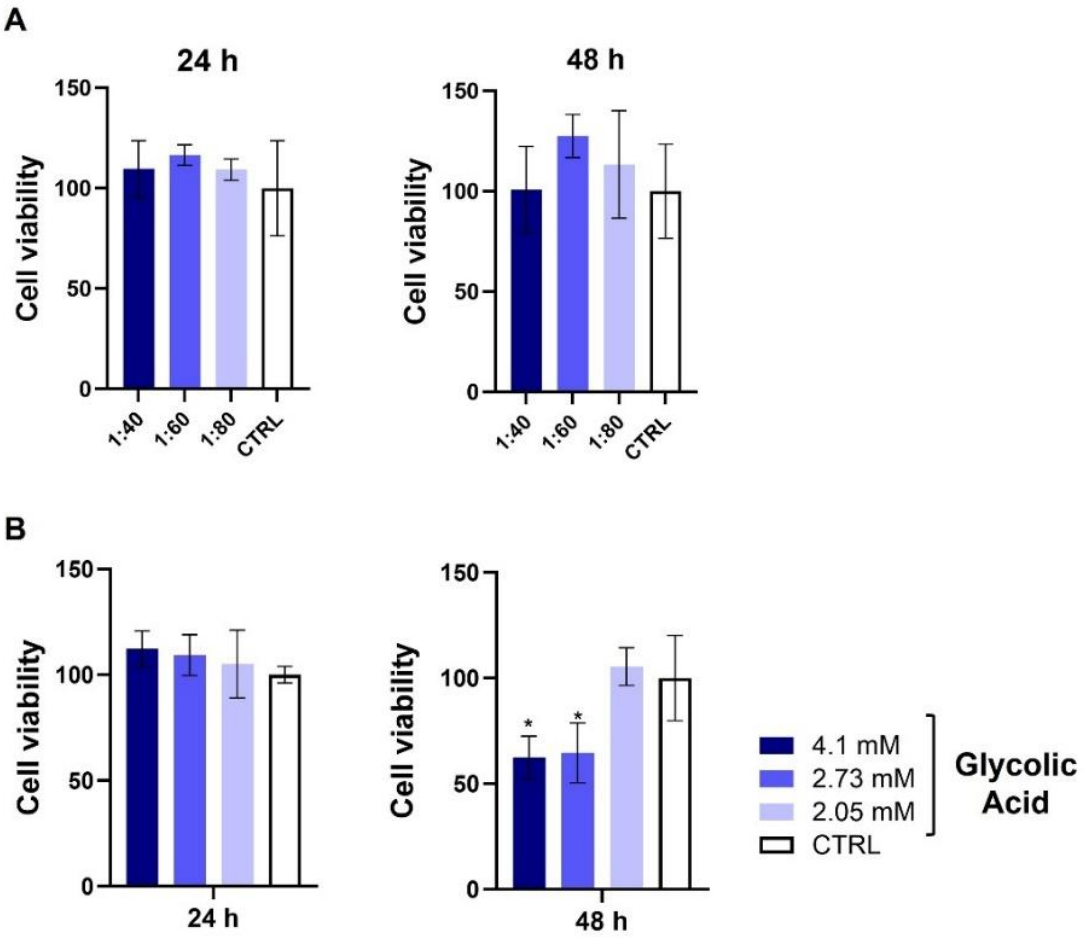


Figure 19: Cell viability test (MTT) performed on HaCaT cells exposed to SS (1:40, 1:60, and 1:80 dilutions) (**A**) and GA (4.1, 2.73, and 2.05 mM) (**B**) for 24 and 48 h. Data are expressed as percentage of viable cells relative to control. Bars represent mean ± SD of three independent experiments. * $p < 0.05$ vs. CTRL.

3.2.1.2 Evaluation of GA's and SS's Effects on Cytotoxicity

At both experimental time points (14 and 24 h), SS treatment markedly decreased LDH release at all tested dilutions (1:40, 1:60, and 1:80) when compared with both GA and control (Figure 20). In contrast, GA induced a significant elevation in LDH release after 14 h relative to the control group.

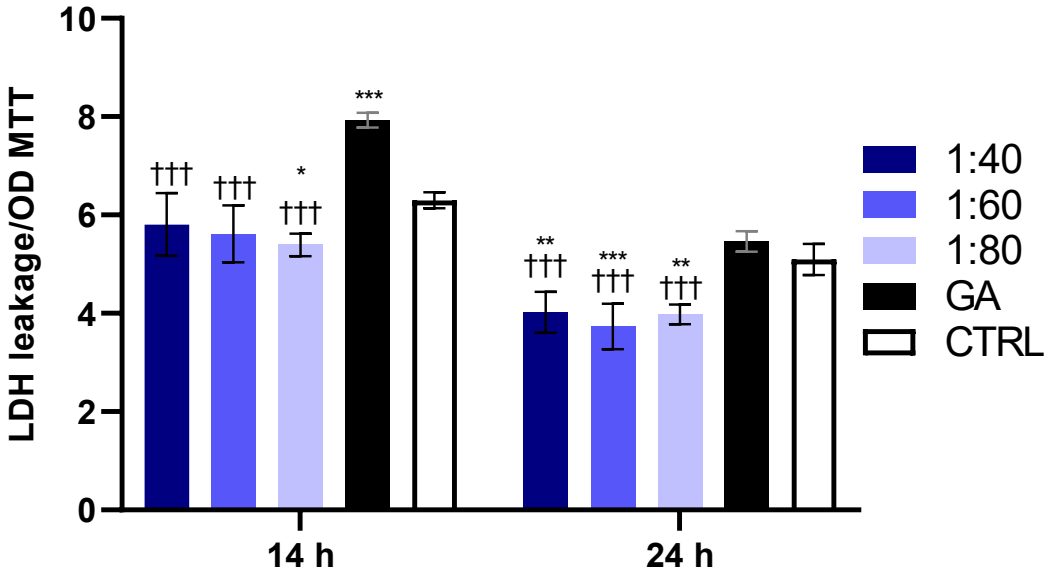


Figure 20: LDH release in HaCaT cells exposed to SS at 1:40, 1:60, and 1:80 dilutions and to GA (4.1 mM) for 14 and 24 h. LDH leakage values were normalized on MTT OD values. Data are presented as mean ± SD of three independent experiments; 14 h: * $p < 0.05$ vs. CTRL; *** $p < 0.01$ vs. CTRL; ††† $p < 0.001$ vs. GA; 24 h: ** $p < 0.01$ vs. CTRL; *** $p < 0.001$ vs. CTRL; ††† $p < 0.001$ vs. GA.

3.2.1.3 Measurement of ROS Level after SS and GA Treatment

To assess the impact of SS and GA on intracellular ROS generation, flow cytometric analysis was conducted on H2DCFDA-labeled HaCaT cells. After 6 h of exposure, the 1:60 and 1:80 SS dilutions, as well as GA, produced a significant elevation in ROS levels relative to the control, whereas the 1:40 SS dilution resulted in a reduction in ROS production. Notably, all SS-treated groups displayed lower ROS accumulation compared to GA-treated cells (Figure 21A). By 18 h, ROS levels reached a plateau, with no significant differences observed between SS- or GA-treated cells and the control, nor among cells exposed to the various SS dilutions in comparison with GA-treated cells (Figure 21B).

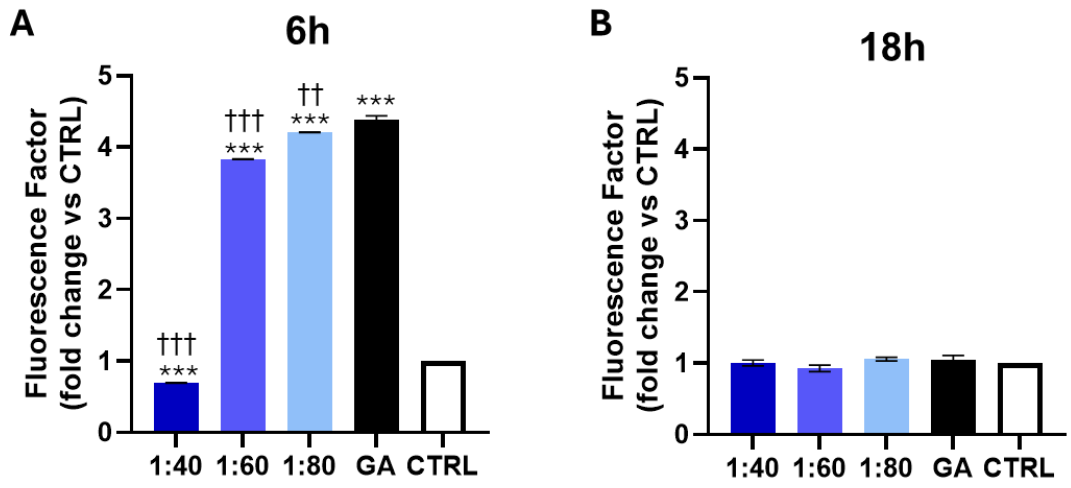


Figure 21: ROS levels measured by flow cytometry after 6 (**A**) and 18 h (**B**) of treatment with SS at 1:40, 1:60, and 1:80 dilutions and with GA (4.1 mM). Histograms represent median values ± SD of three independent experiments in which the Y axis reports mean fluorescence intensity (MFI) generated by the oxidation of H2DCFDA (generation of intracellular ROS) and is reported as fold change vs. CTRL. *** $p < 0.001$ vs. CTRL; ††† $p < 0.001$ vs. GA; †† $p = 0.01$ vs. GA.

3.2.1.4 Effect of SS and GA Treatment on PI3K/Akt/NF-κB Protein levels

The PI3K/Akt/NF-κB signaling axis is a central regulatory cascade activated in response to ROS accumulation, particularly during conditions of mild inflammation. For this reason, the protein expression profiles of these mediators were examined following 14 and 24 h of treatment with SS and GA. After 14 h, PI3K expression was significantly elevated across all SS-treated groups (1:40, 1:60, and 1:80) as well as in the GA-treated group (4.1 mM), relative to control. Nevertheless, PI3K levels in the 1:40 and 1:60 SS-treated samples were significantly lower when compared with GA-treated cells. By 24 h, PI3K expression was markedly reduced in all SS- and GA-exposed groups compared to the control, with the 1:80 SS dilution exhibiting an additional significant decrease relative to GA-treated cells (Figure 22A).

Regarding the p-Akt/Akt ratio, a 14 h exposure period was sufficient to induce a significant increase in all SS- and GA-treated groups relative to the control. Within this timeframe, treatment with the 1:40 SS dilution resulted in a significant reduction in the p-Akt/Akt ratio compared with GA, whereas the 1:80 SS dilution produced a significant increase relative to GA. After 24 h, both the 1:40 and 1:80 SS groups displayed a

significant decrease in the p-Akt/Akt ratio when compared to the control and to GA-treated cells (Figure 22B).

For NF-κB, protein expression was significantly elevated after 14 h in cells treated with the 1:60 and 1:80 SS dilutions, as well as in GA-treated cells, relative to the control. However, NF-κB levels in the 1:40 and 1:60 SS groups were significantly lower than those observed in GA-treated cells. After 24 h, NF-κB expression was significantly reduced in all SS- and GA-treated samples compared to the control. Notably, the 1:40 SS dilution resulted in a further significant decrease relative to GA-treated cells (Figure 22C).

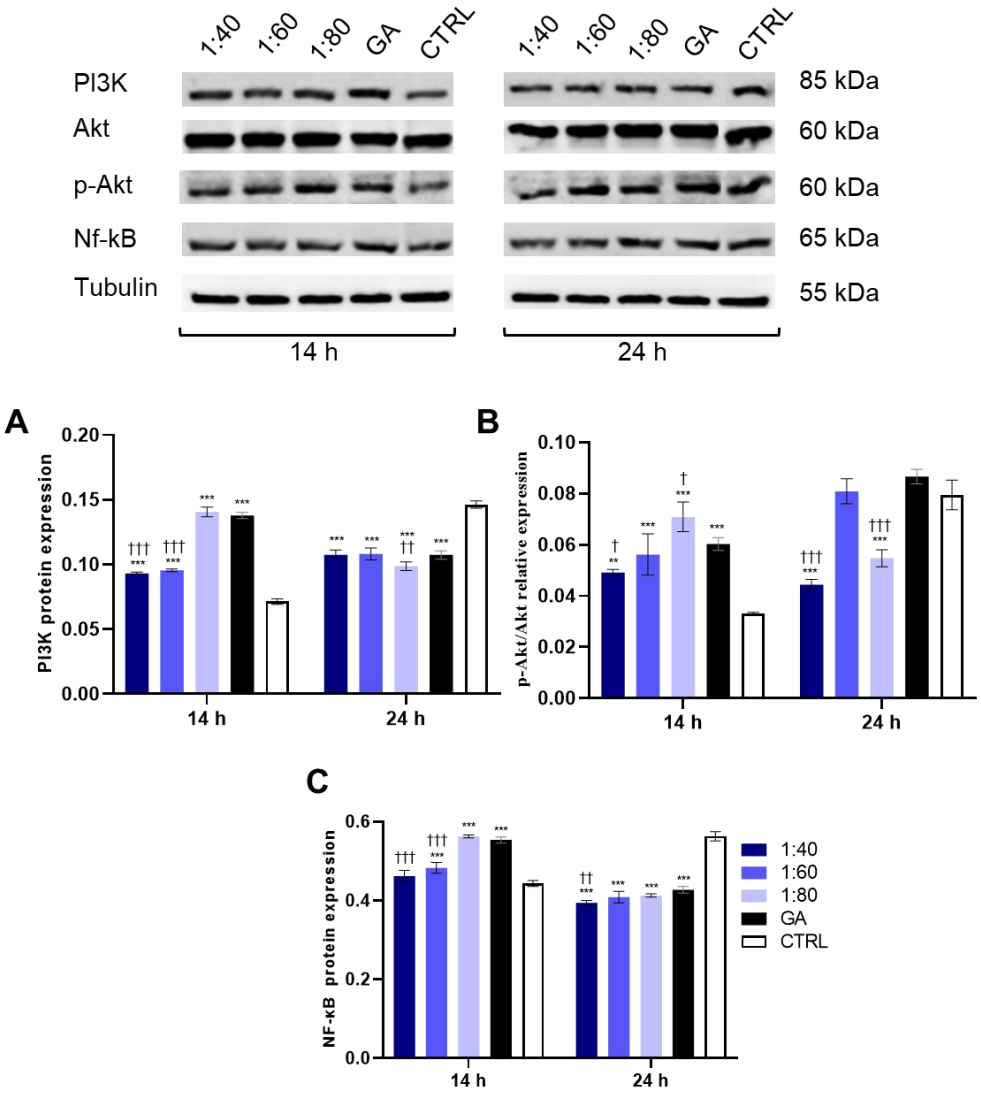


Figure 22: Densitometric analysis of Western blotting of PI3K (**A**), Phospho-Akt (p-Akt) and Akt (**B**), and NF-kB (**C**) expression levels in HaCaT cells treated with SS at 1:40,

1:60, and 1:80 dilutions and with GA (4.1 mM) for 14 and 24 h. The graphs represent a densitometric analysis of protein expression levels normalized on tubulin expression levels. Data are presented as the mean ± SD of three independent experiments. A: 14 h: *** $p < 0.001$ vs. CTRL; ††† $p < 0.001$ vs. GA; 24 h: *** $p < 0.001$ vs. CTRL; †† $p < 0.01$ vs. GA. B: 14 h: ** $p < 0.01$ vs. CTRL; *** $p < 0.001$ vs. CTRL; † $p < 0.05$ vs. GA; 24 h: *** $p < 0.001$ vs. CTRL; ††† $p < 0.001$ vs. GA. C: 14 h: *** $p < 0.001$ vs. CTRL; ††† $p < 0.001$ vs. GA; 24 h: *** $p < 0.001$ vs. CTRL; †† $p < 0.01$ vs. GA.

3.2.1.5 Assessment of SS Modulated Inflammatory Response

To assess the inflammatory response of HaCaT cells following exposure to SS and GA, COX-2 gene and protein expression levels were examined. COX-2 mRNA expression was quantified after 6 and 24 h of treatment. At 6 h, all SS-treated groups exhibited a statistically significant reduction in COX-2 gene expression compared to the control. Moreover, the 1:40 and 1:80 SS dilutions showed a further significant decrease relative to GA-treated cells. At 24 h, GA treatment resulted in a significant upregulation of COX-2 gene expression compared to the control, whereas all SS dilutions (1:40, 1:60, 1:80) displayed a significant downregulation relative to GA-treated cells (Figure 23A).

COX-2 protein expression was evaluated after 48 h of treatment. GA induced a statistically significant increase in COX-2 protein levels compared to the control, while none of the SS-treated samples demonstrated significant changes relative to the control. Notably, the 1:60 and 1:80 SS dilutions elicited a significant reduction in COX-2 protein expression compared to GA-treated cells (Figure 23C).

To further support these observations, IL-6 release into the culture supernatant was quantified after 48 h of treatment using ELISA. The 1:60 SS condition resulted in a statistically significant decrease in IL-6 secretion compared to both the control and GA-treated groups (Figure 23B).

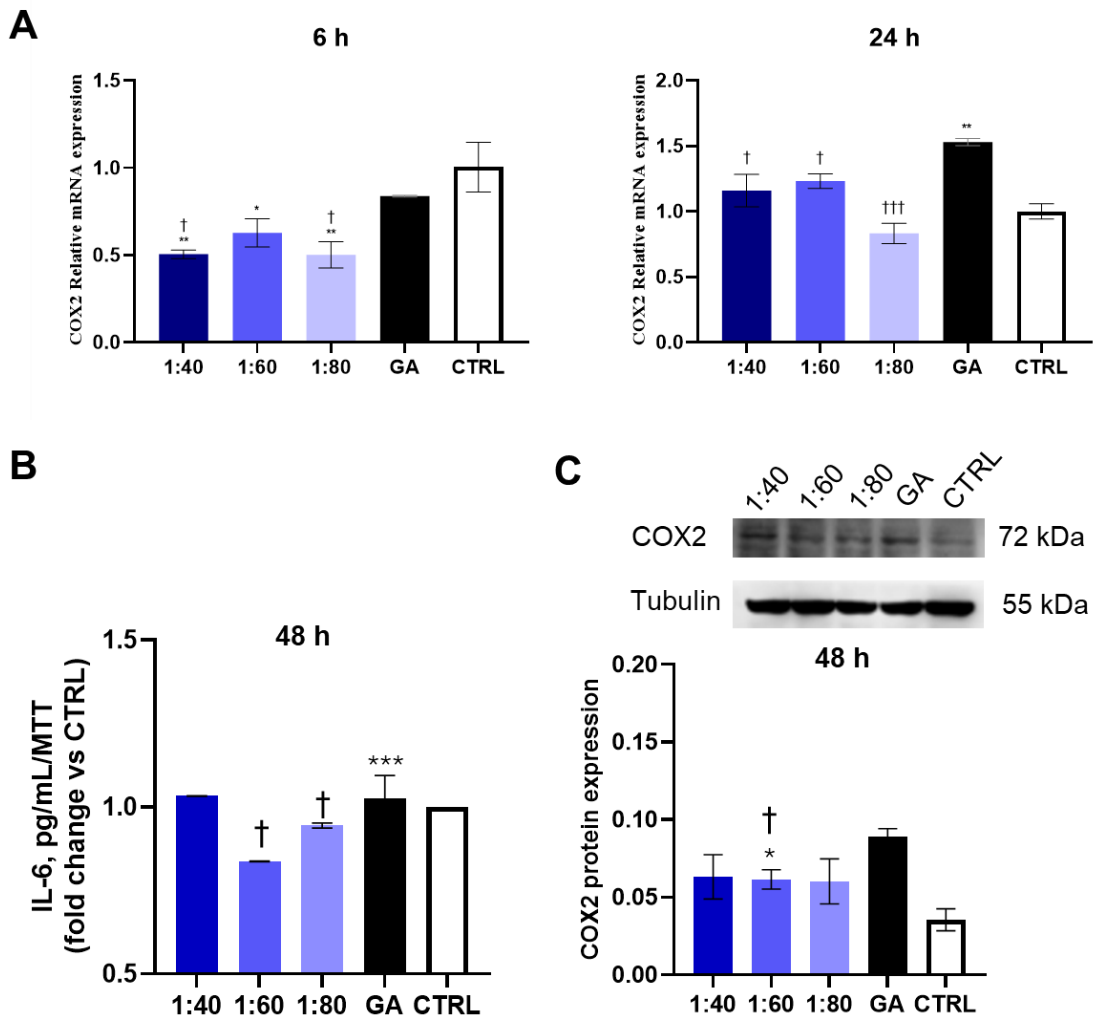


Figure 23: A: COX2 gene expression in HaCaT cells treated with SS at 1:40, 1:60, and 1:80 dilutions and with GA (4.1 mM) for 6 and 24 h, analyzed by RT-PCR. COX2 gene expression was normalized with respect to GAPDH. Data are presented as mean ± SD; 6 h: ** $p < 0.01$ vs. CTRL; * $p< 0.05$ vs. CTRL; † $p < 0.05$ vs. GA; 24 h: ** $p < 0.01$ vs. CTRL; † $p < 0.05$ vs. GA; ††† $p < 0.001$ vs. GA. **B**: ELISA assay for IL−6 secretion after 48 h of SS and GA treatment. IL−6 levels are reported as pg/mL normalized on MTT and presented as fold change vs. CTRL. * $p < 0.05$ vs. CTRL; † $p < 0.05$ vs. GA. **C**: COX2 protein expression levels in HaCaT cells treated with SS at 1:40, 1:60, and 1:80 dilutions and with GA (4.1 mM) for 48 h. The graph represents a densitometric analysis of protein expression levels normalized on tubulin. Data are presented as mean ± SD of three independent experiments. *** $p < 0.001$ vs. CTRL; † $p < 0.05$ vs. GA.

3.2.1.6 Analysis of Matrix Metalloproteinases (MMPs) Gene Expression

To investigate the effects of SS and GA on extracellular matrix (ECM) remodeling, the expression of MMPs was evaluated in HaCaT following 6 and 24 h of treatment. Specifically, the gene expression levels of MMP-2 and MMP-9 were assessed. After 6 h, the 1:40 and 1:80 SS-treated groups exhibited a statistically significant increase in MMP-2 expression compared to both the control and GA-treated cells. At 24 h, only the 1:80 SS dilution sustained a significantly elevated MMP-2 expression level relative to the control and GA-treated groups (Figure 24A).

Regarding MMP-9, the 1:40 SS-treated group showed a significant upregulation at 6 h compared to both the control and GA-treated cells. After 24 h, the 1:40 and 1:80 SS-treated groups, as well as GA-treated cells, displayed significantly increased MMP-9 expression relative to the control (Figure 24B).

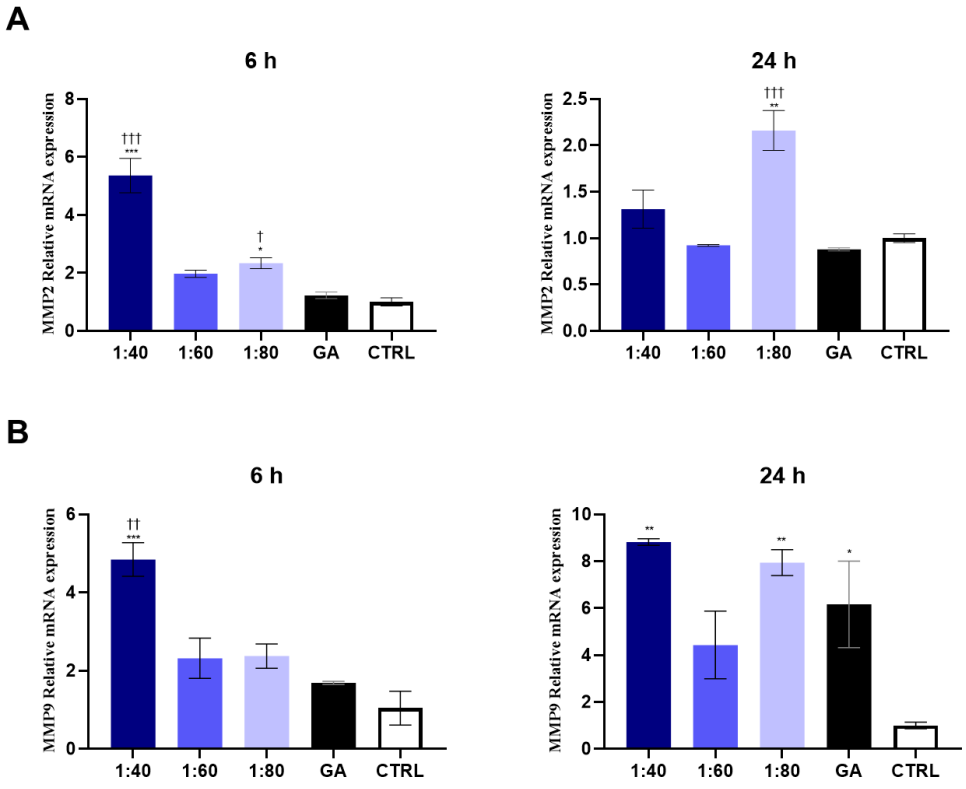


Figure 24: MMP−2 (**A**) and MMP−9 (**B**) gene expression in HaCaT cells treated with SS at 1:40, 1:60, and 1:80 dilutions and with GA (4.1 mM) for 6 and 24 h, analyzed by RT-PCR. Data are normalized on GAPDH and are expressed as mean ± SD of three independent experiments. A: 6 h: *** $p < 0.001$ vs. CTRL; * $p < 0.05$ vs. CTRL; ††† $p <$

0.001 vs. GA; † $p < 0.05$ vs. GA; 24 h: ** $p < 0.01$ vs. CTRL; ††† $p < 0.001$ vs. GA. B: 6 h: *** $p < 0.001$ vs. CTRL; †† $p < 0.01$ vs. GA; 24 h: ** $p < 0.01$ vs. CTRL; * $p = 0.05$ vs. CTRL.

3.2.1.7 Wound Healing Assessment after SS and GA Treatment

To assess the influence of SS and GA on keratinocyte migration, an essential process in epidermal repair, a wound healing (scratch) assay was conducted. A linear scratch was created in each well to mimic a mechanical injury, and images were captured at 0 h to establish the baseline wound area. Cells were subsequently exposed to SS (1:40, 1:60, 1:80) or GA (4.1 mM), and the extent of wound closure was evaluated after 24 and 48 h by quantifying the remaining wound area relative to baseline. The results revealed that SS enhanced HaCaT motility in a dilution-dependent fashion. At both 24 h and 48 h, the 1:40 and 1:80 SS treatments produced significantly greater wound closure compared to the untreated control. GA also promoted a significant increase in migration at 48 h; however, its effect was consistently lower than that observed with the 1:40 SS condition at both time points (Figure 25). Overall, these observations reinforce the superior regenerative capacity of SS compared to isolated GA in facilitating re-epithelialization.

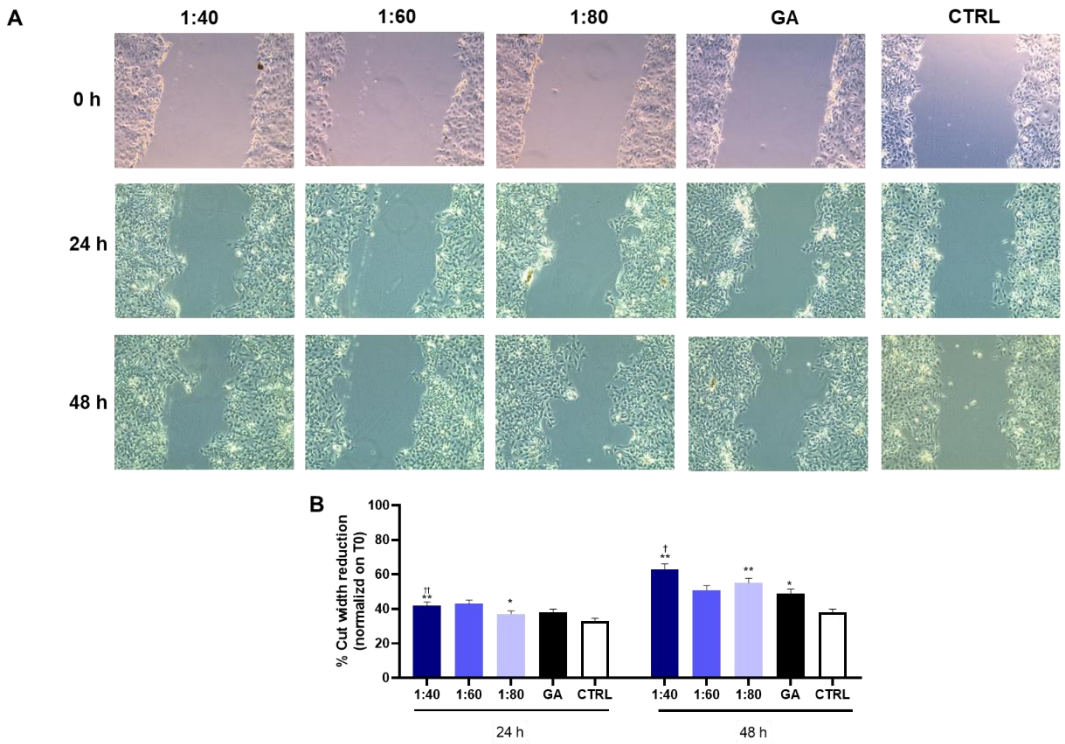


Figure 25: Wound healing assay in HaCaT cells after treatment with SS at different concentrations (1:40, 1:60, 1:80) and GA (4.1 mM). **A**: Representative images are

reported, acquired at 10X magnification. **B**: Bar graph displays the percentage of cut width reduction after 24 h and 48 h of treatment, normalized on the cut measurement at T0. * $p < 0.05$ vs. CTRL; ** $p < 0.01$ vs. CTRL; † $p < 0.05$ vs. GA; †† $p < 0.01$ vs. GA.

3.2.2 Human Endothelial Cells (ECs) (EA.hy926)

3.2.2.1 Evaluation of Cell Viability

The metabolic activity of EA.hy926 cells was quantified using the MTT assay following 24, 48, and 72 h of exposure to SS and GA. At the 24 h time point, cells treated with the 1:40 SS dilution exhibited a significant decrease in viability relative to GA-treated cells, whereas the 1:60 SS condition resulted in a marked increase in metabolic activity compared to both the GA group and the control. After 48 h, treatments with 1:40 and 1:60 SS led to significantly enhanced cell viability when compared with GA-exposed cells as well as the control. By 72 h, all SS dilutions (1:40, 1:60, 1:80) produced a notable elevation in viability, surpassing both GA-treated cells and the untreated control (Figure 26).

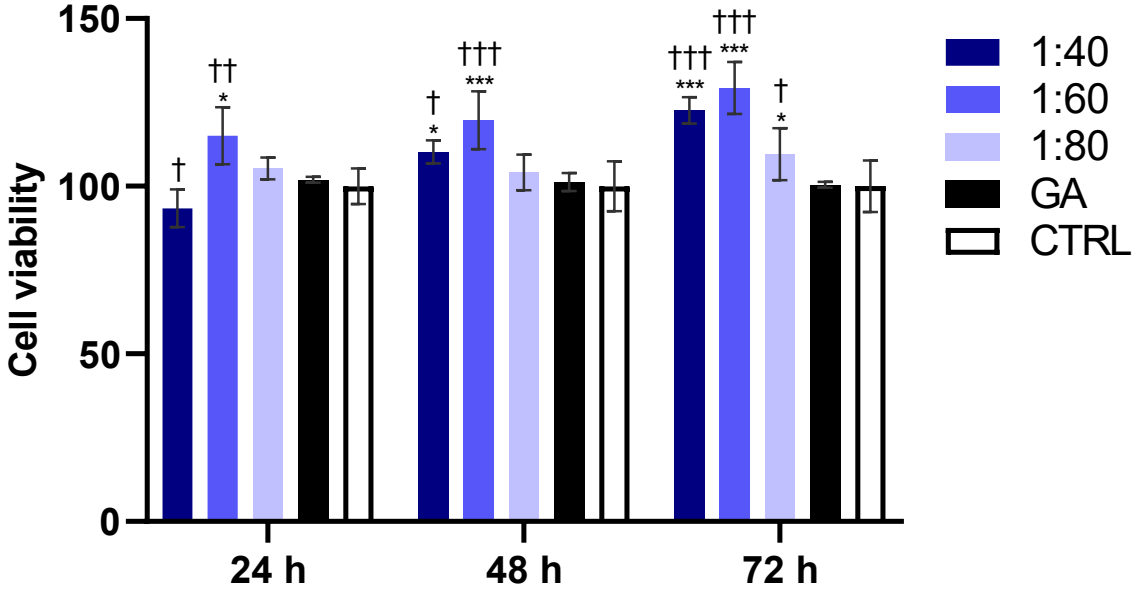


Figure 26: MTT assay performed on EA.hy926 after treatment with 1:40, 1:60, and 1:80 SS dilutions and with GA (4.1 mM) for 24, 48, and 72 h. Percentage of viable cells was normalized with control treated with DMEM and adjusted at 100 %. Data are shown as mean ± SD of three independent experiments. For 24 h: * $p < 0.01$ vs. CTRL; † $p < 0.05$

vs. GA; †† $p < 0.01$ vs. GA; for 48 h: * $p < 0.05$ vs. CTRL; *** $p < 0.001$ vs. CTRL; † $p < 0.05$ vs. GA; ††† $p < 0.001$ vs. GA; for 72 h: * $p < 0.05$ vs. CTRL; *** $p < 0.001$ vs. CTRL; † $p < 0.05$ vs. GA; ††† $p < 0.001$ vs. GA.

3.2.2.2 Wound Healing Assessment after SS and GA Treatments

The wound healing assay was conducted in endothelial EA.hy926 cells to assess their migratory behavior following exposure to SS and GA. A linear scratch was introduced into each well containing confluent monolayers, and images of the wound area were captured immediately prior to treatment (0 h). Cells were subsequently treated with SS at dilutions of 1:40, 1:60, and 1:80, or with GA, and wound closure was evaluated after 18 h by acquiring a second set of images. Quantitative analysis of the wound area was then performed to calculate the percentage of closure relative to baseline.

After 18 h of treatment, all SS dilutions (1:40, 1:60, and 1:80) significantly enhanced endothelial cell migration, resulting in greater wound closure compared to GA-treated cells. In contrast, GA exposure led to a statistically significant reduction in wound closure relative to the control, indicating an impaired migratory response under these conditions (Figure 27). Collectively, these findings demonstrate that SS promotes endothelial cell migration more effectively than isolated GA, further supporting its potential role in facilitating tissue regeneration.

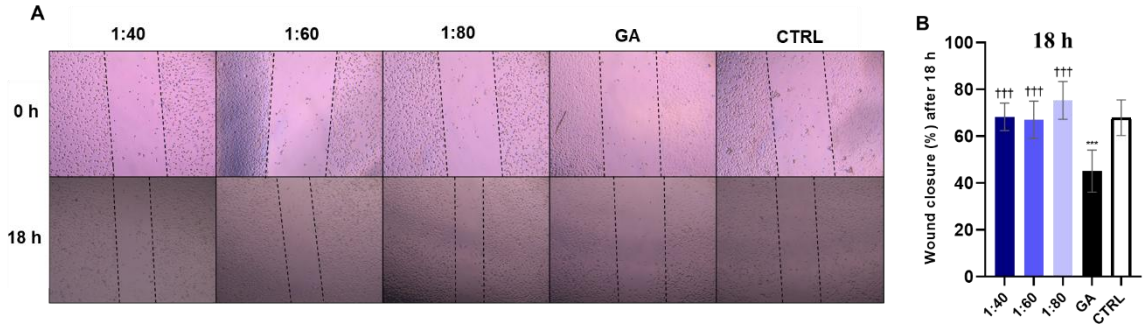


Figure 27: Wound healing assay in EA.hy926 cells after treatment with SS at different concentrations (1:40, 1:60, 1:80) and GA (4.1 mM). **A**: Representative images are reported, acquired at 5X magnification. **B**: Bar graph displays percentage of cut width reduction after 18 h of treatment, normalized on cut measurement at T0. *** $p < 0.001$ vs. CTRL; ††† $p < 0.001$ vs. GA.

3.2.3 Normal Human Dermal Fibroblasts (NHDFs)

3.2.3.1 Evaluation of Cell Viability

Considering the growing use of SS in dermatological formulations, its impact on dermal fibroblasts was determined using an MTT assay, which measures cell metabolic activity and, indirectly, cell viability. NHDFs were treated with three different concentrations of SS, 1:40, 1:60, and 1:80 up to 48 h. After 24 h, cells exposed to SS 1:40 and 1:80 dilutions show a significant increase in cell viability compared to control. After 48 h of treatment, this trend appears even more pronounced and all the SS dilutions (1:40, 1:60, 1:80) lead to record a marked and significant increase in cell metabolic activity with respect to control (Figure 28).

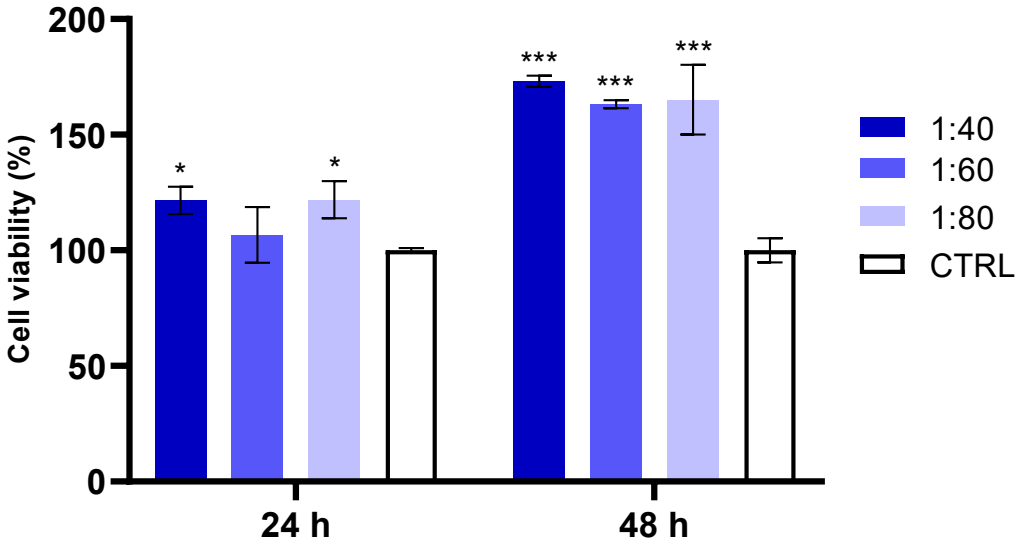


Figure 28: MTT test performed on NHDFs treated with different dilutions of SS (1:40, 1:60, 1:80) for 24 and 48 h. The reported percentage of viable cells is relative to the control and adjusted at 100 %. Bars show the mean ± SD versus control. For 24 h *vs CTRL $p<0.05$; for 48 h ***vs CTRL $p<0.0001$.

NHDF viability was also measured by the Alamar blue assay after 24, 48 and 72 h of SS treatment. After 24 h of treatment, no significant change in cell viability was detected, after 48 h of treatment, SS 1:40 and after 72 h, SS 1:60 significantly increased the cell viability with respect to control (Figure 29).

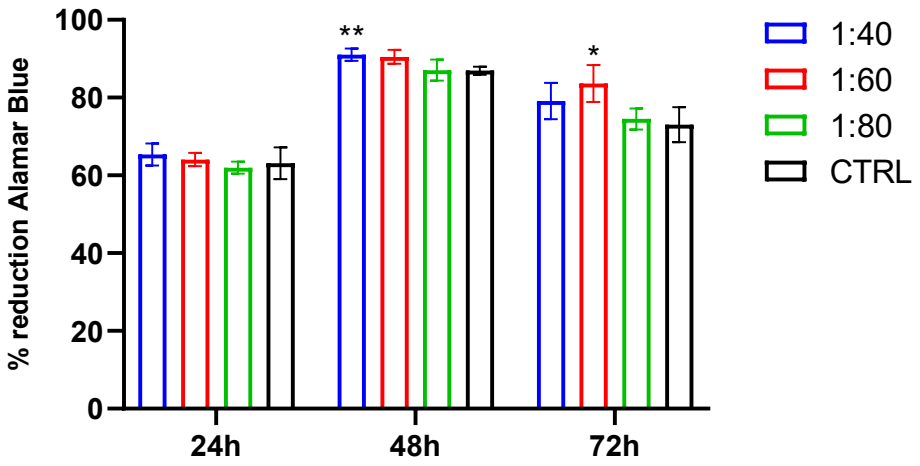


Figure 29: Alamar blue assay in NHDFs, treated with different concentrations of SS (1:40, 1:60, 1:80) for 24, 48, and 72 h. The histogram represents Alamar blue reduction percentage; data shown are the mean (±SD) of three separate experiments. 48h: ** *vs* CTRL $p<0.001$, 72h **vs* CTRL $p<0.01$

3.2.3.2 Proteomics Results

Protein groups detected and quantified in all the triplicates of a treatment group were selected for analysis and only the SS 1:60 after 48 h of treatment shows a significant number of protein groups against the control . Venn diagram shows the DAP obtained by statistically analysing the individual proteins against the CTRL with $p<0.05$. While only 62 DEP were common to all SS concentrations (1:40, 1:60, 1:80) at 24 h, this number increased dramatically to 361 common proteins after 48 h (Figure 30).

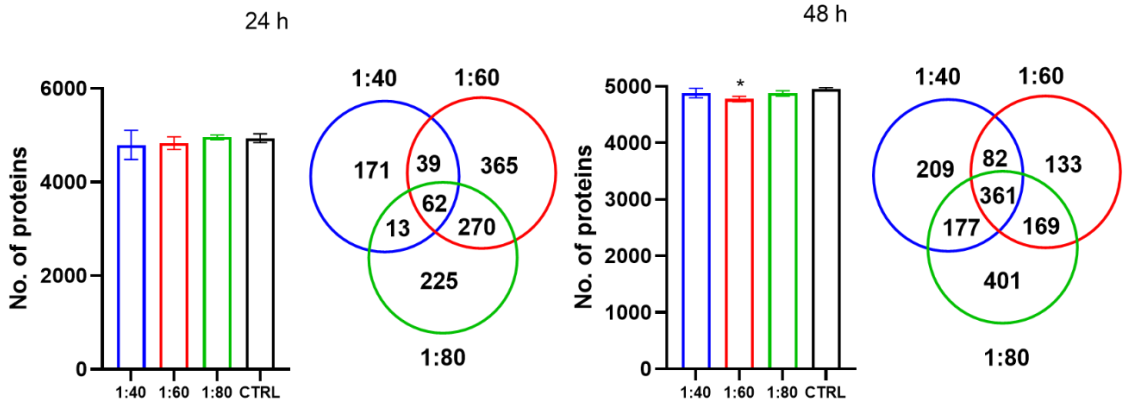


Figure 30: The mean number of proteins detected in each treatment group exposed to different dilutions of SS after 24 and 48 h. The bars represent the proteins quantified in

three replicates of each treatment group. *p < 0.05 *vs* CTRL. Venn diagrams show the DEP in each treatment group compared to the control, with p < 0.05.

a. String Network Analysis

The unique proteins obtained from the Venn diagrams above, after 24 and 48 h of SS treatment, were merged and a string analysis was performed for protein visualization and to determine the protein-protein interactions (PPIs). The string network in Figure 31 shows three highly connected clusters that correspond to functional modules or protein complexes that work together to perform specific biological processes and some small clusters are also present.

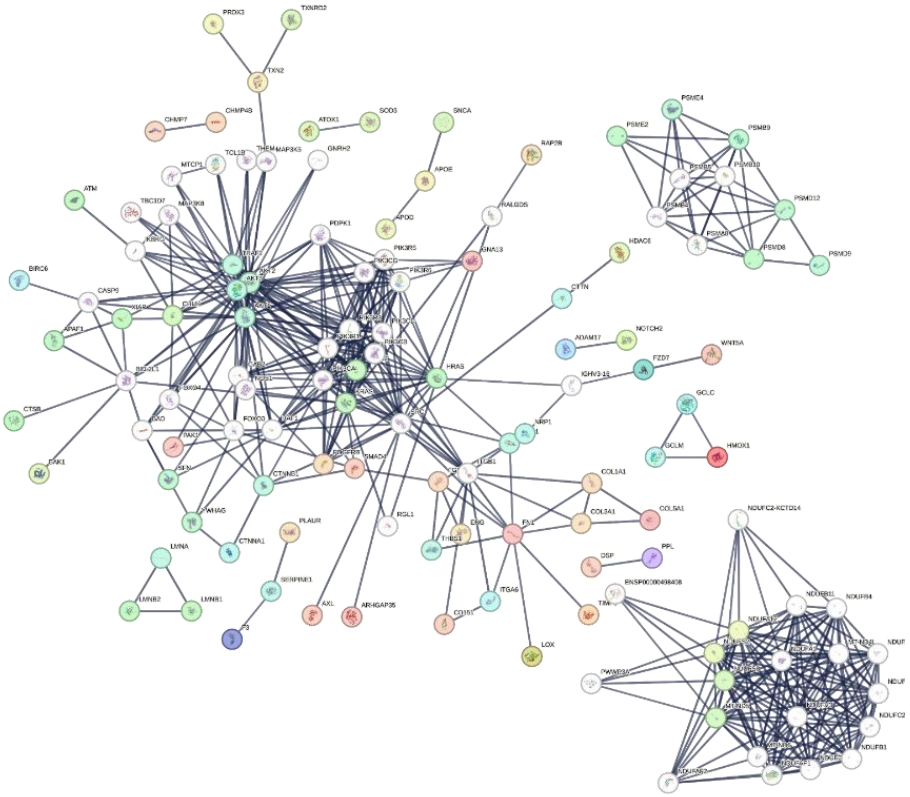


Figure 31: String network analysis of differentially abundant proteins (DAP). The confidence set to the highest (0.9) with the second shell having no more than 50 interactors, while keeping the disconnected nodes hidden in the network.

b. Gene Ontology (GO) Enrichment

The GO enrichment of selected terms was also performed, showing the five most abundant biological functions based on gene count (Figure 32). The group similarity was

set to 0.8 and the hight number of genes counted (n=65) for the regulation of programmed cell death, followed by others response to oxidative stress (n=52), wound healing (n=45), positive regulation of cell migration (n=34) and a few for aging (n=10).

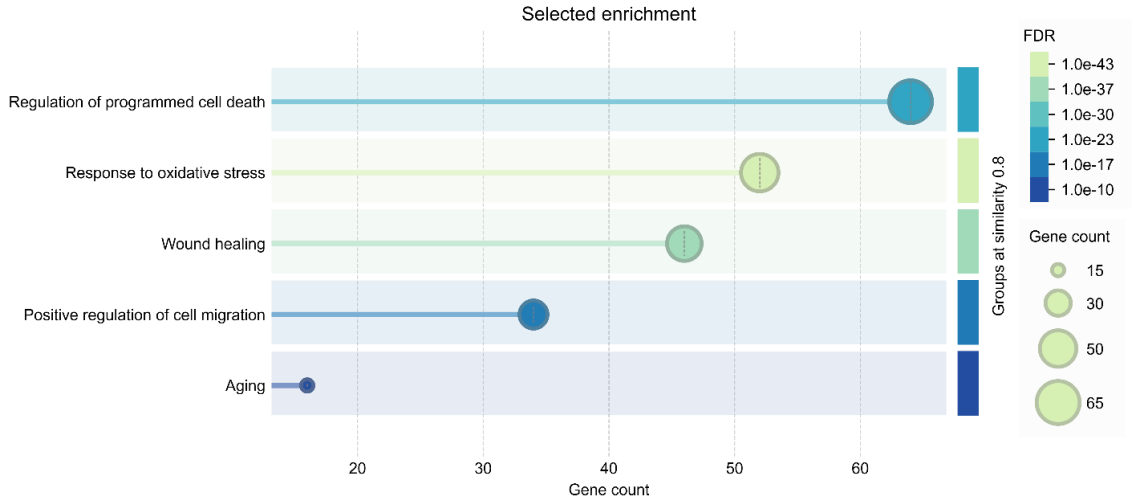


Figure 32: Functional enrichment visualization of selected terms by GO for DAP. The group similarity was set to 0.8 and terms were sorted based on gene count.

c. CytoHubba Analysis

The top 10 hub proteins were identified from the DAP and results show that AKT family, also known as protein kinase B (PKB), is a family of serine/threonine-specific protein kinases, is present in highest number followed by PI3K (Phosphoinositide 3-Kinase) family, SRC (Proto-oncogene tyrosine-protein kinase Src) and the KRAS family (Figure 33). All these proteins are involved in various cell signalling pathways that control cell growth, metabolism, and cell survival and related functions.

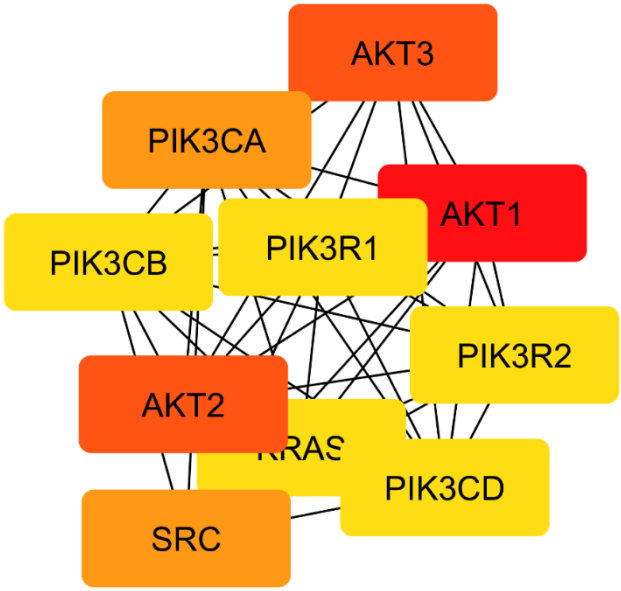


Figure 33: Top 10 hub proteins identified by CytoHubba Cytoscape plugin. Proteins with the highest number of connections in the network are detected as hub proteins. The image shows the degree of importance of hubs through a color scale ranging from red (high) to yellow (low).

3.2.3.3 Evaluation of programmed cell death occurrence

SS effect on NHDF apoptosis and necrosis induction was analyzed through a flow cytometry application, in order to validate the proteomic data. After 24 h of SS treatment a statistically significant increase of live cells percentage (Annexin V^-/PI^-) is detected comparing all the three SS dilutions (1:40, 1:60 and 1:80) with the control. The percentage of necrotic cells (Annexin V^-/PI^+) and early apoptotic cells (Annexin V^+/PI^-) after SS administration appears comparable to those observed in the CTRL and, nevertheless, accounted for a negligible proportion (approximately 2%). The percentage of late apoptotic cells (Annexin V^+/PI^+) after treatment with 1:40, 1:60 and 1:80 is significantly lower compared to the percentage recorded in the control group. After 48 h, an opposite pattern was observed: a slight, but statistically significant reduction (around 20%) in the percentage of live cells is detected after treatment with the three SS dilution with respect to control, with a major extent for 1:80 dilution. The amount of necrotic and early apoptotic cells remains unchanged compared with that observed after 24 h of treatment, while the percentage of late apoptotic cells appear significantly increased after SS exposure with respect to the control, again with a major extent for 1:80 dilution (Figure 34).

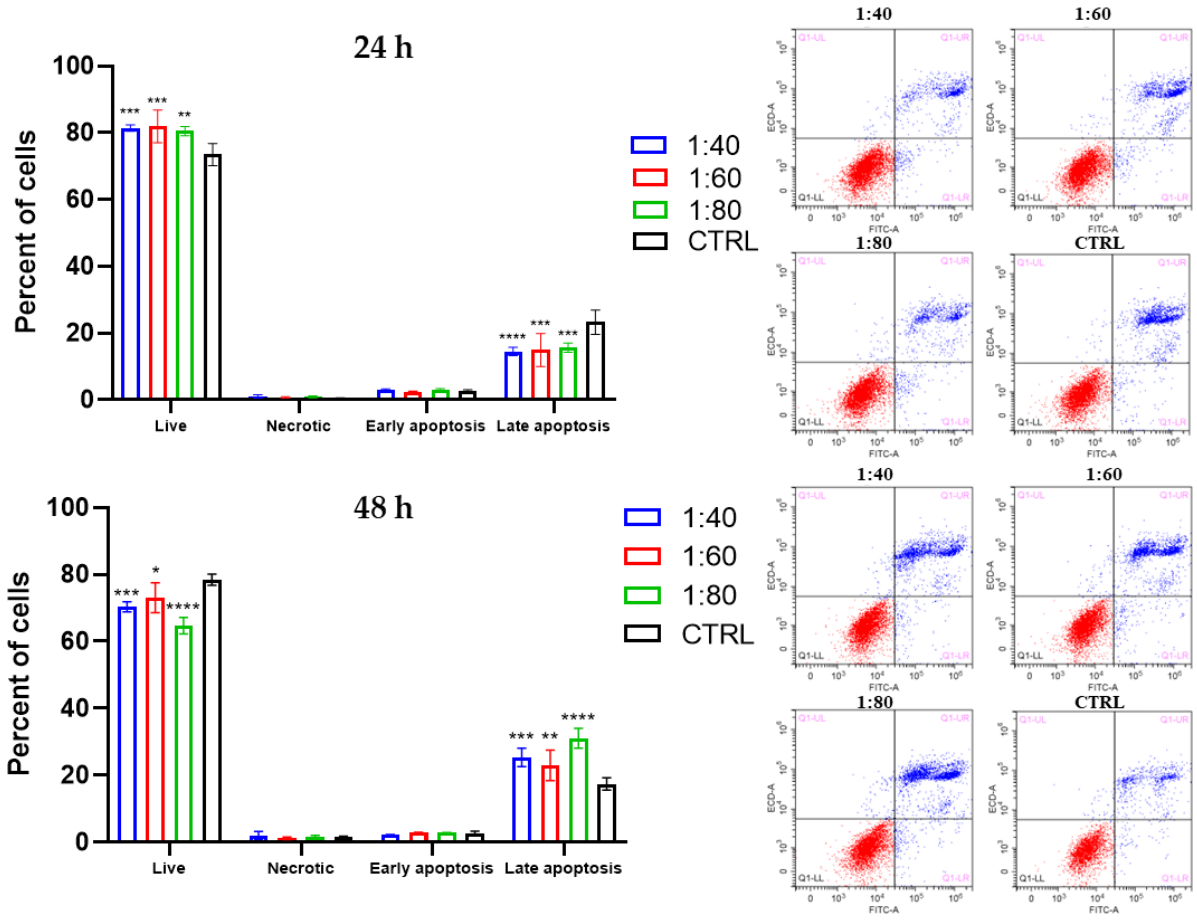


Figure 34: Flow cytometry analysis of apoptosis induction in NHDFs after 24 and 48 h of SS (1:40, 1:60, 1:80) treatment. Percentages of Annexin/PI-stained cells analyzed by flow cytometry are shown. Histograms represent the percentage of total apoptotic cells (Annexin V^+/PI^+) reported as mean ± SD of three independent experiments. Representative dual-parameter fluorescence density dot plots are displayed close to the histograms. For 24 h: ****p<0.0001, ***p<0.0005, **p<0.005 *vs* CTRL; for 48 h: ****p<0.0001, ***p<0.0005, **p<0.01, *p<0.05 *vs* CTRL.

3.2.3.4 Pro and Antiapoptotic Protein Expression Analysis

The two main proteins that work antagonistically during the process of programmed cell death are Bax a proapoptotic, and Bcl-2 an antiapoptotic. To measure the effect of SS treatment on programmed cell death in NHDFs by a non-proteomic method, Bax and Bcl-2 protein expression were evaluated by western blot analysis. After 24 h of SS treatment, Bax expression level in all the SS 1:40 and 1:80 treatment groups were significantly higher and in 1:80 it was significantly lower than control while after 48 h it was significantly higher in SS 1:40 and decreased significantly in SS 1:60 and 1:80 with

respect to control (Figure 35A). Conversely, in the case of Bcl-2, all the SS treated groups show significantly higher protein expression than the control after 24 and 48 h (Figure 35B).

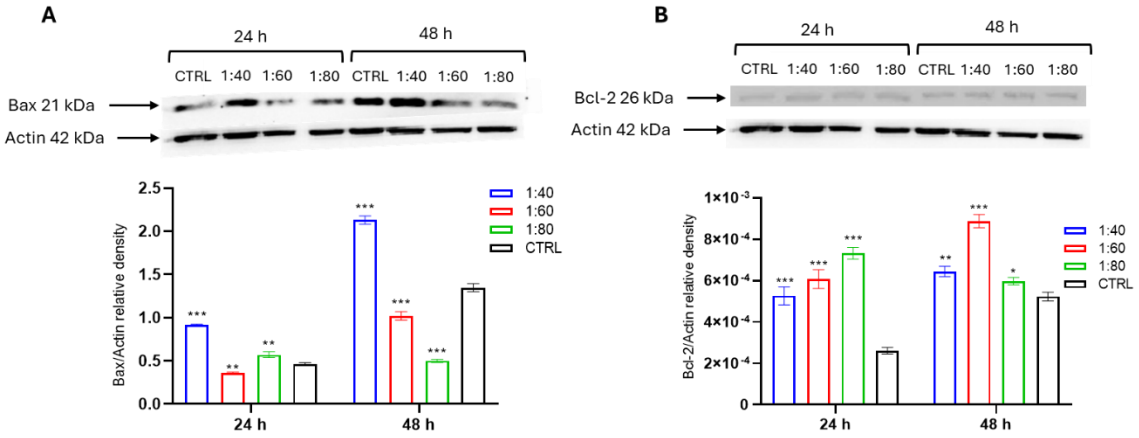


Figure 35: Western blot analysis of (**A**) Bax and (**B**) Bcl-2 in NHDFs exposed to different dilutions of SS (1:40, 1:60, 1:80) and CTRL. The graph represents a densitometric analysis of protein expression levels normalized to actin expression levels. Data are presented as the mean ± SD of three independent experiments. ***p<0.0001, **p<0.005, *p<0.05 *vs* respective CTRL.

3.2.3.5 Antioxidant Capacity Assessment

The antioxidant capacity of NHDFs was quantified following a 24-h treatment with various dilutions of SS (1:40, 1:60, 1:80). A significant increase in antioxidant activity was observed in all SS-treated groups compared to the control, indicating that SS treatment robustly enhances the free radical scavenging potential of dermal fibroblasts (Figure 36A).

Intracellular ROS release level in NHDFs was measured after 6 and 24 h of SS (1:40, 1:60, 1:80) treatment by flow cytometry. After 6 h of treatment, the ROS release level was significantly higher in all the treatment groups compared to control, while after 24 h of treatment, SS significantly reduced the ROS release level in all the treatment groups in a dose-dependent manner (Figure 36C and 36C).

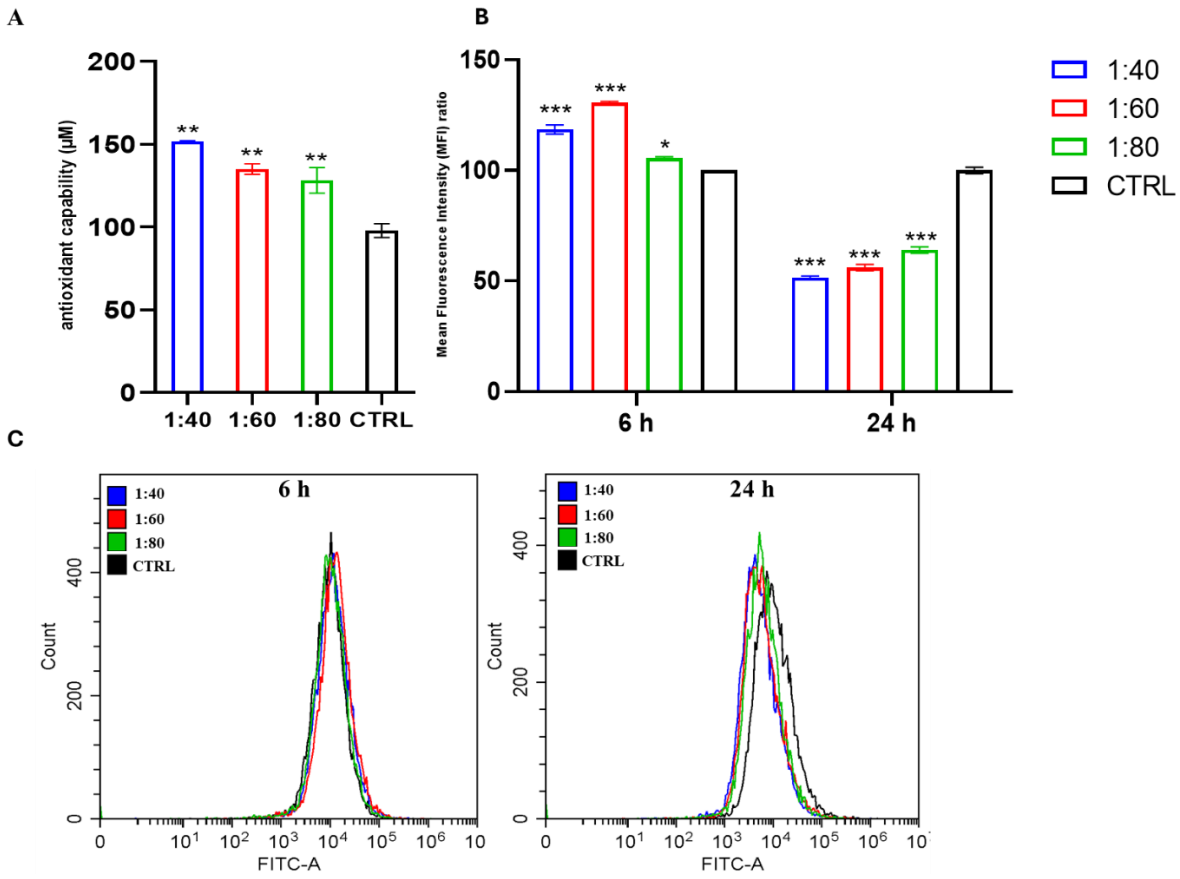


Figure 36: (**A**) Antioxidant capacity in NHDFs treated with 1:40, 1:60, and 1:80 dilutions of SS for 24 h. Histograms represent median values ± SD of three independent experiments. Statistical analysis was performed using one-way ANOVA, followed by Dunnett's multiple comparisons test: ** *vs* CTRL p<0.001. (**B**) Effects of SS at dilutions of 1:40, 1:60, and 1:80 on intracellular ROS production in NHDFs. Intracellular ROS levels were assessed by flow cytometry after 6 and 24 h of treatment. The histogram represents the median fluorescence intensity (MFI), reported as fold change versus control (CTRL), and are expressed as mean ± SD of three independent experiments. (**C**) Representative overlay plots are shown. The Y-axis indicates MFI generated by the oxidation of H_2DCFDA, reflecting intracellular ROS production. 6 h, ***p < 0.0001 and *p < 0.01 *vs* CTRL; 24 h, ***p < 0.0001 *vs* CTRL.

3.2.3.6 Wound Healing Analysis

The effect of SS on cell migration was evaluated using a scratch wound healing assay. Treatment with all SS dilutions (1:40, 1:60, 1:80) resulted in a statistically significant enhancement of NHDFs migration compared to the control. Remarkably, all SS-treated

groups achieved complete wound closure (100%) within the 24-h experimental period, demonstrating the potent pro-migratory activity of SS (Figure 37).

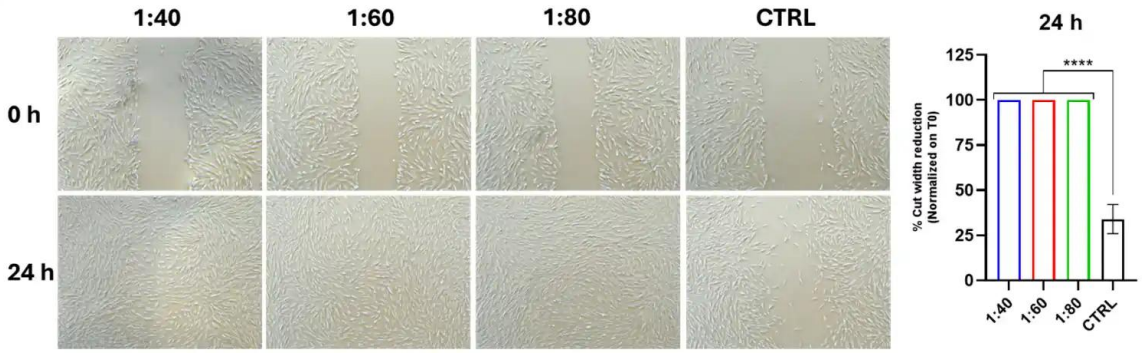


Figure 37: Wound healing assay in NHDFs after treatment with SS at different concentrations. Representative images are reported, acquired at 5X magnification at 0 h and 24 h after treatment. Bar graph displays the percentage of cut width reduction after 24 h of treatment, normalized on the cut measurement at T0. ****$p<0.0001$ *vs* CTRL.

4 DISCUSSION

4.1 Chemical Characterization of Snail Slime

Recent developments in analytical methodologies have significantly expanded our ability to characterize the chemical composition of complex mixtures such as SS. Using MS and NMR spectroscopy, Vassilev *et al.* [34] identified more than twenty metabolites in *Helix aspersa* mucus, offering important insights into its diverse biological functions. Similarly, GC–MS investigations on the mucus of *Monacha obstructa*, *Theba pisana*, and *Eobania vermiculata* revealed nine predominant volatile constituents, with hexamethylcyclotrisiloxane (MW 222.06) and methoxy phenyl oxime (MW 151.06) being the most abundant [35]. Moreover, elemental profiling via ICP-AES and FAAS has shown that *A. fulica* slime contains appreciable quantities of key trace minerals, including Ca, Mg, Fe, Zn, Cu, and Co [31, 36].

Considering the lack of previous chemical investigations on stabilized and non-stabilized SS, we have deepened our findings to figure that both stabilized and non-stabilized slime samples share an overall comparable NMR metabolite pattern from a qualitative standpoint, although notable quantitative variations are evident. Among the detected metabolites, citrate emerged as the predominant compound in each formulation, with the non-stabilized material exhibiting the highest concentration. This observation aligns with industrial practices, since citrate is routinely incorporated during processing to chemically promote mucus secretion. Sorbate and benzoate were also detected at substantial levels, and as expected, the stabilized formulation displayed nearly double the amount of these compounds, reflecting their deliberate inclusion as preservation agents. For the remaining metabolites, the stabilized preparation generally contained higher quantities relative to the non-stabilized version, with fumarate and alanine representing the only exceptions; however, their variations did not reach statistical significance. Collectively, the data highlight how processing and formulation steps substantially influence the chemical composition of SS, ultimately affecting its functional properties and potential applications. Similar trends have been documented for slime preparations differing in molecular weight [34] and in samples produced in the presence or absence of gold nanoparticles [124].

The SPME-GC/MS findings further demonstrate the extent to which processing treatments alter the volatile fraction of SS. The changes observed in the chromatographic

profiles confirm that the instrumental approach employed is capable of sensitively detecting compositional modifications arising from distinct handling procedures applied to the same biological matrix. To our knowledge, this work represents the first comprehensive investigation of the volatile profile of SS obtained through Headspace-SPME-GC/MS analysis.

IR spectroscopic examination provided confirmatory evidence of several functional groups characteristic of SS [125]. The signal at 516 cm^{-1} is likely attributable to skeletal bending vibrations commonly associated with polysaccharides and structurally complex carbohydrates. Similarly, the absorption near 594 cm^{-1} may correspond to out-of-plane C–H bending typical of glycosidic or polysaccharide linkages. Peaks at 651 cm^{-1} and 682 cm^{-1} can reasonably be assigned to C–S stretching modes, arising from sulfur-containing amino acids such as cysteine within protein constituents. Vibrational bands around 798 cm^{-1} and 887 cm^{-1} reflect C–C and C–O deformations from mucopolysaccharides. A prominent band at 933 cm^{-1} suggests C–H rocking from carbohydrate backbones, whereas the absorption near 1126 cm^{-1}, ascribed to C–O stretching in glycosylated proteins, confirms the strong contribution of glycoproteins to the slime matrix. The 1198 cm^{-1} band corresponds to amide III vibrations, indicative of protein secondary structure, primarily α-helical motifs. A peak at 1323 cm^{-1} may arise from CH_2 symmetric bending or N–H deformation linked to polysaccharides and amino acids. The broad feature at approximately 1400 cm^{-1} reflects vibrations from sugar moieties and amino acid chains. The 1581 cm^{-1} absorption represents amide II (N–H bending coupled with C–N stretching), while the peak centered at 1700 cm^{-1} is attributed to C=O stretching, largely influenced by citric acid but potentially incorporating signals from other carboxylated species. A minor band around 2538 cm^{-1}, although uncommon, may correspond to weakly hydrogen-bonded SH groups or related interactions. Aliphatic C–H stretching appears near 2947 cm^{-1}, whereas aromatic C–H stretching at 3078 cm^{-1} points to phenyl-bearing protein residues. The broad O–H stretching band at 3417 cm^{-1} is consistent with contributions from water, polysaccharides, and glycoproteins.

Raman spectroscopy provided complementary structural insights. The distinctive band at 369 cm^{-1} likely originates from lattice or skeletal vibrational modes typical of carbohydrate-rich matrices. The 684 cm^{-1} peak, associated with OCN bending (amide IV–VII), reflects the protein backbone characteristic of mucin glycoproteins. Peaks positioned at 795 cm^{-1} and 877 cm^{-1} correspond to β-glycosidic C–C/C–O ring modes

and indole vibrations, respectively, the latter evidencing tryptophan residues. The 1005 cm^{-1} band confirms the presence of phenylalanine through benzene ring breathing, while the 1092 cm^{-1} peak indicates C–O stretching, underscoring the role of GAGs and mucopolysaccharides. The 1157 cm^{-1} feature derives from tryptophan's indole ring, and Amide III (1268 cm^{-1}) and amide I (1630 cm^{-1}) bands highlight abundant proteinaceous content. At 1390 cm^{-1}, N–C–N vibrations are evident, and the signal at 1449 cm^{-1} corresponds to CH_2/CH_3 deformations suggestive of lipid traces. Consistent with IR analysis, the peak at 1717 cm^{-1} reflects C=O stretching influenced by citric acid. Aliphatic C–H stretching bands (2943 and 2990 cm^{-1}) confirm hydrocarbon chains from lipids or polysaccharides, while the 3078 cm^{-1} aromatic C–H band suggests aromatic residues such as tyrosine or phenylalanine. The broad N–H stretch near 3195 cm^{-1} evidences protein amide groups, and the analyzed samples, which were lyophilized, the broad water band typical of 3100–3400 cm^{-1} was not present.

TGA analysis revealed several distinct stages of mass loss, reflective of the complex chemical nature of SS. At lower temperatures (35–175 °C), substantial mass loss occurred under both atmospheres, corresponding to the elimination of moisture and the volatilization of small, hygroscopic constituents such as cyclic ethers and furan derivatives. Between 300 and 550 °C, decomposition of organic acids and aromatic components became evident. Under oxidative conditions, compounds such as benzoic acid degraded rapidly, whereas pyrolytic decomposition occurred more gradually under nitrogen. In the 550–600 °C region, more stable constituents, including long-chain carboxylic acids and phenolic derivatives, underwent decomposition, enhanced by oxidation in air and slower pyrolysis under inert conditions. At temperatures of 600–800 °C, degradation of lipids and complex aromatics was observed, with air promoting combustion and nitrogen yielding carbonaceous residues. Above 800 °C, the release of thermally resistant inorganic constituents occurred. In air, this corresponded to residual carbon oxidation and the breakdown of salts such as calcium carbonate, while in nitrogen, a greater proportion of non-combustible material persisted. These observations collectively reflect the intricate mixture of volatile compounds, organic acids, aromatic molecules, lipids, and mineral components present in SS [126, 127].

DSC analysis did not reveal distinct melting temperature (Tm) or crystallization temperature (Tc) transitions for either the liquid or lyophilized SS samples, although the technique effectively characterized their stability under varying thermal conditions [128,

129]. The commercial liquid samples exhibited no structural changes up to 50 °C (Figure 16a), confirming stability within this temperature range. Conversely, the lyophilized material showed broader stability (Figure 16b), preserving integrity up to 70 °C. After cycling at 90 °C, a melting peak emerged at roughly 81 °C, and the similarity between Tm and Tc enthalpies (3.8244 J/g vs. 3.6069 J/g) suggested reversible internal rearrangements rather than destructive degradation. At 100 °C, however, the divergence in Tm (6.1383 J/g) and Tc (4.8116 J/g) enthalpies indicated substantial and partly irreversible structural alterations. Repeated cycling to 100 °C yielded fluctuating Tc values in both enthalpy and peak shape, highlighting the complex thermal behavior of lyophilized SS and the influence of cumulative heat exposure [130, 131].

Growing industrial interest in natural antioxidant sources has stimulated research into phenolic-rich biological materials. SS has recently attracted attention as a potential reservoir of such compounds. Stabilized SS contained a higher total phenolic content (2.56 mg GAE/g) than the non-stabilized sample (1.48 mg GAE/g), values within the broad range previously reported. Alkhadhrh *et al.* [132] documented a significantly higher phenolic content in *Helix aspersa* mucus (150.28 mg GAE/g extract), while Aouji *et al*. [133] reported values spanning 0.16–1.26 mg/g depending on solvent and extraction method. Because phenolic molecules act as radical scavengers and reducing agents, they play an essential role in mitigating oxidative damage. Synthetic antioxidants are widely used in food and pharmaceutical products but exhibit undesirable toxicological profiles, strengthening the case for natural alternatives [134]. The antioxidant response of SS was therefore assessed through several assays, including radical scavenging (ABTS, DPPH), reducing capacity (CUPRAC, FRAP, phosphomolybdenum), and metal chelation. The stabilized formulation exhibited measurable DPPH (3.14 mg TE/g) and ABTS (0.62 mg TE/g) scavenging effects, whereas the non-stabilized sample showed no activity. Earlier studies reported variable antioxidant capacities across different snail species and extraction methods [79, 132, 133]. In all reducing-power assays, the stabilized sample showed superior performance. The non-stabilized slime, however, exhibited greater metal-chelating capacity (5.41 mg EDTAE/g compared with 3.23 mg EDTAE/g), likely attributable to its elevated citrate content, given citrate's well-established chelating properties [135, 136]. The enhanced scavenging and reducing activities of stabilized SS may be linked to the presence of benzoic acid and 2,4-dimethylbenzaldehyde, compounds previously reported to possess moderate antioxidant effects [123, 137]. Structural features

particularly hydroxyl, methoxy, and carboxyl substituents, are known to influence antioxidant capacity across benzoic acid derivatives as discussed by Velika and Kron [138] and Chen *et al* [123].

Enzyme inhibition is another biologically relevant property, particularly with regard to managing metabolic and neurodegenerative disorders such as diabetes, obesity, and Alzheimer's disease. Synthetic inhibitors, including acarbose and galantamine, are clinically effective but may induce adverse effects during long-term treatment [96, 98, 139-141]. This underscores the need for natural inhibitor sources. Only a limited number of studies have evaluated the enzyme-modulating properties of snail mucus. In a previous work by Alkhadhrh *et al.* [132] the tyrosinase inhibitory action of *Helix aspersa* snail mucus was reported with an IC_{50} of 35 µg/mL. The presence of benzoic acid in stabilized slime can be ascribed to its enzyme inhibiting characteristics [142-144]. For example, Liu *et al.* [145] identified benzoic acid as a strong inhibitor of mushroom tyrosinase, demonstrating a non-competitive mode of action. In another study conducted by Guan et [142], benzoic acid and its derivatives were tested for anti-amylase action and benzoic acid exhibited a weak anti-amylase effect with the IC_{50}= 45.25 mM. Additionally, the authors often mentioned that benzene ring with more hydroxyl groups usually improves the ability of the compounds to inhibit amylase. Budryn *et al* [146] examined the inhibitory effects of hydroxybenzoic acid derivatives on cholinesterase and found that the hydrophobic characteristics of benzene rings may enhance these inhibitory effects. In addition, the presence of benzoic acid, 2,5-furandione, 3-methyl can interact with enzymes by covalently or non-covalently modifying functional amino groups (typically lysine residues) in proteins and enzymes, and thus enzymatic activity can be inhibited [147].

The chemical analysis performed on SS underlines that it contains a diverse array of biomolecules likely capable of modulating multiple enzymatic systems through different modes of inhibition, including competitive, non-competitive, and structural modification mechanisms. Such multimodal inhibitory behavior reflects the complex chemical nature of SS and supports the notion that its bioactive components may interact with enzymatic targets through both direct active-site engagement and indirect conformational modulation. This broad inhibitory potential underscores the relevance of SS as a promising natural source of enzyme-modulating molecules, which may provide a viable and potentially safer alternative to widely used synthetic inhibitors, particularly in

therapeutic areas such as metabolic and neurodegenerative disorders, where cholinesterase and related enzymatic pathways play a pivotal role. Taken together, these findings reinforce the hypothesis that SS can serve as a natural reservoir of enzyme inhibitory compounds and may represent an attractive substitute for current synthetic agents. Collectively, SS is rich in bioactive metabolites with antimicrobial and antioxidant properties, and its composition includes glycoproteins, organic acids, and phenolic compounds, supporting its dermatological and pharmaceutical potential. These findings link SS chemical composition to bioactivity, highlighting it as a versatile natural biomaterial whose therapeutic properties are influenced by processing conditions.

4.2 Biological Evaluation of Snail Slime

Previous literature has demonstrated that SS enhances human gingival fibroblasts (HGFs) viability and activates cellular recovery pathways, also due to Erk-mediated signaling. Moreover, SS exhibits notable anti-inflammatory properties, evidenced by a marked downregulation of COX-2 expression, combined with pro-angiogenic and ECM-regulatory effects characterized by increased *Angiopoietin-1* gene expression and elevated collagen-I secretion [11]. Building upon these findings, this work extends the investigation to keratinocytes, the predominant cell population of the epidermis, to clarify how SS contributes to epidermal renewal and skin regeneration. Given that GA is one of the principal constituents of SS, this section provides the first direct comparative evaluation of SS and GA, highlighting their differential modulation of controlled pro-inflammatory events essential for exfoliation and re-epithelialization. Furthermore, recognizing that effective epidermal repair requires adequate vascular support, we also assessed SS biocompatibility in ECs, focusing on its ability to sustain EC migration and angiogenic function. Overall, the study addresses three central aspects: (i) an in-depth assessment of SS effects on HaCaT, representing the outermost epidermal layer; (ii) a comparative evaluation of GA administered alone versus its natural SS matrix, with emphasis on pro-inflammatory activation and ECM remodeling; and (iii) a preliminary analysis of SS effects on EC viability and migration as a basis for future studies on deeper dermal layers.

A first essential step was to assess SS tolerability and potential cytotoxicity in HaCaT cell line, since keratinocytes are directly exposed to topical treatments. HaCaT were treated with SS and GA alone, keeping in mind that GA is well known for its abundance in SS

and for its established role as a mild exfoliating agent that promotes cell turnover at low concentrations and short exposure times [148], primarily through upregulation of GAGs and stimulation of collagen synthesis. Viability results indicated that SS was well tolerated by HaCaT at dilutions between 1:40 and 1:80, whereas GA at equivalent concentrations exhibited a more limited temporal window of biological tolerance. Specifically, in contrast to SS, GA induced a keratinolytic response when exposure was extended to 48 h. This outcome supports the hypothesis that the complex biochemical matrix of SS mitigates the strong keratinolytic activity of GA, even when GA content is higher (as in the 1:40 dilution), likely due to the presence of multiple bioactive molecules. This interpretation is further supported by cytotoxicity assays measuring LDH release. The results revealed a stark contrast between treatments: SS markedly reduced LDH release, indicating high cellular tolerability, whereas GA induced a significant increase in LDH levels, indicative of cytotoxicity. These observations are consistent with the classical findings of Van Scott *et al.*, who reported that prolonged application of GA (over 10 minutes) results in intrinsic cytotoxicity due to deeper skin penetration and conversion to the free acid form, leading to apoptosis, pruritus, edema, and erythema [149]. Collectively, these data underscore a major advantage of SS: it preserves the beneficial exfoliating properties of GA while preventing excessive cytotoxicity, thereby attenuating stress responses in epidermal cells.

HaCaT continuously undergoes cycles of regeneration and exfoliation. This physiological turnover maintains skin hydration and a youthful appearance by replacing senescent cells with newly differentiated HaCaT [150]. Disruption of this balance, whether through impaired regeneration or insufficient desquamation, can trigger inflammatory responses and contribute to dermatological disorders such as acne and melasma [151]. Thus, controlled physical exfoliation of dead HaCaT, combined with anti-inflammatory or antibacterial support, is essential [152]. SS, containing a unique blend of multifunctional macromolecules, provides both gentle exfoliation and established anti-inflammatory activity [20, 87]. Nevertheless, transient inflammation can also serve as a beneficial physiological stimulus by activating immune responses, eliminating debris, and coordinating early wound-healing processes [153]. Formulations containing GA are known to induce a short-lived inflammatory event required to initiate exfoliation and renewal of the outer epidermis [154]. Our results support the hypothesis that GA alone triggers a strong and prolonged inflammatory response, whereas GA embedded within the

SS matrix induces a more attenuated and better controlled event. This effect became particularly evident upon investigation of the PI3K/Akt/NF-κB signaling cascade.

Recent evidence highlights the central role of the PI3K/Akt axis in regulating skin development, differentiation, and homeostasis [155], partly through activation of the NF-κB transcription factor. NF-κB controls numerous cellular processes, including proliferation, differentiation, migration, angiogenesis, and metabolic regulation [156]. Importantly, NF-κB is strongly associated with inflammation; upon activation, it translocate to the nucleus and drives the expression of pro-inflammatory genes such as ILs, chemokines, and TNF-α [157]. Activation typically involves PI3K-mediated phosphorylation of Akt, which in turn activates NF-κB signaling [158]. Our results indicate that exposure of HaCaT cells to GA alone induced a pronounced inflammatory response, evidenced by coordinated upregulation of PI3K, Akt, and NF-κB after 14 h. SS also activated this pathway but to a significantly lesser degree, suggesting induction of a brief, more controlled inflammatory event. Moreover, when higher amounts of SS were administered, PI3K, Akt, and NF-κB were predominantly downregulated, supporting the hypothesis that the complex SS composition reduces the magnitude of inflammatory activation induced by GA alone. These findings align with Liu *et al.* [156], who described a feedback mechanism whereby NF-κB upregulation initiates both pro-inflammatory signaling and subsequent activation of cell-survival and anti-apoptotic pathways (e.g., via c-Myc inhibition) [159]. This dual behavior facilitates the resolution of inflammation and initiation of protective responses [157]. Our observations mirror this model: NF-κB upregulation is followed by pathway downregulation, indicating progression toward inflammatory resolution.

One of the principal NF-κB-regulated genes is COX-2 [160], a key mediator of inflammation. COX-2 modulates chemokine production and influences the recruitment of regulatory T cells, thereby contributing to cell-mediated immune responses and tissue protection [161]. Transient COX-2 induction is also essential in initiating wound-healing events, although excessive or prolonged COX-2 activity can impair tissue repair [162]. To evaluate the inflammatory imprint of SS and GA, we measured COX-2 expression at both mRNA and protein level in HaCaT, along with IL-6 secretion as an additional inflammatory marker. Our data suggest that PI3K/Akt/NF-κB pathway activation by GA alone results in elevated COX-2 gene expression after 24 h, confirming strong pro-inflammatory stimulation and correlating with reduced viability after 48 h. In contrast,

although SS induced early activation of PI3K/Akt/NF-κB, this activation did not translate into increased COX-2 gene expression at 24 h, reinforcing the notion that SS attenuates inflammatory progression. COX-2 protein expression at 48 h further demonstrated that GA induces a sustained inflammatory response, whereas SS-treated groups showed no significant increase relative to control. Notably, the 1:60 and 1:80 SS dilutions reduced COX-2 protein levels relative to GA, suggesting that SS not only prevents excessive inflammatory signaling but may actively counteract GA-induced COX-2 upregulation. IL-6 analysis corroborated these findings: both 1:60 and 1:80 dilutions produced lower IL-6 release than GA after 48 h. Collectively, these results support the conclusion that SS elicits a moderate, controlled inflammatory response while preventing the sustained, aggressive activation characteristic of GA. This controlled profile positions SS as a safer and more physiologically compatible agent for topical applications, especially in formulations intended for sensitive, inflamed, or damaged skin. Additionally, the balanced inflammatory response induced by SS aligns with its known benefits in wound healing, where tightly regulated inflammatory signaling is essential to prevent chronic irritation, fibrosis, or impaired regeneration [163].

In healthy skin, HaCaT interacts closely with fibroblasts to maintain cutaneous homeostasis, particularly through the regulation of extracellular matrix (ECM) remodeling. Acting via paracrine signaling, HaCaT stimulates fibroblasts to secrete ECM-modulating factors, while also directly contributing to ECM reorganization, as noted by Pfisterer *et al.* [164] and Russo *et al*. [165]. Within the broader context of ECM remodeling, gelatinases represent essential mediators that degrade ECM components and thereby create spatial pathways required for the migration of cells from deeper dermal layers toward the epidermal surface [166], further supporting the concept that MMP activation constitutes a necessary event for cell migration [167]. Specifically, MMP-2 (gelatinase A) and MMP-9 (gelatinase B) are key enzymes involved in collagen degradation and ECM turnover, both of which are fundamental to wound re-epithelialization [168]. Beyond their proteolytic functions, these gelatinases also facilitate cell migration, angiogenesis, cell-cycle regulation, and connective tissue remodeling [169]. As reported by Krishnaswamy *et al.* [170], MMP-2 and MMP-9 are expressed by HaCaT at the leading edge of wounds to promote re-epithelialization. Gelatinases are also the most abundant MMPs detected in chronic wound tissues, exhibiting broader substrate specificities than collagenases (MMP-1 and MMP-13), thereby degrading a wider

spectrum of ECM molecules. Nevertheless, because additional MMP isoforms including MMP-1, MMP-3, and MMP-13 play substantial roles in remodeling events, further investigations are required to elucidate the effect of SS on the entire MMP network [171, 172]. This concept is well supported by our experimental findings, in which an initial, short-term inflammatory phase was followed by pronounced upregulation of MMP-2 and MMP-9 gene expression. This sequence indicates an accelerated ECM remodeling response, which appeared markedly more robust with SS treatment than with GA alone, reinforcing the idea that SS administration significantly enhances and sustains the remodeling process.

Although reactive oxygen species (ROS) are indispensable in several signaling pathways and physiological functions, including tissue repair, their biological effects remain "double-edged": beneficial when transient and controlled, yet detrimental when chronically elevated [173]. Measuring intracellular ROS levels, therefore provides crucial insights into the oxidative profile induced by topical agents such as SS and GA. The early increase in ROS observed with the 1:60 and 1:80 SS dilutions suggests that these concentrations transiently activate oxidative signaling, potentially serving as a stimulus for proliferation, differentiation, and other cellular processes. Conversely, the 1:40 SS dilution led to reduced ROS levels, indicating a possible antioxidant or ROS-scavenging effect at higher SS concentrations. These results suggest that SS components may exert concentration-dependent activities, promoting redox signaling at intermediate levels while providing antioxidant protection at higher levels. GA treatment, in contrast, produced a strong and statistically significant ROS surge after 6 h, greater than that observed with any SS dilution, consistent with its established keratinolytic and exfoliative mechanisms that commonly involve oxidative stress. The comparative profiles of SS- and GA-treated cells therefore support the hypothesis that SS's natural biological matrix buffers the oxidative stress typically associated with GA.

By 18 h, ROS levels in all treatment and control groups converged, indicating the activation of compensatory mechanisms and restoration of redox balance over time. The absence of prolonged ROS elevation, particularly in SS-treated cells underscores that SS does not induce persistent oxidative stress, a critical consideration for avoiding chronic inflammation and cellular injury. Collectively, these findings highlight SS's redox-modulating capacity. Unlike GA, which evokes a more substantial oxidative burst, SS elicits a controlled and transient ROS response that may support cellular activation

without causing sustained oxidative damage. This further emphasizes SS's potential as a safer and more tolerable alternative for skin-regeneration strategies involving regulated oxidative cues.

Keratinocyte migration represents a fundamental process in the re-epithelialization phase of wound repair and skin regeneration [174]. Using a wound-healing assay, we evaluated the effects of SS and GA on keratinocyte migration. SS significantly enhanced HaCaT migration in a dose-dependent manner, with both the 1:40 and 1:80 dilutions markedly accelerating wound closure at 24 and 48 h. Although GA also promoted wound closure at 48 h, its effect was notably less significant than that of SS, particularly when compared with the 1:40 SS dilution, which maintained superior performance at both time points. This differential behavior may reflect the limited functional scope of GA, which, despite its keratinolytic efficacy, lacks the diverse bioactive compounds present in SS [175] that collectively support migration, proliferation, and ECM remodeling. The enhanced migratory response induced by SS underscores its potential as a multifunctional regenerative agent applicable to dermatological treatments.

Angiogenesis, an essential driver of tissue repair, involves a complex multistep mechanism regulated by a balance between pro- and anti-angiogenic factors [176]. This process is closely linked to MMP activity, which facilitates basement membrane degradation, ECM remodeling, and the controlled release of angiogenic mediators, as well as the mobilization of endogenous inhibitors [177]. Skin regeneration and re-epithelialization likewise require the contribution of dermal blood vessels, mirroring mechanisms observed in wound healing [178]. Accordingly, we conducted a preliminary evaluation of SS's effects on ECs to determine its capacity to support proper skin regeneration. SS increased EC viability up to 72 h, outperforming both GA and the control. Moreover, SS significantly promoted EC migration, a major determinant of angiogenic activity and new vessel formation [179]. Notably, this pro-migratory effect was even more pronounced at higher SS dilutions, achieving 75% wound closure, in contrast to GA, which reached only 45%. This behavior aligns with previous findings demonstrating the pro-angiogenic potential of SS during skin wound repair [180]. Overall, our findings show that SS is well tolerated by skin cells, unlike GA, and induces a transient, controlled inflammatory response that supports regeneration and skin homeostasis. By modulating ROS signaling, reducing COX-2 and IL-6, and enhancing

MMP-mediated ECM remodeling, SS emerges as a promising regulator of skin regeneration and wound healing, warranting further *in vivo* validation.

4.3 Proteomics Analysis

Proteins serve as structural support, biochemical catalysts, hormones, enzymes, building blocks, and initiators of cellular death. On the other hand, proteins act as the machinery of cellular metabolism and communication [181]. To better understand the biological pathways involved in a normal biological function or dysfunction, including diseases, the identification and/or measurement of the production and release of proteins is essential [182]. Multi-omics, including proteomics, not only simplified the ways to identify and quantify the proteins involved in various biological functions, but also helps to unfold the complex mixture of proteins [183].

Considering the previous results of SS on HaCaT and ECs, it is believed that SS exerts a significant impact on the production and expression of several proteins involved in key biological functions of cell proliferation, wound healing, antioxidant capability, and inflammation [11, 107, 184-186] which demonstrates that SS exerts complex and time-dependent effects on NHDFs.

Given SS's expanding application in cosmetic formulations, we assessed its impact on the viability of NHDFs, the predominant cell type in the dermal layer by MTT assay. SS produced even higher viability responses in NHDFs, with a marked increase at 48 h, suggesting strong biocompatibility and favorable cellular interaction, as similarly reported by Deng *et al.* [187]. Trapella *et al.* [4] likewise confirmed that SS is non-toxic, well-tolerated by skin, and capable of significantly enhancing fibroblast viability. Our findings further corroborate these observations, supporting the view that SS is well accepted by connective-tissue cell populations and demonstrates a substantial capacity to promote fibroblast viability [11]. Cell viability was also assessed by the Alamar Blue assay, validating the MTT results that SS is very well tolerated by NHDFs even after 72 h of exposure, underlining the outcomes of previous research on HaCaT, HGFs and ECs [11, 107]. Considering the results of the cell viability assay, we further deepen our findings on NHDFs at the proteomic level after SS treatment and making this study the first ever to do so. The unique PG obtained after applying filters from the DAP dataset were used for string network analysis yields the GO enrichment thus confirming the role of SS in five

highly influenced biological functions: (i) regulation of programmed cell death, referred as apoptosis (ii) reduction of oxidative stress, (iii) wound healing, (iv) cell migration, and (v) anti-aging. Many of these biological functions have already confirmed by other researchers by non-proteomic means. In fact, Ho *et al*. [188] mentioned that *Achatina fulica* slime induced programmed cell death through the extrinsic apoptotic pathway in the triple-negative breast cancer cell line, via activation of *Fas* pathway, while downregulating the apoptosis in normal cells. Similarly, Cabibbo *et al*. [189] confirmed that SS elevates the activities of antioxidant enzymes such as glutathione and superoxide dismutase, and Rashad *et al*. [107] reported the reduction in ROS release in HaCaT after SS treatment, corroborating the role of SS in counteracting the occurrence of oxidative stress. Functions such as wound healing, cell migration and anti-aging after SS treatment are also well documented in previous studies of our group on SS [11, 107].

Proteins with the highest number of connections in the network are detected as hub proteins, and in this study top 10 hub proteins belong to AKT, PI3K, SRC and KRAS families. In detail, AKT plays a key role in the PI3K/Akt signaling pathway, promoting cell proliferation and preventing apoptosis; PI3Ks control vital cellular functions by key PI3K/Akt/mTOR signaling pathways and regulate cell growth, metabolism, and survival [190]. The SRC protein acts as a crucial signaling molecule regulating cell growth, proliferation, migration, adhesion, and survival [191]. The KRAS protein is a key part of the RAS/MAPK signaling pathway that acts like an "on-off" switch for cell growth and division; in healthy cells, this cycle controls growth, differentiation, and cell survival [192]. Collectively, the enrichment of AKT, PI3K, SRC, and KRAS family members as hub proteins indicates that SS-driven proteomic changes converge on central signaling nodes that coordinate multiple repair-related processes rather than acting on isolated pathways. These hub proteins integrate survival, migratory, and stress-response signals, thereby synchronizing apoptosis regulation, antioxidant capability and proliferative responses required for effective wound healing. Their high connectivity suggests that SS modulates upstream regulatory points capable of orchestrating broad cellular programs, enabling a coordinated balance between cell survival, controlled turnover, and migration. This approach allowed to further validate, in a subsequent step, the selected enrichment functions by non-proteomics methodologies.

The regulation of programmed cell death, more specifically apoptosis, was cross-verified by Annexin/PI staining, by flow cytometry, with an additional investigation of Bax and

Bcl-2 expression, two main regulators of the apoptotic process. The increase of living cells after 24 h of SS treatment, along with the reduction of apoptotic cells compared to control (no apoptosis induction), combined with the opposite situation recorded after 48 h, in which a reduction of SS-treated living cells and an increase of apoptotic events occurs, suggests that SS can act over time triggering a turnover thus leading to a beneficial cell renewal. Indeed, from 24 h, the level of Bax increases in the 1:40 and 1:80 samples, probably triggering an activation of the intrinsic apoptotic cascade, thus supporting the increase of apoptotic events recorded by Annexin/PI after 48 h. The 1:60 dilution, even inducing the same Annexin/PI result of 1:40 and 1:80, does not induce the same Bax higher level: considering that the apoptotic process is orchestrated by different pathways and that Bax is only one of the actors involved [107], it can be argued that in the 1:60 dilution other molecules, (*e.g.* molecules related to the extrinsic apoptotic pathway), are involved to obtain the same result induced by 1:40 and 1:80. As a consequence, the increment of apoptotic cells can be considered an induction of physiological cellular turnover for two main reasons: I) the reduction of living cells and the increase of apoptotic cells from Annexin/PI is low, being around 15-20%, is not a massive effect; II) the Alamar blue data, at 48 and 72 h, indicate that cells remain healthy and viable after prolonged treatment. This hypothesis is corroborated by the reduced levels of Bax after 48 h, suggesting a transitory apoptotic stimulus, correctly balanced by the activity of Bcl-2 anti-apoptotic protein, in order to prevent a massive apoptosis induction. In fact, it can be evidenced that Bax and Bcl-2 show the same trend: the higher Bax levels are paralleled by increased Bcl-2 levels, indicating that Bcl-2 may act to counterbalance the pro-apoptotic effect of Bax, as elsewhere confirmed also by Qian *et al*. [193] which states that Bcl-2 is able to inhibit apoptosis by forming a heterodimer with Bax and to ensure cell survival by regulating the Ca^{2+} concentration and antioxidant effect. Additionally, it can also inhibit the activities of caspase-9, 3, 6, and 7, thereby inhibiting apoptosis.

Oxidative stress is a central regulator of fibroblast function, where controlled ROS act as critical signaling mediators in wound healing, while excessive or sustained ROS accumulation impairs regeneration and induces cellular damage [194]. In this study, SS finely modulated intracellular redox homeostasis, inducing a biphasic ROS response characterized by a transient early increase at 6 h followed by a pronounced reduction at 24 h across all tested dilutions. This pattern reflects a hormetic redox effect, where an

initial oxidative signal primes endogenous defense mechanisms, ultimately enhancing antioxidant capacity and cellular resilience, making these results coherent with previous findings [107]. Importantly, this redox modulation is supported by proteomic evidence: GO analysis revealed enrichment of proteins involved in oxidative stress responses, indicating coordinated remodeling of redox-regulatory networks. These findings align with previous studies showing that SS enhances key antioxidant enzymes, including glutathione peroxidase and superoxide dismutase, thereby reinforcing intrinsic detoxification systems [195].

Functionally, the ROS dynamics induced by SS were accompanied by regulated apoptotic signaling, with controlled Bax modulation and elevated Bcl-2 expression, supporting cell survival over oxidative stress–driven death. Simultaneously, the reduction in ROS at 24 h, coupled with enhanced antioxidant capacity, likely establishes a permissive environment for fibroblast migration, which may be mediated through redox-sensitive activation of the PI3K/AKT signaling pathway, promoting cytoskeletal remodeling and pro-migratory programs [155]. This dual effect, attenuating oxidative stress while sustaining pro-migratory signaling, positions SS as a redox-modulating biomaterial capable of orchestrating a dynamic balance between ROS signaling, antioxidant protection, and regenerative activity. These mechanistic insights, integrated with the proteomic reprogramming observed, provide a robust rationale for the pro-healing and anti-aging effects of SS in human dermal fibroblasts.

The most striking finding is the potent pro-migratory activity of SS that regulates the wound healing and aging process. Thus, to confirm the proteomic data, the scratch assay results were assessed, revealing that all tested dilutions of SS significantly accelerated wound closure, achieving 100% gap closure within 24 h, a stark contrast to the control. This suggests that SS contains bioactive compounds that powerfully stimulate the cellular migration, essential for wound repair, already witnessed by previous findings [20, 87, 196]. It has been in fact demonstrated that a superficial scar in albino rats treated with SS achieved 64% of healing after 14 days compared to a standard Madecassol ointment, which took 21 days [20]. Similarly, Gubitosa *et al.* mentioned that gold nanoparticles of SS significantly increase the urokinase-type plasminogen activator receptor (uPAR), essential for keratinocyte adhesion, spreading, and migration [87]. Simultaneously, SS enhanced the cellular antioxidant capacity, indicating a role in bolstering cellular defence against oxidative stress. The profound reprogramming of the cellular proteome observed

suggests that SS may induce a controlled stress response that redirects energy from proliferation to migration and defence mechanisms. This action, promoting migration while enhancing antioxidant activity, positions SS as a promising agent for supporting wound healing, where rapid tissue closure and protection from ROS are critical passages.

5 CONCLUSIONS

SS has been employed since antiquity for the management of burns, inflammatory conditions, and a wide range of skin disorders, and these traditional practices have laid the foundation for sustained scientific interest in this complex biological secretion. Contemporary research has progressively expanded its scope, exploring SS not only in cosmetic and sunscreen formulations but also as a bioactive material endowed with antimicrobial, anti-inflammatory, antioxidant, and wound-healing properties across diverse delivery platforms. More recently, attention has shifted toward advanced formulation strategies, including SS-based patches, nanocarriers, and site-specific delivery systems, designed to enhance bioavailability, stability, and therapeutic precision for the treatment of different pathological conditions. Within this evolving framework, the present work provides an integrated and in-depth chemical, biological, and molecular characterization of *Helix aspersa's* slime, reinforcing its relevance as a multifunctional natural biomaterial.

The chemical profiling performed in this study demonstrates that SS is characterized by a rich and heterogeneous composition, encompassing glycoproteins, organic acids, phenolic derivatives, peptides, and low-molecular-weight metabolites. These constituents collectively underpin the antimicrobial, antioxidant, and enzyme-inhibitory properties observed, thereby supporting the suitability of SS for dermatological and pharmaceutical applications. Importantly, the comparative evaluation of stabilized and non-stabilized formulations highlights that processing and preservation strategies significantly influence both chemical integrity and bioactivity, suggesting that appropriate stabilization can preserve or even enhance specific functional attributes of SS. By coupling advanced analytical techniques with functional assays, this work establishes a clear relationship between chemical composition and biological performance, emphasizing the need for rational processing approaches to optimize SS-based products.

From a biological perspective, the data consistently indicate that SS is well tolerated by skin-resident cells and does not exert the cytotoxic burden observed with isolated GA. Instead, SS elicits a finely tuned cellular response characterized by transient and regulated inflammatory activation rather than sustained stress or damage. This balanced behavior is reflected in the controlled modulation of intracellular reactive oxygen species, the downregulation of pro-inflammatory mediators such as COX-2 and IL-6, and the

preservation of cell viability across keratinocytes, fibroblasts, and endothelial cells. Such responses are particularly relevant in the context of skin regeneration, where a brief inflammatory phase is necessary to initiate repair, but prolonged inflammation can impair healing and tissue homeostasis. In this regard, SS appears capable of attenuating the harsh effects associated with GA while maintaining or enhancing regenerative signaling.
Furthermore, SS markedly promotes key processes involved in tissue remodeling and repair. The upregulation of matrix metalloproteinases, together with enhanced keratinocyte and endothelial cell migration, underscores its ability to actively support extracellular matrix remodeling, re-epithelialization, and angiogenic responses. The positive effects observed on endothelial cell viability and migration further suggest that SS can act not only on epidermal components but also on the deeper dermal compartment, an essential aspect for effective wound healing and tissue regeneration. Taken together, these findings reinforce the concept of SS as a regulator of multiple interconnected cellular pathways rather than a simple growth-promoting agent.

At the molecular level, proteomic and complementary non-proteomic analyses further substantiate the multifunctional nature of SS. The modulation of proteins involved in cell survival, apoptosis regulation, oxidative stress response, and wound healing indicates that SS initially primes fibroblasts for repair by enhancing migration and antioxidant defenses, followed by broader and more sustained adjustments in the proteomic landscape that may contribute to long-term cellular protection and tissue homeostasis. These molecular adaptations provide mechanistic support for the observed biological effects, ranging from regulating cell viability, cellular turnover by programmed cell death, and oxidative stress mitigation to wound healing, thus highlighting the capacity of SS to orchestrate complex cellular responses through coordinated signaling networks.

Overall, this work positions snail slime as a sophisticated biological modulator with significant potential in dermatological, cosmetic, and biomedical applications. By integrating chemical characterization, cellular assays, and molecular analyses, the study offers a comprehensive view of how SS composition translates into functional outcomes relevant to skin regeneration and repair. While the present findings provide robust mechanistic insights through *in vitro* models, future investigations employing *in vivo* systems will be essential to validate these effects under physiological conditions, particularly with regard to wound closure kinetics, granulation tissue formation, and collagen remodeling. Such studies will be crucial to strengthen the translational relevance

of SS and to fully exploit its potential as a sustainable, multifunctional, and biologically active natural resource.

6 FUTURE PROSPECTIVES

Building on the comprehensive chemical, biological, and proteomic characterization presented in this thesis, several future research directions emerge to further advance the translational potential of SS.

First, given the demonstrated influence of processing and stabilization strategies on SS composition and bioactivity, future work should prioritize the optimization and standardization of extraction, preservation, and formulation protocols. This will be crucial for ensuring batch-to-batch reproducibility, long-term stability, and regulatory compliance, particularly for clinical and industrial applications.

Second, deeper mechanistic investigations focusing on the specific signaling pathways and key regulatory proteins identified through proteomic analysis, such as those involved in PI3K/Akt, MAPK, oxidative stress response, and extracellular matrix remodeling, will be necessary to fully elucidate how SS orchestrates its multifunctional effects. Targeted pathway inhibition or gene-silencing approaches may help clarify causal relationships and refine our understanding of SS-driven cellular modulation.

Third, the development of advanced SS-based delivery systems, such as hydrogels, patches, nanocarriers, or site-specific formulations, represents a promising avenue to enhance bioavailability, control release kinetics, and tailor therapeutic effects for specific dermatological and wound-healing indications.

Finally, *in vivo* validation using appropriate animal models will be essential to confirm the regenerative effects observed *in vitro*, particularly with respect to wound closure dynamics, granulation tissue formation, angiogenesis, and collagen deposition. Such studies will provide critical insight into the temporal and spatial coordination of SS-induced repair processes under physiological conditions.

Together, these future studies will not only strengthen the clinical relevance of SS but also pave the way for its rational integration into next-generation biomaterials and regenerative medicine strategies.

7 FUNDING

This thesis was produced while attending the PhD program in Biomolecular and Pharmaceutical Sciences at the “G. d’Annunzio” University of Chieti-Pescara, Cycle XXXVIII, with the support of a scholarship financed by the Ministerial Decree no. 351 of 9th April 2022, based on the National Recovery and Resilience Plan (NRRP) - funded by the European Union - NextGenerationEU - Mission 4 "Education and Research", Component 1 "Enhancement of the offer of educational services: from nurseries to universities” - Investment 3.4 “Advanced teaching and university skills”.

8 ACKNOWLEDGMENTS

It is a great pleasure to acknowledge my deepest thanks and sincere gratitude to my supervisor, **Prof. Susi Zara**, Associate Professor at the Department of Pharmacy, “G. d’Annunzio” University of Chieti-Pescara, whose continuous support, motivation, huge understanding, vast knowledge, and expertise has made this research possible. Without her patience, support, and guidance, I would not be able to complete this academic challenge. It is a great honor for me to work under her supervision.

I would like to take this opportunity to say warm thanks to **Prof. Éva Csősz**, Proteomics Core Facility, Department of Biochemistry and Molecular Biology, Faculty of Medicine, University of Debrecen, Debrecen, Hungary, for providing me the opportunity to work in the facility, continuous support and guidance in experimental design and proteomics analysis.

Lastly, I express my heartiest gratitude to all the colleagues and lab members from the University of Chieti, Italy, especially, **PhD. Alessia Ricci** and **PhD. Marwa Balaha** and from the University of Debrecen, Hungary, who helped me a lot during this research work.

The results presented in the thesis were obtained thanks to the collaboration between University “G. d’Annunzio” Chieti-Pescara and Lumacheria Italiana S.r.l. (Cherasco, Italy) in accordance with the agreement signed on 04/02/2025.

9 REFERENCES

1. Sajjadi, N., *Chemical Ecology of Biocompounds in Molluscs*, in *Biological Resources of Water*, S. Ray, Editor. 2018, IntechOpen: London.
2. McDermott, M., et al., *Advancing Discovery of Snail Mucins Function and Application.* Frontiers in Bioengineering and Biotechnology, 2021. **Volume 9 - 2021**.
3. Cilia, G. and F. Fratini, *Antimicrobial properties of terrestrial snail and slug mucus.* Journal of Complementary and Integrative Medicine, 2018. **15**(3).
4. Olaniyan, O.T. and C.O. Adetunji, *Biological, Biochemical, and Biodiversity of Biomolecules from Marine-Based Beneficial Microorganisms: Industrial Perspective*, in *Microbial Rejuvenation of Polluted Environment: Volume 3*, C.O. Adetunji, D.G. Panpatte, and Y.K. Jhala, Editors. 2021, Springer Singapore: Singapore. p. 57-81.
5. Chase, R., *Behavior and its neural control in gastropod molluscs*. 2002: Oxford University Press.
6. Guiller, A. and L. Madec, *Historical biogeography of the land snail Cornu aspersum: a new scenario inferred from haplotype distribution in the Western Mediterranean basin.* BMC Evolutionary Biology, 2010. **10**(1): p. 18.
7. Apostolou, K., et al., *Bacterial Diversity Associated with Terrestrial and Aquatic Snails.* Microorganisms, 2025. **13**(1): p. 8.
8. Rizzi, V., et al., *Snail slime-based gold nanoparticles: An interesting potential ingredient in cosmetics as an antioxidant, sunscreen, and tyrosinase inhibitor.* Journal of Photochemistry and Photobiology B: Biology, 2021. **224**: p. 112309.
9. Liegertová, M. and J. Malý, *Gastropod Mucus: Interdisciplinary Perspectives on Biological Activities, Applications, and Strategic Priorities.* ACS Biomaterials Science & Engineering, 2023. **9**(10): p. 5567-5579.
10. Vincent, J.F., *Defense and attack strategies and mechanisms in biology*, in *Biomimetics*. 2005, CRC Press. p. 359-382.
11. Ricci, A., et al., *Snail slime extracted by a cruelty free method preserves viability and controls inflammation occurrence: a focus on fibroblasts.* Molecules, 2023. **28**(3): p. 1222.
12. McDermott, M.B., *Mucinomics: A Bioinformatic Analysis of Snail Mucins, and Their Function.* 2021.
13. Smith, A.M., *Gastropod secretory glands and adhesive gels*. 2010: Springer.
14. Greistorfer, S., et al., *Snail mucus − glandular origin and composition in Helix pomatia.* Zoology, 2017. **122**: p. 126-138.
15. Greistorfer, S., et al., *Snail mucus− glandular origin and composition in Helix pomatia.* Zoology, 2017. **122**: p. 126-138.
16. Bansil, R. and B.S. Turner, *The biology of mucus: Composition, synthesis and organization.* Advanced drug delivery reviews, 2018. **124**: p. 3-15.
17. Okeniyi, F.A., et al., *Antimicrobial potentials of mucus mucin from different species of giant African land snails on some typed culture pathogenic bacteriab.* Asian Journal of Agriculture and Biology, 2022. **2022**(04).
18. Noothuan, N., et al., *Snail mucus from the mantle and foot of two land snails, Lissachatina fulica and Hemiplecta distincta, exhibits different protein profile and biological activity.* BMC Research Notes, 2021. **14**(1): p. 138.
19. Phrompanya, P., et al., *Biological properties of mucus from land snails (Lissachatina fulica) and freshwater snails (Pomacea canaliculata) and histochemical study of mucous cells in their foot.* PeerJ, 2023. **11**: p. e15827.
20. Aouji, M., et al., *Chemical composition, mineral profile, anti-bacterial, and wound healing properties of snail slime of Helix aspersa Müller.* BioMedicine, 2023. **13**(4): p. 10.
21. Dinica, R.M., et al., *Allantoin from valuable Romanian animal and plant sources with promising anti-inflammatory activity as a nutricosmetic ingredient.* Sustainability, 2021. **13**(18): p. 10170.
22. EFSA Panel on Nutrition, N.F., et al., *Safety of HelixComplex snail mucus (HSM) as a novel food pursuant to Regulation (EU) 2015/2283.* EFSA Journal, 2024. **22**(1): p. e8492.
23. Brieva, A., et al., *Molecular basis for the regenerative properties of a secretion of the mollusk Cryptomphalus aspersa.* Skin Pharmacology and Physiology, 2008. **21**(1): p. 15-22.
24. Ellijimi, C., et al., *Helix aspersa maxima mucus exhibits antimelanogenic and antitumoral effects against melanoma cells.* Biomed Pharmacother, 2018. **101**: p. 871-880.
25. Gubitosa, J., et al., *Biomolecules from snail mucus (Helix aspersa) conjugated gold nanoparticles, exhibiting potential wound healing and anti-inflammatory activity.* Soft Matter, 2020. **16**(48): p. 10876-10888.

26. Fabi, S.G., et al., *The effects of filtrate of the secretion of the Cryptomphalus aspersa on photoaged skin.* J Drugs Dermatol, 2013. **12**(4): p. 453-457.
27. Rashad, M., et al., *Biological activities of gastropods secretions: snail and slug slime.* Natural Products and Bioprospecting, 2023. **13**(1): p. 42.
28. Tsoutsos, D., D. Kakagia, and K. Tamparopoulos, *The efficacy of Helix aspersa Müller extract in the healing of partial thickness burns: a novel treatment for open burn management protocols.* Journal of Dermatological Treatment, 2009. **20**(4): p. 219-222.
29. Kim, K., et al., *Cosmeceutical properties of levan produced by Zymomonas mobilis.* International journal of cosmetic science, 2006. **28**(3): p. 231-231.
30. Rattanawiwatpong, P., et al., *Anti-aging and brightening effects of a topical treatment containing vitamin C, vitamin E, and raspberry leaf cell culture extract: a split-face, randomized controlled trial.* Journal of cosmetic dermatology, 2020. **19**(3): p. 671-676.
31. Zhu, K., et al., *Extraction, structure, pharmacological activities and applications of polysaccharides and proteins isolated from snail mucus.* International Journal of Biological Macromolecules, 2024. **258**: p. 128878.
32. Dn, H.M., I.L. Kriswandini, and E.A. R, *Antimicrobial proteins of Snail mucus (Achatina fulica) against Streptococcus mutans and Aggregatibacter actinomycetemcomitans.* Dental Journal, 2014. **47**(1): p. 31-36.
33. Zhong, J., et al., *A novel cysteine-rich antimicrobial peptide from the mucus of the snail of Achatina fulica.* Peptides, 2013. **39**: p. 1-5.
34. Vassilev, N.G., et al., *An (1)H NMR- and MS-Based Study of Metabolites Profiling of Garden Snail Helix aspersa Mucus.* Metabolites, 2020. **10**(9).
35. Sallam, A.A.A., S.A. El-Massry, and I.N. Nasr, *Chemical analysis of mucus from certain land snails under Egyptian conditions.* Archives of Phytopathology and Plant Protection, 2009. **42**(9): p. 874-881.
36. Liudmyla, K., C. Olena, and S. Nadiia, *Chemical properties of Helix aspersa mucus as a component of cosmetics and pharmaceutical products.* Materials Today: Proceedings, 2022. **62**: p. 7650-7653.
37. Barajas-Ledesma, E. and C. Holland, *Probing the compositional and rheological properties of gastropod locomotive mucus.* Frontiers in Soft Matter, 2023. **3**.
38. Trapella, C., et al., *HelixComplex snail mucus exhibits pro-survival, proliferative and pro-migration effects on mammalian fibroblasts.* Scientific Reports, 2018. **8**(1): p. 17665.
39. Wargala, E., et al., *Snail mucus as an innovative ingredient used in the cosmetology and medical industry.* Aesth. Cosmetol. Med, 2023. **12**: p. 45-49.
40. Laneri, S., et al., *Dosage of bioactive molecules in the nutricosmeceutical Helix aspersa muller mucus and formulation of new cosmetic cream with moisturizing effect.* Natural Product Communications, 2019. **14**(8): p. 1934578X19868606.
41. El Mubarak, M.A.S., F.N. Lamari, and C. Kontoyannis, *Simultaneous determination of allantoin and glycolic acid in snail mucus and cosmetic creams with high performance liquid chromatography and ultraviolet detection.* Journal of Chromatography A, 2013. **1322**: p. 49-53.
42. Cilia, G. and F. Fratini, *Antimicrobial properties of terrestrial snail and slug mucus.* J Complement Integr Med, 2018. **15**(3).
43. Mencucci, R., et al., *GlicoPro, Novel Standardized and Sterile Snail Mucus Extract for Multi-Modulative Ocular Formulations: New Perspective in Dry Eye Disease Management.* Pharmaceutics, 2021. **13**(12).
44. Salem, M.B., et al., *Cornu aspersum mucin attenuates indomethacins-induced gastric ulcers in mice via alleviating oxidative stress and inflammation.* Heliyon, 2023. **9**(5): p. e15677.
45. Singh, N., A.N. Brown, and M.H. Gold, *Snail extract for skin: A review of uses, projections, and limitations.* Journal of Cosmetic Dermatology, 2024. **23**(4): p. 1113-1121.
46. Dolashka, P., et al., *Antimicrobial activity of molluscan hemocyanins from Helix and Rapana snails.* Current pharmaceutical biotechnology, 2016. **17**(3): p. 263-270.
47. Pitt, S., et al., *Antimicrobial properties of mucus from the brown garden snail Helix aspersa.* British Journal of Biomedical Science, 2015. **72**(4): p. 174-181.
48. Rygało-Galewska, A., K. Zglińska, and T. Niemiec, *Edible Snail Production in Europe.* Animals, 2022. **12**(20): p. 2732.
49. Ballard, K. and B. PsycSc, *The Bioactivity and Functionality of the Molecular and Microbial Components of the Trail Mucus in the Invasive Land Snails Theba pisana and Cernuella virgata*. University of the Sunshine Coast, Queensland.

50. Perpelek, M., et al., *Bioactive snail mucus-slime extract loaded chitosan scaffolds for hard tissue regeneration: The effect of mucoadhesive and antibacterial extracts on physical characteristics and bioactivity of chitosan matrix.* Biomedical Materials, 2021. **16**(6): p. 065008.
51. Liegertová, M. and J. Malý, *Gastropod mucus: Interdisciplinary perspectives on biological activities, applications, and strategic priorities.* ACS Biomaterials Science & Engineering, 2023. **9**(10): p. 5567-5579.
52. Deng, T., et al., *A natural biological adhesive from snail mucus for wound repair.* Nature Communications, 2023. **14**(1): p. 396.
53. Adikwu, M. and B. Alozie, *Application of snail mucin dispersed in detarium gum gel in wound healing.* Sci Res Essay, 2007. **2**(6): p. 195-198.
54. Sarkar, P., D. Iyengar, and K. Mukhopadhyay, *Emergence of snail mucus as a multifunctional biogenic material for biomedical applications.* Acta Biomaterialia, 2025. **200**: p. 21-46.
55. Dolashki, A., et al., *Structure and antibacterial activity of isolated peptides from the mucus of garden snail Cornu aspersum.* Bulg. Chem. Commun. C, 2018. **50**: p. 195-200.
56. Santana, W.A., et al., *Evaluación de la Actividad Antimicrobiana y la Cicatrización Potencial de la Secreción Mucosa de Achatina fulica.* International Journal of Morphology, 2012. **30**(2): p. 365-373.
57. Iguchi, S.M.M., et al., *An N-acetylneuraminic acid-specific lectin from the body surface mucus of African giant snail.* Comparative Biochemistry and Physiology Part B: Comparative Biochemistry, 1985. **81**(4): p. 897-900.
58. Etim, L.B., C. Aleruchi, and G.A. Obande, *Antibacterial properties of snail mucus on bacteria isolated from patients with wound infection.* British microbiology research journal, 2016. **11**(2): p. 1-9.
59. Santana, W.A., et al., *Assessment of Antimicrobial Activity and Healing Potential of Mucous Secretion of Achatina fulica.* International Journal of Morphology, 2012. **30**: p. 365-373.
60. Dolashki, A., et al., *Antimicrobial Activities of Different Fractions from Mucus of the Garden Snail Cornu aspersum.* Biomedicines, 2020. **8**(9).
61. Bortolotti, D., et al., *Antimicrobial properties of mucus from the brown garden snail Helix aspersa.* British Journal of Biomedical Science, 2016. **73**(1): p. 49-50.
62. Abiona, J., et al., *Comparative evaluation of inhibitory activity of Epiphgram from albino and normal skinned giant African land snail (Archachatina marginata) against selected bacteria isolates.* Ethiopian journal of environmental studies and management, 2013. **6**(2): p. 177-181.
63. Etim, L., C. Aleruchi, and G. Obande, *Antibacterial properties of snail mucus on bacteria isolated from patients with wound infection.* British microbiology research journal, 2016. **11**(2): p. 1-9.
64. Ulagesan, S. and H.J. Kim, *Antibacterial and antifungal activities of proteins extracted from seven different snails.* Applied Sciences, 2018. **8**(8): p. 1362.
65. Ulagesan, S., A. Kuppusamy, and H.J. Kim, *Antimicrobial and antioxidant activities of protein hydrolysate from terrestrial snail Cryptozona bistrialis.* Journal of Applied Pharmaceutical Science, 2018. **8**(12): p. 012-019.
66. Gentili, V., et al., *HelixComplex snail mucus as a potential technology against O3 induced skin damage.* PLOS ONE, 2020. **15**(2): p. e0229613.
67. Cole, R., C.S. Richards, and T. Popkin, *Novel bacterium infecting an African snail.* Journal of Bacteriology, 1977. **132**(3): p. 950-966.
68. Abd El Hafez ., M.S.M. and et al., *Antibacterial Potential of Tridacna sp. and Pearl Oyster Aqueous Extracts on Food Spoilage Salmonella enterica.* Egyptian Journal of Aquatic Biology and Fisheries, 2022. **26**(6): p. 737-749.
69. Nantarat, N., Y. Tragoolpua, and P. Gunama, *Antibacterial activity of the Mucus Extract from the Giant African Snail (Lissachatina fulica) and Golden Apple Snail (Pomacea canaliculata) against pathogenic bacteria causing skin diseases.* Tropical Natural History, 2019. **19**(2): p. 103-112.
70. Nagarajan, K., et al., *Purification and Characterization of Trochus radiatus derived low molecular weight bactericidal polypeptide active against ESKAPE Pathogens.* International Journal of Peptide Research and Therapeutics, 2021. **27**: p. 1615-1631.
71. Pereira, A., et al., *Achatina fulica Haemocyanin-Derived Peptides as Novel Antimicrobial Agents.* bioRxiv, 2023: p. 2023.08.15.553437.
72. Pagano, C., et al., *Development and characterization of an emulgel based on a snail slime useful for dermatological applications.* International Journal of Pharmaceutics, 2024. **660**: p. 124337.
73. El-Zawawy, N.A. and M.M. Mona, *Antimicrobial efficacy of Egyptian Eremina desertorum and Helix aspersa snail mucus with a novel approach to their anti-inflammatory and wound healing potencies.* Sci Rep, 2021. **11**(1): p. 24317.

74. Fabi, S.G., et al., *The Effects of Filtrate of the Secretion of the Cryptomphalus Aspersa on Photoaged Skin.* J Drugs Dermatol, 2013. **12**(4): p. 453-7.
75. Nuryana, C.T., et al., *Achatina fulica mucus ameliorates uvb-induced human dermal fibroblast photoaging via the TGF-β/Smad pathway.* The Indonesian Biomedical Journal, 2023. **15**(6): p. 375-82.
76. Koo, J., et al., *Oral Administration of Edible Snail Extract Powder Prevents UVB-Induced Skin Damage.* Food Science & Nutrition, 2025. **13**(11): p. e71215.
77. Marchlewicz, M., et al., *Effect of Helix aspersa Mucus on the Regeneration of Skin with Photoaging Features in Different Methods of Application.* Applied Sciences, 2024. **14**(16): p. 7394.
78. Pagano, C., et al., *Development and characterization of an emulgel based on a snail slime useful for dermatological applications.* Int J Pharm, 2024. **660**: p. 124337.
79. Kandeil, M.A. and M.M. Mona, *Evaluation of antioxidant, antityrosinase, and anticancer activity of mucus extract from both Egyptian land snails, Eremina desertorum and Helix aspersa, with emphasis on their chemical profiles.* Journal of Experimental Zoology Part A: Ecological and Integrative Physiology, 2024. **341**(2): p. 182-192.
80. Rizzi, V., et al., *Snail slime-based gold nanoparticles: An interesting potential ingredient in cosmetics as an antioxidant, sunscreen, and tyrosinase inhibitor.* J Photochem Photobiol B, 2021. **224**: p. 112309.
81. Errajouani, F., et al., *Exploring the Potential Anti-Inflammatory and Wound-Healing Proprieties of Cepaea hortensis Snail Mucin.* Cosmetics, 2023. **10**(6): p. 170.
82. Ibrahim, A.M., et al., *The antioxidant and anti-inflammatory effects of Eremina desertorum snail mucin on experimentally induced intestinal inflammation and testicular damage.* Biosci Rep, 2022. **42**(10).
83. Messina, L., et al., *Snail Mucus Filtrate Reduces Inflammation in Canine Progenitor Epidermal Keratinocytes (CPEK).* Animals (Basel), 2022. **12**(14).
84. Alogna, A., A. Liboni, and R. Rizzo, *Evaluation of Biological Properties and Beneficial Effects for a Sustainable and Conscious Exploitation of Achatina fulica Snails.* Biology, 2025. **14**(2): p. 190.
85. Espinoza-Monje, M., et al., *Characterization of Weissella viridescens UCO-SMC3 as a Potential Probiotic for the Skin: Its Beneficial Role in the Pathogenesis of Acne Vulgaris.* Microorganisms, 2021. **9**(7).
86. Di Filippo, M.F., et al., *Novel drug-loaded film forming patch based on gelatin and snail slime.* International Journal of Pharmaceutics, 2021. **598**: p. 120408.
87. Gubitosa, J., et al., *Biomolecules from snail mucus (Helix aspersa) conjugated gold nanoparticles, exhibiting potential wound healing and anti-inflammatory activity.* Soft Matter, 2020. **16**(48): p. 10876-10888.
88. Bonnemain, B., *Helix and Drugs: Snails for Western Health Care From Antiquity to the Present.* Evidence-Based Complementary and Alternative Medicine, 2005. **2**: p. 583043.
89. Georgieva, A., et al., *Hemocyanins from Helix and Rapana Snails Exhibit in Vitro Antitumor Effects in Human Colorectal Adenocarcinoma.* Biomedicines, 2020. **8**(7).
90. Kantawong, F., et al., *Mucus of Achatina fulica stimulates mineralization and inflammatoryresponse in dental pulp cells.* Turkish Journal of Biology, 2016. **40**(2): p. 353-359.
91. WALUGA-KOZŁOWSKA, E., et al., *SNAIL MUCUS-A NATURAL ORIGIN SUBSTANCE WITH POTENTIAL USE IN MEDICINE.* Acta Poloniae Pharmaceutica, 2021. **78**(6).
92. Hendrawati, H., H.N. Agustha, and R. Sari, *Topical application of snail mucin gel enhances the number of osteoblasts in periodontitis rat model.* Majalah Kedokteran Gigi, 2019. **52**(2): p. 61-65.
93. Swastini, I., T.G.B. Mahadewa, and I.P.E. Widyadharma, *Alveolar Bone Osteoclast Profile in the Periodontitis Wistar Rats Model with the Snail Slime (Achatina Fulica) Application.* Open Access Maced J Med Sci, 2019. **7**(10): p. 1680-1684.
94. Ajadi, A.R., et al., *Evaluación de la Glucosamina y Mucina de Caracol en la Progresión de la Osteoartritis Experimental de Rodilla en Perros.* International Journal of Morphology, 2013. **31**(1): p. 280-286.
95. Swastini, I., G. Dewi, and I. Arjani, *Optimization of snail (Achatina fulica) mucus gel formula with CMC-Na as a gelling agent healing periodontitis.* Biomedical & Pharmacology Journal, 2024. **17**(2): p. 1301-1306.
96. Saadullah, M., et al., *Pharmacological evaluation of the hypoglycemic and anti-Alzheimer's activities of aerial parts of Breynia distachia (Phyllanthaceae).* Tropical Journal of Pharmaceutical Research, 2022. **21**(3): p. 579-587.

97. Saadullah, M., et al., *Evaluation of molecular mechanisms responsible for in vivo anti-Alzheimer's property of Euphorbia cotinifolia methanol extract.* Journal of King Saud University - Science, 2023. **35**(6): p. 102785.
98. Saadullah, M., et al., *Molecular modeling study of novel lancifolamide bioactive molecule as an inhibitor of acetylcholinesterase (AChE), herpes simplex virus (HSV-1), and anti-proliferative proteins.* Molecules, 2022. **27**(17): p. 5480.
99. Saadullah, M., et al., *Exploration of neuroprotective and cognition boosting effects of Mazus pumilus in Alzheimer's disease model.* Journal of Complementary and Integrative Medicine, 2024.
100. Saadullah, M., et al., *Chapter 4 - Biosynthesis of phytonutrients*, in *Phytonutrients and Neurological Disorders*, H. Khan, M. Aschner, and H. Mirzaei, Editors. 2023, Academic Press. p. 57-105.
101. Matusiewicz, M., et al., *In Vitro Influence of Extracts from Snail Helix aspersa Müller on the Colon Cancer Cell Line Caco-2.* Int J Mol Sci, 2018. **19**(4).
102. Ho, C.Y., et al., *Snail Mucus Enhances Chemosensitivity of Triple-negative Breast Cancer Via Activation of the Fas Pathway.* Anticancer Res, 2022. **42**(2): p. 845-855.
103. Chen, B.-R. and W.-C. Huang, *849 Snail mucus increases the anti-cancer activity of anti-PD-L1 antibody in melanoma.* Journal for ImmunoTherapy of Cancer, 2023. **11**(Suppl 1): p. A948-A948.
104. El Ouar, I., et al., *Effect of Helix aspersa extract on TNFα, NF-κB and some tumor suppressor genes in breast cancer cell line Hs578T.* Pharmacogn Mag, 2017. **13**(50): p. 281-285.
105. Coelho, L.C., et al., *Lectins, Interconnecting Proteins with Biotechnological/Pharmacological and Therapeutic Applications.* Evid Based Complement Alternat Med, 2017. **2017**: p. 1594074.
106. Ciulla, M., et al., *Characterization of Mucins, Glycosaminoglycans, and Bioactive Compounds in Helix aspersa's slime by Spectroscopic and Biochemical Analysis.* Journal of Molecular Structure, 2025: p. 143838.
107. Rashad, M., et al., *Nature's Synergy: Cellular and Molecular Evaluation of Snail Slime and Its Principal Component, Glycolic Acid, on Keratinocytes, with Preliminary Evidence from Endothelial Cells.* Biomolecules, 2025. **15**(9): p. 1302.
108. Cairone, F., et al., *Pomegranate Juices: Analytical and Bio-Toxicological Comparison of Pasteurization and High-Pressure Processing in the Development of Healthy Products.* Foods, 2025. **14**(2): p. 315.
109. Kirby, A.J. and R.J. Schmidt, *The antioxidant activity of Chinese herbs for eczema and of placebo herbs—I.* Journal of ethnopharmacology, 1997. **56**(2): p. 103-108.
110. Shekhar, T.C. and G. Anju, *Antioxidant activity by DPPH radical scavenging method of Ageratum conyzoides Linn. leaves.* American journal of ethnomedicine, 2014. **1**(4): p. 244-249.
111. Dawidowicz, A.L., D. Wianowska, and M. Olszowy, *On practical problems in estimation of antioxidant activity of compounds by DPPH method (Problems in estimation of antioxidant activity).* Food chemistry, 2012. **131**(3): p. 1037-1043.
112. Re, R., et al., *Antioxidant activity applying an improved ABTS radical cation decolorization assay.* Free radical biology and medicine, 1999. **26**(9-10): p. 1231-1237.
113. Apak, R., et al., *Novel total antioxidant capacity index for dietary polyphenols and vitamins C and E, using their cupric ion reducing capability in the presence of neocuproine: CUPRAC method.* Journal of agricultural and food chemistry, 2004. **52**(26): p. 7970-7981.
114. Benzie, I.F. and J.J. Strain, *The ferric reducing ability of plasma (FRAP) as a measure of "antioxidant power": the FRAP assay.* Analytical biochemistry, 1996. **239**(1): p. 70-76.
115. Prieto, P., M. Pineda, and M. Aguilar, *Spectrophotometric quantitation of antioxidant capacity through the formation of a phosphomolybdenum complex: specific application to the determination of vitamin E.* Analytical biochemistry, 1999. **269**(2): p. 337-341.
116. Dinis, T.C., V.M. Madeira, and L.M. Almeida, *Action of phenolic derivatives (acetaminophen, salicylate, and 5-aminosalicylate) as inhibitors of membrane lipid peroxidation and as peroxyl radical scavengers.* Archives of biochemistry and biophysics, 1994. **315**(1): p. 161-169.
117. Ellman, G.L., et al., *A new and rapid colorimetric determination of acetylcholinesterase activity.* Biochemical pharmacology, 1961. **7**(2): p. 88-95.
118. Masuda, T., et al., *Screening for tyrosinase inhibitors among extracts of seashore plants and identification of potent inhibitors from Garcinia subelliptica.* Bioscience, biotechnology, and biochemistry, 2005. **69**(1): p. 197-201.
119. Šafašík, I., *Rapid Detection of Alpha-Amylase Inhibitors.* Journal of Enzyme Inhibition, 1990. **3**(3): p. 245-247.
120. Ting, L., et al., *A microplate-based screening method for alpha-glucosidase inhibitors.* Chinese Journal of Clinical Pharmacology and Therapeutics, 2005. **10**(10): p. 1128.

121. di Giacomo, V., et al., *Cold atmospheric plasma activated media selectively affects human head and neck cancer cell lines.* Oral Diseases, 2025. **31**(2): p. 401-416.
122. De Colli, M., et al., *In vitro comparison of new bisphosphonic acids and zoledronate effects on human gingival fibroblasts viability, inflammation and matrix turnover.* Clinical oral investigations, 2016. **20**(8): p. 2013-2021.
123. Chen, J., et al., *Structure-antioxidant activity relationship of methoxy, phenolic hydroxyl, and carboxylic acid groups of phenolic acids.* Scientific reports, 2020. **10**(1): p. 2611.
124. Onzo, A., et al., *Untargeted analysis of pure snail slime and snail slime-induced Au nanoparticles metabolome with MALDI FT-ICR MS.* Journal of Mass Spectrometry, 2021. **56**(5): p. e4722.
125. Alogna, A., et al., *Design of Liposomes Carrying HelixComplex Snail Mucus: Preliminary Studies.* Molecules, 2021. **26**(16): p. 4709.
126. Di Filippo, M.F., et al., *Influence of the extraction method on functional properties of commercial snail secretion filtrates.* Scientific Reports, 2024. **14**(1): p. 22053.
127. Dong, R., et al., *Co-pyrolysis of vineyards biomass waste and plastic waste: Thermal behavior, pyrolytic characteristic, kinetics, and thermodynamics analysis.* Journal of Analytical and Applied Pyrolysis, 2024. **179**: p. 106506.
128. Sheng, M., et al., *Practical Use of Differential Scanning Calorimetry for Thermal Stability Hazard Evaluation.* Organic Process Research & Development, 2019. **23**(10): p. 2200-2209.
129. Obas, F.-L., et al., *Characterization of the thermal behavior and structural properties of a commercial high-solids confectionary gel made with gelatin.* Food Hydrocolloids, 2024. **148**: p. 109432.
130. Wen, J., et al., *Applications of Differential Scanning Calorimetry for Thermal Stability Analysis of Proteins: Qualification of DSC.* Journal of Pharmaceutical Sciences, 2012. **101**(3): p. 955-964.
131. Maule, I., et al., *Thermal Stability Evaluation of Nitroalkanes with Differential Scanning Calorimetry.* Organic Process Research & Development, 2021. **25**(4): p. 781-788.
132. Alkhadhrh, M., et al., *Investigating the inhibitory effects of carotenoids-fortified Helix aspersa slime on oxidative stress, collagenase and tyrosinase enzyme activities.* J Cosmet Dermatol, 2024. **23**(11): p. 3757-3766.
133. Aouji, M., et al., *Chemical composition, mineral profile, anti-bacterial, and wound healing properties of snail slime of Helix aspersa Müller.* Biomedicine (Taipei), 2023. **13**(4): p. 10-19.
134. Halliwell, B., *Understanding mechanisms of antioxidant action in health and disease.* Nature Reviews Molecular Cell Biology, 2024. **25**(1): p. 13-33.
135. Shinta, Y.C., B. Zaman, and S. Sumiyati, *Citric Acid and EDTA as chelating agents in phytoremediation of heavy metal in polluted soil: a review.* IOP Conference Series: Earth and Environmental Science, 2021. **896**(1): p. 012023.
136. Mattar, G., et al., *Are Citric Acid-Iron II Complexes True Chelates or Just Physical Mixtures and How to Prove This?* Foods, 2023. **12**(2): p. 410.
137. Szwajgier, D., J. Pielecki, and Z. Targoński, *Antioxidant activities of cinnamic and benzoic acid derivaties.* Acta Scientiarum Polonorum Technologia Alimentaria, 2005. **4**(2): p. 129-142.
138. Velika, B. and I. Kron, *Antioxidant properties of benzoic acid derivatives against Superoxide radical.* Free Radicals and Antioxidants, 2012. **2**(4): p. 62-67.
139. Rauf, A. and N. Jehan, *Natural Products as a Potential Enzyme Inhibitors from Medicinal Plants*, in *Enzyme Inhibitors and Activators*, M. Şentürk, Editor. 2017, IntechOpen: Rijeka.
140. Nour, H., et al., *Exploration of natural products for the development of promising cholinesterase inhibitors in Alzheimer's disease treatment.* Heliyon, 2025. **11**(4): p. e42479.
141. Kumar, A., V. Kumar Singh, and A.M. Kayastha, *Studies on α-amylase inhibition by acarbose and quercetin using fluorescence, circular dichroism, docking, and dynamics simulations.* Spectrochimica Acta Part A: Molecular and Biomolecular Spectroscopy, 2024. **314**: p. 124160.
142. Guan, L., et al., *A Structure-Activity Relationship Study of the Inhibition of α-Amylase by Benzoic Acid and Its Derivatives.* Nutrients, 2022. **14**(9).
143. Yildiz, M., et al. *Acetylcholinesterase inhibitory properties of some benzoic acid derivatives*. in *AIP Conference Proceedings*. 2016. AIP Publishing LLC.
144. Chen, Q.-X., et al., *Inhibitory effects on mushroom tyrosinase by p-alkoxybenzoic acids.* Food Chemistry, 2005. **91**(2): p. 269-274.
145. Xiaodan, L., H. Huang, and C. Qingxi, *Studies on inhibitory effects of benzoic acid on mushroom tyrosinase.* Xiamen da xue xue bao. Zi ran ke xue ban= Journal of Xiamen University. Natural Science, 2003. **42**(1): p. 102-106.
146. Budryn, G., et al., *Hydroxybenzoic acids as acetylcholinesterase inhibitors: Calorimetric and docking simulation studies.* Nutrients, 2022. **14**(12): p. 2476.

147. Butler, P.J., et al., *The use of maleic anhydride for the reversible blocking of amino groups in polypeptide chains.* Biochem J, 1969. **112**(5): p. 679-89.
148. Houshmand, E.B., *Effect of glycolic acid, phytic acid, soothing complex containing Emulsion on Hyperpigmentation and skin luminosity: A clinical evaluation.* Journal of Cosmetic Dermatology, 2021. **20**(3): p. 776-780.
149. Prabakaran, L., et al., *Current trends and requirements in sensors for hydroxy acid-based skincare treatments: A mini-review.* Journal of Industrial and Engineering Chemistry, 2025. **144**: p. 723-734.
150. Fuchs, E. and S. Raghavan, *Getting under the skin of epidermal morphogenesis.* Nature Reviews Genetics, 2002. **3**(3): p. 199-209.
151. Knutsen-Larson, S., et al., *Acne vulgaris: pathogenesis, treatment, and needs assessment.* Dermatologic clinics, 2012. **30**(1): p. 99-106.
152. Conforti, C., et al., *Chemical peeling for acne and melasma: current status and innovations.* Giornale Italiano di Dermatologia e Venereologia, 2020. **155**(3): p. 280-285.
153. Chen, L., et al., *Inflammatory responses and inflammation-associated diseases in organs.* Oncotarget, 2017. **9**(6): p. 7204.
154. Denda, S., et al., *Glycolic acid induces keratinocyte proliferation in a skin equivalent model via TRPV1 activation.* Journal of dermatological science, 2010. **57**(2): p. 108-113.
155. Teng, Y., et al., *The PI3K/Akt Pathway: Emerging Roles in Skin Homeostasis and a Group of Non-Malignant Skin Disorders.* Cells, 2021. **10**(5): p. 1219.
156. Bai, D., L. Ueno, and P.K. Vogt, *Akt-mediated regulation of NFκB and the essentialness of NFκB for the oncogenicity of PI3K and Akt.* International journal of cancer, 2009. **125**(12): p. 2863-2870.
157. Liu, T., et al., *NF-κB signaling in inflammation.* Signal transduction and targeted therapy, 2017. **2**(1): p. 1-9.
158. Lee, D.H. and C.S. Lee, *Flavonoid myricetin inhibits TNF-α-stimulated production of inflammatory mediators by suppressing the Akt, mTOR and NF-κB pathways in human keratinocytes.* European Journal of Pharmacology, 2016. **784**: p. 164-172.
159. Romashkova, J.A. and S.S. Makarov, *NF-κB is a target of AKT in anti-apoptotic PDGF signalling.* Nature, 1999. **401**(6748): p. 86-90.
160. Tak, P.P. and G.S. Firestein, *NF-κB: a key role in inflammatory diseases.* The Journal of Clinical Investigation, 2001. **107**(1): p. 7-11.
161. Kalinski, P., *Regulation of Immune Responses by Prostaglandin E2.* The Journal of Immunology, 2012. **188**(1): p. 21-28.
162. Futagami, A., et al., *Wound Healing Involves Induction of Cyclooxygenase-2 Expression in Rat Skin.* Laboratory Investigation, 2002. **82**(11): p. 1503-1513.
163. Zhou, J., et al., *Simultaneous silencing of TGF-β1 and COX-2 reduces human skin hypertrophic scar through activation of fibroblast apoptosis.* Oncotarget, 2017. **8**(46).
164. Pfisterer, K., et al., *The Extracellular Matrix in Skin Inflammation and Infection.* Frontiers in Cell and Developmental Biology, 2021. **Volume 9 - 2021**.
165. Russo, B., N.C. Brembilla, and C. Chizzolini, *Interplay Between Keratinocytes and Fibroblasts: A Systematic Review Providing a New Angle for Understanding Skin Fibrotic Disorders.* Frontiers in Immunology, 2020. **Volume 11 - 2020**.
166. Newby, A.C., *Matrix metalloproteinases regulate migration, proliferation, and death of vascular smooth muscle cells by degrading matrix and non-matrix substrates.* Cardiovascular Research, 2006. **69**(3): p. 614-624.
167. Nabeshima, K., et al., *Matrix metalloproteinases in tumor invasion: Role for cell migration.* Pathology International, 2002. **52**(4): p. 255-264.
168. Caley, M.P., V.L.C. Martins, and E.A. O'Toole, *Metalloproteinases and Wound Healing.* Advances in Wound Care, 2015. **4**(4): p. 225-234.
169. Safwan Kamarazaman, I., et al., *Baeckea frutescens L. Promotes wound healing by upregulating expression of TGF-β, IL-1 β, VEGF and MMP-2.* Saudi Pharmaceutical Journal, 2024. **32**(7): p. 102110.
170. Krishnaswamy, V.R., D. Mintz, and I. Sagi, *Matrix metalloproteinases: The sculptors of chronic cutaneous wounds.* Biochimica et Biophysica Acta (BBA) - Molecular Cell Research, 2017. **1864**(11, Part B): p. 2220-2227.
171. Han, Y.-P., et al., *TNF-α stimulates activation of pro-MMP2 in human skin through NF-κB mediated induction of MT1-MMP.* Journal of Cell Science, 2001. **114**(1): p. 131-139.
172. Shakibaei, M., et al., *Suppression of NF-κB activation by curcumin leads to inhibition of expression of cyclo-oxygenase-2 and matrix metalloproteinase-9 in human articular chondrocytes:*

Implications for the treatment of osteoarthritis. Biochemical Pharmacology, 2007. **73**(9): p. 1434-1445.
173. Ukaegbu, K., E. Allen, and K.K.H. Svoboda, *Reactive Oxygen Species and Antioxidants in Wound Healing: Mechanisms and Therapeutic Potential.* International Wound Journal, 2025. **22**(5): p. e70330.
174. Ciulla, M., et al., *Characterization of mucins, glycosaminoglycans, and bioactive compounds in Helix aspersa's slime by spectroscopic and biochemical analysis.* Journal of Molecular Structure, 2026. **1349**: p. 143838.
175. Balaha, M., et al., *CAPE derivatives: Multifaceted agents for chronic wound healing.* Archiv der Pharmazie, 2024. **357**(10): p. e2400165.
176. Furtado, J. and A. Eichmann, *Chapter Nine - Vascular development, remodeling and maturation*, in *Current Topics in Developmental Biology*, M. Mallo, Editor. 2024, Academic Press. p. 344-370.
177. Bajbouj, K., R.K. Ramakrishnan, and Q. Hamid, *Role of Matrix Metalloproteinases in Angiogenesis and Its Implications in Asthma.* Journal of Immunology Research, 2021. **2021**(1): p. 6645072.
178. Takeo, M., W. Lee, and M. Ito, *Wound healing and skin regeneration.* Cold Spring Harb Perspect Med, 2015. **5**(1): p. a023267.
179. Petrillo, S., et al., *Endothelial Cells Promote Osteogenesis by Establishing a Functional and Metabolic Coupling With Human Mesenchymal Stem Cells.* Frontiers in Physiology, 2022. **Volume 12 - 2021**.
180. Rosanto, Y., et al., *Effect of snail mucus on angiogenesis during wound healing [version 2; peer review: 1 approved, 2 approved with reservations].* F1000Research, 2021. **10**(181).
181. Parray, Z.A., M. Shahid, and A. Islam, *Insights into Fluctuations of Structure of Proteins: Significance of Intermediary States in Regulating Biological Functions.* Polymers, 2022. **14**(8): p. 1539.
182. Morris, R., Katrina A. Black, and Elliott J. Stollar, *Uncovering protein function: from classification to complexes.* Essays in Biochemistry, 2022. **66**(3): p. 255-285.
183. Chandramouli, K. and P.Y. Qian, *Proteomics: challenges, techniques and possibilities to overcome biological sample complexity.* Hum Genomics Proteomics, 2009. **2009**.
184. Adole, U.J., *Antibacterial susceptibility of Staphylococcus aureus, Salmonella typhi, Bacillus subtilis and Escherichia coli to snail slime.* African Health Sciences, 2023. **23**(4): p. 177-182.
185. Ellijimi, C., et al., *Helix aspersa maxima mucus exhibits antimelanogenic and antitumoral effects against melanoma cells.* Biomedicine & Pharmacotherapy, 2018. **101**: p. 871-880.
186. Gubitosa, J., et al., *Chitosan/snail slime films as multifunctional platforms for potential biomedical and cosmetic applications: Physical and chemical characterization.* Journal of Materials Chemistry B, 2023. **11**(12): p. 2638-2649.
187. Ukaegbu, K., E. Allen, and K.K. Svoboda, *Reactive Oxygen Species and Antioxidants in Wound Healing: Mechanisms and Therapeutic Potential.* International Wound Journal, 2025. **22**(5): p. e70330.
188. HO, C.-Y., et al., *Snail Mucus Enhances Chemosensitivity of Triple-negative Breast Cancer Via Activation of the Fas Pathway.* Anticancer Research, 2022. **42**(2): p. 845-855.
189. Cabibbo, M., et al., *From nature to medicine: snail slime-based functional excipients for oral dosage forms.* International Journal of Pharmaceutics, 2025. **682**: p. 125914.
190. Barrett, D., et al., *Targeting the PI3K/AKT/mTOR signaling axis in children with hematologic malignancies.* Paediatr Drugs, 2012. **14**(5): p. 299-316.
191. Roskoski, R., *Src protein-tyrosine kinase structure, mechanism, and small molecule inhibitors.* Pharmacological Research, 2015. **94**: p. 9-25.
192. Kim, H.J., et al., *Oncogenic KRAS: Signaling and Drug Resistance.* Cancers, 2021. **13**(22): p. 5599.
193. Qian, S., et al., *The role of BCL-2 family proteins in regulating apoptosis and cancer therapy.* Frontiers in Oncology, 2022. **Volume 12 - 2022**.
194. Pizzino, G., et al., *Oxidative Stress: Harms and Benefits for Human Health.* Oxidative Medicine and Cellular Longevity, 2017. **2017**(1): p. 8416763.
195. Putranti, I.O., et al., *The Role of Achatina Fulica Snail Slime Extract Enzymatic Antioxidants as Photoprotector in Sunburn Model Mice.* International Journal of Medical Science and Clinical Research Studies, 2022. **2**(07): p. 624-630.
196. Harti, A.S., et al., *The effectiveness of snail slime and chitosan in wound healing.* International Journal of Pharma Medicine and Biological Sciences, 2016. **5**(1): p. 76-80.

10 PUBLICATIONS

a. Published articles (*Corresponding author)

1. **Rashad, M.**, Ricci, A., Pilato, S., Cataldi, A., Balaha, M., Zara, S. (2025). Nature's Synergy: Cellular and Molecular Evaluation of Snail Slime and Its Principal Component, Glycolic Acid, on Keratinocytes, with Preliminary Evidence from Endothelial Cells. *Biomolecules*, 2025. 15(9): p. 1302. https://doi.org/10.3390/biom15091302
2. Ciulla, M., **Rashad, M***. Spano, M., et al. (2025). Characterization of Mucins, Glycosaminoglycans, and Bioactive Compounds in *Helix aspersa*'s slime by Spectroscopic and Biochemical Analysis. *Journal of Molecular Structure*. 143838. https://doi.org/10.1016/j.molstruc.2025.143838
3. Di Nicolantonio, L., Trebbi, G., Vargas Peregrina, D., **Rashad, M.,** Censi, R., Zara, S., et al. (2025). Development and characterization of a new cosmetic formulation enriched with optimized Thanaka bark extract (*H. crenulata*). *Journal of Drug Delivery Science and Technology,* 113, 107343. https://doi.org/10.1016/j.jddst.2025.107343
4. Sahin, A. F., Carradori, S., Ricci, A., **Rashad, M.,** Akdemir, A. (2025). The Quest for Ligands Against Kinesin Motor Protein Eg5. *Archiv der Pharmazie, 358*(5), e70010. https://doi.org/10.1002/ardp.70010
5. **Rashad, M***., Sampò, S., Cataldi, A., Zara, S. (2025). From Nature to Nurture: The Science and Applications of Snail Slime in Health and Beauty. *Journal of Cosmetic Dermatology,* 24(2), e70002. https://doi.org/10.1111/jocd.70002
6. Talpur, S. A., **Rashad, M.,** Ahmed, A., Rosatelli, G., Baloch, M. Y. J., Khan, A. H. A., et al. (2025). Pollution indicators and human health risk assessment of fluoride contaminated drinking groundwater in southern Pakistan. *HydroResearch,* 8, 167-177. https://doi.org/10.1016/j.hydres.2024.10.005
7. Saadullah, M., Batool, JA., **Rashad, M*.**, Asif, M., Chauhdary, Z., Bibi, A. (2024). Exploration of neuroprotective and cognition boosting effects of *Mazus pumilus* in Alzheimer's disease model. *Journal of Complementary and Integrative Medicine.* 2024;21(4): 461-471. https://doi.org/10.1515/jcim-2024-0231
8. Daud, S., Abid, O. u. R., Saadullah, M., Fakhar-e-Alam, M., Carradori, S., Sardar,

A., Niaz, B., Atif, M., Zara, S., **Rashad, M*.** (2024). Isatin-based ibuprofen and mefenamic acid Schiff base derivatives as dual inhibitors against urease and α–glucosidase: In vitro, in silico and cytotoxicity studies. *Journal of Saudi Chemical Society, 28*(5), 101905. https://doi.org/10.1016/j.jscs.2024.101905

9. Fakhar-e-Alam, M., Amjad, I., Saadullah, M., Tahir, M., Jawad, M., Asif, M., Atif, M., Zara, S. & **Rashad, M***. (2024). Antitumor activity of zinc oxide nanoparticles fused with green extract of Nigella sativa. *Journal of Saudi Chemical Society*, 28, 101814. https://doi.org/10.1016/j.jscs.2024.101814
10. **Rashad, M**., Sampò, S., Cataldi, A. et al. (2023). Biological activities of gastropods secretions: snail and slug slime. *Natural Products and Bioprospecting* 13, 42 (2023). https://doi.org/10.1007/s13659-023-00404-0
11. Saadullah, M., Fakhar-e-Alam, M., Muzammil, S., Asif, M., Siddique, M. H., **Rashad, M*.,** Afzal, M. (2023). Evaluation of molecular mechanisms responsible for in vivo anti-Alzheimer's property of Euphorbia cotinifolia methanol extract. *Journal of King Saud University - Science*, 35(6), 102785. https://doi.org/10.1016/j.jksus.2023.102785

b. Articles under review

1. **Rashad, M*.**, Ricci, A., Balaha, M., Darula, Z., Pap, A., Cataldi, A., Csősz, É., Zara, S. Unraveling the Regenerative Proteomic Signature of *Helix aspera*'s Slime in Human Dermal Fibroblasts by Data-driven Proteomics Approach. Under review in the FEBS Journal, and a preprint is available at https://doi.org/10.64898/2026.03.08.709924
2. Arif, H., Khalid, H., Hussain, R., Rehman, A. Carradori S., **Rashad M**., Balaha M., et al. Synthesis, characterization, biological evaluation and in-silico study of 3,5-di-substituted-1,2,4-triazole derivatives.

11 CONFERENCES AND SEMINARS

- [14/10/2025 – 17/10/2025] Budapest, Hungary

  19th Central and Eastern European Proteomic Conference (CEEPC) – 2025

  Abstract title: Proteomics Profiling of Snail Slime-Treated Human Dermal Fibroblast Using High-End Mass Spectrometry

  Link: https://proteomics.ttk.hu/19ceepc/Book_of_Abstracts.pdf

- [18/09/2025 – 20/09/2025] Ravenna, Italy

  78th Congress of the Italian Society of Anatomy and Histology

  Abstract title: Molecular mechanisms underlying inflammatory and remodeling events differently regulated by cruelty-free method-extracted snail slime and glycolic acid

  Link: https://oajournals.fupress.net/index.php/ijae/issue/view/713/298

- [20/03/2025 – 22/03/2025] Bologna, Italy

  Cosmoprof Worldwide Bologna 56th Edition

  Abstract title: Snail Slime Extracted by Cherasco Method Promotes Skin Regeneration and Counteracts Inflammation

- [12/09/2024 – 14/09/2024] Genova, Italy

  77th Congress of the Italian Society of Anatomy and Histology

  Abstract title: Snail slime obtained through Cherasco method as a promising strategy to counteract inflammation occurrence and to promote viability in human gingival fibroblasts

  Link: https://oajournals.fupress.net/index.php/ijae/issue/view/654/256

- [04/09/2024 – 07/09/2024] Lisbon, Portugal

  European Society for Dermatological Research (ESDR) (53rd Annual Meeting)

  Abstract title: Anti-aging and antioxidant effect of *H. Crenulata* (thanaka) extracts: from *in vitro* evaluation to cosmetic formulations

  Link: https://esdrmeeting.org/wp-content/uploads/2024/08/ESDR2024_AbstractsBook_2024.08.19.pdf

- [11/09/2023 – 13/09/2024] Modena, Italy

  76th Congress of the Italian Society of Anatomy and Histology

  Abstract title: Innovative 3D-printed titanium specimens favor a balanced modulation of inflammation in DPSCs during liposome-triggered mineralization

  Link: https://oajournals.fupress.net/index.php/ijae/issue/view/624/215